２０２３年度

青山学院大学審査学位論文

主査　　平田　普三　教授

Development of Evaluation Techniques for Hepatic Carcinogenicity and Reproductive/Developmental Toxicity

肝発がん性及び生殖発生毒性の評価技術開発に関する研究

理工学研究科

理工学専攻

劉　舒婕

Table of Contents

Abstract

Carcinogenicity, reproductive toxicity, and developmental toxicity are the critical outcomes of safety assessments that notably affect human health. Traditional methods for detecting these toxicities have historically relied on the use of mammalian animals, often involving long-term assessments spanning two–three years and incurring substantial costs. However, a growing need persists in developing evaluation methods based on the 3R (reduction, replacement, and refinement) principles from the perspective of animal welfare. In particular, the chemical and cosmetic industries are seeking complete replacements for animal experiments in the safety testing of novel materials. While developing alternative assessment methods, the adverse outcome pathways (AOPs) of toxicity must be elucidated. The present study aimed to address the mechanisms underlying carcinogenicity, reproductive toxicity, and developmental toxicity and to develop evaluation methods based on AOPs.

Investigation and Technological Development in Carcinogenicity

Carcinogenic mechanisms can be attributed to both genetic and non-genetic factors. However, AOPs for non-genetic carcinogenicity have not been fully elucidated and alternative mechanistic testing methods have not yet been established. This study focused on the liver, which is the primary target of hepatic carcinogenesis. In most cases, liver hypertrophy is the initial change observed in hepatic carcinogenesis. Distinguishing between hypertrophy that leads to carcinogenesis and that which does not, is challenging and necessitates a two-year carcinogenicity test. In this study, toxicogenomic analysis was used to conduct a molecular investigation of the mechanisms underlying carcinogenic liver hypertrophy. Analysis of the genomic data associated with the 134 compounds revealed that the known mechanisms of liver hypertrophy are not directly linked to carcinogenesis. Oxidative stress and factors related to lipid metabolism, including *Gpx2* and *Acot1*, were identified in the process leading to carcinogenesis. These genes have been proposed as valuable markers for distinguishing between adaptive liver hypertrophy and hypertrophic liver carcinogenesis, indicating their roles in crucial molecular events that lead to hepatic carcinogenesis.

Investigation and Technological Development in Reproductive and Developmental Toxicity

Due to the complexity of the toxicity response in hazard evaluation standardized alternative test methods for reproductive and developmental toxicity are scarce. To address this gap, AOPs must be elucidated; however, very few AOPs have been reported, particularly for developmental toxicity. This study focused on craniofacial malformations which are major target defects of teratogenic substances and identified a conserved AOP caused by exposure to teratogenic substances during development in mammals and zebrafish. Contrarily, zebrafish have gained attention as an emerging model for predicting teratogenicity owing to their high-throughput capabilities, cost-effectiveness, and the

availability of various tools for investigating teratogenic mechanisms. With a focus on animal welfare, utilizing zebrafish embryos exposed to 120 h of fertilization is regarded as an alternative testing method that falls outside the realm of experimental animals. Embryos were exposed to 12 teratogens that induce craniofacial abnormalities in humans and other mammals, all of which displayed craniofacial malformations after teratogen treatment. Further observations revealed characteristic disruptions in chondrocyte number, shape, and stacking. These findings suggest aberrant development of cranial neural crest cells (CNCCs), which was confirmed by gene expression analysis of the CNC. These findings indicate that chemical-induced craniofacial malformations are caused by aberrant development of the neural crest. Next, we focused on the relationship between CNCC disruption and craniofacial abnormalities and generated transgenic zebrafish (*sox10:EGFP, sox10:Dendra2, sox10:EGFP-CAAX*) to visualize neural crest cells. The developmental process of CNCCs can be classified into three steps: CNCC migration, first pharyngeal arch (PA1) formation, and outgrowth of craniofacial placodes. The embryos were treated with five well-known teratogens: valproic acid, salicylic acid, caffeine, warfarin, and methotrexate. Upon exposure to these teratogens, CNCC migration and subsequent morphogenesis of the first pharyngeal arch (PA1) were impaired 24 hours post-fertilization (hpf). Morphological changes in PA1 were correlated with craniofacial anomalies, suggesting that these morphological changes originated from early CNCC defects. Furthermore, we observed altered cell proliferation and apoptosis in CNCCs during migration due to teratogen exposure, indicating that the cell proliferation and apoptosis of migratory CNCCs are critical events in the AOP of craniofacial formation. Our results demonstrate that chemical-induced craniofacial malformations are caused by the aberrant development of CNCCs during the migration period, leading to impaired PA1 formation, a process considered conserved among vertebrates. The results provide direct evidence that craniofacial abnormalities are induced by the abnormal development and differentiation of neural crest cells and elucidate the involvement of AOP. In conclusion, craniofacial abnormalities can be predicted and evaluated using the abnormal development of neural crest cells as an indicator, which is beneficial for assessing teratogenic potential.

Acknowledgements

I extend my appreciation to the members of my dissertation committee, Professors Hiromi Hirata, Yuhei Nishimura, Fumiyoshi Abe, and Shigeru Kitani, for their constructive feedback and valuable suggestions that greatly contributed to improving this dissertation. I also extend my appreciation to Professors Makiko Suwa and Kazuhito Tanabe for their valuable suggestions that contributed to the completion of this dissertation.

I would like to express my sincere gratitude to Professor Koichi Yoshinari and Dr. Hiroshi Honda for their guidance, support, and expertise throughout the process of conducting and completing this research on the investigation and technological development of liver hypertrophic carcinogenicity. I also express my sincere gratitude to Professor Hiroyuki Takeda, Dr. Tasaki Junichi, Dr. Toru Kawanishi, and Dr. Atsuko Shimada for their guidance, support, and expertise during my research on the investigation and technological development of reproductive and developmental toxicity. Their insightful feedback and encouragement are invaluable in shaping the direction and content of this study.

I am indeed grateful to Dr. Osamu Morita, Mr. Naohiro Ikeda, Dr. Masayuki Yamane, Ms. Rika Narumi, Dr. Yuko Nukada, Dr. Takashi Ieki, Mr. Keita Yoshihara, and all those who directly or indirectly contributed to this research. Their collaboration, insights, and assistance were crucial for the successful completion of this work. I would like to thank Dr. Shinichi Meguro and Ms. Sakurako Namba for their support with the zebrafish.

Lastly, I would like to acknowledge the unwavering support of my family and friends. Their encouragement, understanding, and belief in my abilities have been a constant source of motivation. I am grateful for the sacrifices they have made to facilitate my academic pursuits.

Thank you all for your support and contributions.

Chapter 1: Introduction

1.1 Background

Evaluation of carcinogenicity and reproductive toxicity represents the most essential components of safety assessment due to their highest concern. These assessments are of paramount importance owing to their direct implications for human health. Traditionally, the evaluation of these toxicities has relied on the use of mammalian animal models, often necessitating long-term studies spanning two–three years and incur substantial financial costs. However, a growing need exists in developing alternative assessment methods in accordance with the 3R (reduction, replacement, and refinement) principles driven by ethical considerations. This is particularly important in industries, such as chemicals and cosmetics, where the complete replacement of animal testing is actively pursued. Development of alternative evaluation methods depends on a comprehensive understanding of adverse outcome pathways (AOPs). This study aimed to elucidate the mechanisms underlying carcinogenicity and reproductive and developmental toxicity, with the goal of developing AOP-based assessment methods.

1.2 Objectives of the Study

The primary objective of this study was to elucidate the mechanisms underlying carcinogenicity and reproductive and developmental toxicities. Specifically, this study aimed to:

1. Investigate the AOPs for carcinogenicity, differentiating between genetic and non-genetic factors and elucidate the specific AOP in hepatic carcinogenicity.
2. Investigate the AOPs for reproductive and developmental toxicity, with a focus on understanding the relationship between teratogens and chemical-induced craniofacial abnormalities.
3. Develop alternative assessment methods that align with the 3R principles for carcinogenicity and reproductive and developmental toxicity, based on their respective AOPs.

1.3 Significance of the Research

This study has significant implications for toxicology and the broader sphere of public health. The elucidation of AOPs for carcinogenicity and reproductive and developmental toxicity not only offers insights into their underlying mechanisms but also paves the way for the development of novel, ethical, and cost-effective safety assessment methods. These methods have the potential to revolutionize the evaluation of chemical substances, ensuring that they meet stringent safety standards while minimizing the use of animal models.

1.4 Scope and Limitations

The scope and limitations of this study must be acknowledged. This study primarily focused on elucidating AOPs for carcinogenicity and reproductive and developmental toxicity, focusing on the liver and craniofacial abnormalities as the key targets. While this research strives to provide valuable insights, it is important to recognize that the complexity of these toxicities may necessitate further exploration and refinement of the assessment methods.

1.5 Organization of the Study

The remainder of this thesis is organized as follows:

- Chapter 2 reviews the existing literature, provides the context for the research, and highlights the importance of safety assessments.
- Chapter 3 introduces the concept of AOPs, presenting an overview for subsequent discussion.
- Chapters 4 and 5 detail the methodologies and results of the assessments of carcinogenicity and reproductive and developmental toxicities, respectively.
- Chapter 6 concludes the study, summarizes its key findings, acknowledges its limitations, and outlines potential avenues for future research.

Chapter 2: Traditional Animals Test and Alternative Approaches for Carcinogenicity and Reproductive/Developmental toxicity Evaluation

2.1 Significance of Carcinogenicity and Reproductive/Developmental Toxicity Evaluation

The importance of comprehensively studying carcinogenicity as well as reproductive and developmental toxicities stems from its pivotal role in the thorough assessment and management of potential risks posed by various substances. Carcinogens can induce cancer and understanding their effects is essential for safeguarding public health and the environment. Similarly, evaluating reproductive and developmental toxicity helps identify substances that may adversely affect fertility, pregnancy, and the developing fetus. This comprehensive understanding not only ensures the safety of individuals, but also aids regulatory authorities and policymakers in formulating effective guidelines and regulations to mitigate potential hazards. Carcinogenesis is widely acknowledged as a complex, multi-stage process involving the transformation of normal cells into cancerous cells, and is influenced by factors like genetics, environmental factors, age, diet, or hormonal balance. (Adler *et al.*, 2011). Cancer ranks as the second most prevalent cause of mortality in Western nations, surpassed by circulatory diseases (Frankish, 2003). Despite significant efforts and financial resources allocated to cancer research over the past few decades, the disease continues to pose a substantial threat to life. Environmental factors such as chemical exposure, lifestyle choices, dietary habits, and occupational conditions predominantly contribute to its occurrence. Various forms of evidence, spanning studies on migrants and twins to the genetic makeup of populations, collectively point to an approximately 80% contribution of environmental factors to cancer development (Lichtenstein *et al.*, 2000; Roberts *et al.*, 2012; Sokal *et al.*, 2000; Tomatis *et al.*, 1997). In addition, it was predicted that 5–10% of the 75,000 chemicals in commercial use might be carcinogenic to humans (Fung *et al.*, 1995). Assessments of reproductive and developmental toxicity play an indispensable role in identifying potential hazards that may impact the well-being of present and future generations. encompasses phenomena such as diminished fertility, impacts on gonadal function, and disruptions in Gametogenesis. This classification also encompasses developmental toxicity, which denotes consequences such as growth and developmental retardation, congenital anomalies, and functional impairments in progeny. Commonly grouped under the umbrella term Developmental and Reproductive Toxicity (DART), these assessments aim to identify potential hazards to the reproductive cycle, with a specific focus on embryotoxicity. Approximately 2–5% of congenital abnormalities can be attributed to chemical and stressors, predominantly stemming from the inappropriate use of substances such as alcohol and drugs (Mattison, 2010).

Moreover, interest in Carcinogenic, Mutagenic, and Reprotoxic (CMR) substances has been prominent since the early 20th century. Particularly in occupational settings, the recognition of hazards and their impact on workers' health gained attention. Early regulations focused on the handling of CMR substances in workplaces. From the 1960s to the 1980s, advancements in science and technology led to a more sophisticated identification and assessment of CMR substances, accompanied by the evolution of legal regulations. Presently, the evaluation and management of CMR substances are rigorously conducted by international organizations and individual countries. The World Health Organization (WHO) and the International Labour Organization (ILO) provide guidelines on the health impacts of CMR substances. In many regions, legal frameworks have been established with restrictions on the manufacturing and handling of these substances. In addition, in 2020, in line with the European Green Deal's zero pollution goal, the European Commission introduced a sustainability-focused chemicals strategy. Aimed at bolstering citizen and environmental protection, it encourages innovation in secure and sustainable chemicals. The regulation of CMR substances has become increasingly stringent.

2.2 Constraints of Traditional Safety Assessment Methods

Historically, the assessment of carcinogenicity and reproductive and developmental toxicity has predominantly relied on conventional methods that employ mammalian animal models. I also conducted these experiments on many substances, including some supplemented diets, such as alpha-linolenic acid (ALA)-enriched diacylglycerol (DAG) oil (Bushita *et al.*, 2018). However, this approach had several limitations. They often require extended testing periods spanning two–three years, incurring significant financial costs.

The primary method for early detection of carcinogens involves conducting long-term carcinogenesis bioassays on Sprague-Dawley rats by oral administration. These assays were specifically designed to identify the potential carcinogenic effects in humans. A consistent and reliable correlation between the results of long-term bioassays in rodents, predominantly rats and mice, is a key indicator of cancer risk in humans. For these reasons, the 2-year rodent cancer bioassay has been considered the standard method for assessing the cancer-causing potential of a chemical. OECD (Organization for Economic Cooperation and Development) Test Guidelines have been in place since 1981 to regulate this process. However, there is ongoing debate about the accuracy of this assay in predicting cancer risk in humans. There are challenges and uncertainties involved in extrapolating data from rodents to humans, including limited accuracy in quantitative risk estimation. Additionally, the original design of the rodent bioassay does not account for windows of susceptibility throughout an organism's lifetime, which means it may not effectively detect agents that alter susceptibility to tumors, such as Aryl hydrocarbon

receptor chemicals. Conducting these investigations is also a time-intensive and resource-demanding process, prompting ethical concerns related to the well-being of animals. From a regulatory standpoint, there is an escalating acknowledgment of non-genotoxic mechanisms in carcinogenesis, which deviates from the conventional understanding of the correlation between genotoxicity and carcinogenicity. This complicates the interpretation of rodent carcinogenicity findings concerning their applicability to human cancer. The presumed linearity of the dose-response curve for genotoxic carcinogens in regulatory decision-making has sparked controversies over categorizing carcinogens as genotoxic or non-genotoxic, a critical facet of cancer risk assessment. The field of carcinogenicity has experienced renewed attention in recent years due to the increasing recognition of the limitations inherent in current regulatory in vivo testing requirements. Additionally, there are information gaps in legislation, such as the European Registration, Evaluation, Authorization, and Restriction of Chemicals (REACH) and Cosmetics Regulations, which impose restrictions or prohibitions on animal use, and these gaps must be addressed.

Similarly, Developmental and Reproductive Toxicity (DART) has not received much attention in safety assessments for the years following thalidomide disasters. However, the REACH legislation has sparked renewed discussions on this topic owing to its stringent requirements. The timing of these processes creates windows of vulnerability, and they are particularly sensitive to genetic errors and environmental disruptions. Simple lesions can result in complex phenotypes and maternal effects can affect all developmental stages. The most common approach for identifying DART involves the treatment of one or more generations of rats or rabbits with a test chemical. Several OECD Test Guidelines (TGs) have been established to guide this process. These TGs detect malformations, growth alterations, and prenatal mortality in developing offspring to evaluate developmental toxicity. However, tests such as the two-generation study, which can involve up to 3000 animals per substance, are considered among the costliest. In the field of drug development, replacing the use of a second species with human mechanistic assays and evaluating the necessity of using non-human primates as biologicals have been focused. The European ban on testing cosmetic ingredients has also played a significant role in driving these discussions. To address these challenges, the European Center for the Validation of Alternative Methods (ECVAM) conducted various activities, including workshops, to explore alternative approaches. One notable project is the Integrated Project ReProTect, which has pioneered several alternative methods. This was followed by projects such as ChemScreen and the more recent flagship program, EU-ToxRisk. The assessment of developmental processes is difficult.

Further discussion is necessary regarding the relevance of the current carcinogenicity and DART assessments. As society recognizes the need to ensure the safety of drugs, chemicals,

and consumer products, it has become challenging to completely abandon current testing methods. However, lower barriers to implementing alternative approaches are required. Moreover, using animals for toxicity testing raises ethical concerns and necessitates the development of cruelty-free alternatives. The shift towards replacing or refining existing testing protocols is firmly rooted in the principles of the 3R approach: reduction, replacement, and refinement. This paradigm shift in safety assessment aligns with societal values and the pursuit of scientific advancement.

2.3 Requirement for Alternative Assessment Methods Based on the 3R Principle

Considering the constraints posed by traditional safety assessment methods, there is a growing need to embrace alternative approaches that align with the 3R principle. The Reduction principle seeks to minimize the number of animals used, replacement seeks to find non-animal alternatives, and refinement aims to enhance the welfare of animals involved in testing. Chemicals and cosmetics industries are at the forefront of this transformative shift, actively pursuing the development and implementation of alternative assessment methodologies. These endeavors seek not only to enhance the efficiency and cost-effectiveness of safety assessments, but also to uphold the highest ethical standards by reducing reliance on animal models. The need for alternative assessment methods based on the 3R Principle arises from ethical, scientific, and regulatory considerations. There is widespread ethical recognition of the moral imperative to reduce the use of animals in experiments. Scientifically, advancements in technology and methodologies have provided viable alternatives that yield more accurate and reliable results than traditional animal testing methods. From a regulatory standpoint, there is increasing emphasis on incorporating alternative methods to ensure the safety and efficacy of products while aligning with evolving ethical standards. The U.S. Environmental Protection Agency (EPA) has decided to forego the set deadline for discontinuing mammalian toxicity testing by the year 2035. Additionally, the Food and Drug Administration (FDA) also no longer mandates the testing of all drugs on animals prior to initiating human trials.

Currently, growing momentum is present in the adoption and development of alternative assessment methods guided by the 3R principle. Many research institutions, industries, and regulatory bodies actively promote and incorporate these methods in their practices. This includes the development of *in vitro* testing, computational modeling, and other innovative approaches that aim to replace, reduce, or refine the use of animals in research. Ongoing collaboration among stakeholders, scientific communities, and regulatory agencies contributes to the evolution of a more ethical, scientifically robust, and sustainable landscape for assessment methods in various fields.

2.4 Alternative method for Carcinogenicity and Reproductive/developmental toxicity tests.

Considering the constraints posed by traditional safety assessment methods, there is a growing need to embrace alternative approaches that align with the 3R principle. The Reduction principle seeks to minimize the number of animals used, replacement seeks to find non-animal alternatives, and refinement aims to enhance the welfare of animals involved in testing. Chemicals and cosmetics industries are at the forefront of this transformative shift, actively pursuing the development and implementation of alternative assessment methodologies. These endeavors seek not only to enhance the efficiency and cost-effectiveness of safety assessments, but also to uphold the highest ethical standards by reducing reliance on animal models.

Alternative Approach of Carcinogenicity Evaluation

1. Genotoxicity Tests

Genotoxicity assay, which conduct to detect mutagens, have different endpoints such as single- and double-strand breaks, point mutations, deletions, chromosomal aberrations, and micronuclei formation. Over the past decade, notable efforts have been made globally to enhance genotoxicity testing. This includes improving both the basic *in vitro* tests and follow-up *in vivo* studies. The goal was to minimize false-positive results in *in vitro* tests, which can lead to unnecessary animal testing and negative consequences for animal welfare. Recommendations from the ECVAM workshops and strategy papers have supported international initiatives to advance existing *in vitro* genotoxicity tests and identify new test systems with improved sensitivity and specificity. This accumulated knowledge has led to updates to the OECD guidelines for genotoxicity testing. The *in vitro* micronucleus test, evaluated by the ECVAM, has become a key component of the genotoxicity strategy and is often used alongside the Ames test in a two-test battery (Committee on Mutagenicity of Chemicals in Food, Consumer Products, and the Environment). This led to the International Conferences on Harmonization (ICH) establishing Safety Guidelines for the human utilization of pharmaceutical drugs. Furthermore, novel *in vitro* methods, such as genotoxicity assays using 3-D reconstructed human skin models, toxicogenomics-based tests, and biomarker assays for a better understanding of modes of action (MoAs), are under development and validation to fully replace current methods and provide deeper insights into genotoxicity mechanisms (Corvi *et al.*, 2017; Hayashi, 2022).

2. Cell Transformation Assays

In vitro cell transformation assays (CTAs) have been used for approximately 40 years to detect potential carcinogens. Transformation refers to the occurrence of phenotypic changes in cultured cells that resemble tumorigenic cells and are indicative of carcinogenesis. This assay

is considered to detect both genotoxic and non-genotoxic carcinogens. Despite the extensive use of CTAs and the efforts made by the OECD between 1997 and 2016, as well as the validation studies conducted by ECVAM and Japanese Center for the Validation of Alternative Methods (JaCVAM), these assays have not yet been officially adopted as OECD Test Guidelines (TGs). A major obstacle in developing an OECD TG for the SHE CTA which used in Syrian hamster embryo cells was the absence of a comprehensive validation process. Instead, a combination of a Detailed Review Paper (DRP) and a limited prospective validation study was conducted, which necessitated further analysis by the OECD expert group. This also highlights that a DRP does not always serve as a retrospective validation. Furthermore, no Integrated Approaches to Testing and Assessment (IATA) or alternative testing strategies were available for assessing carcinogenicity. Due to the consensus that the assay should not be used as a standalone method, difficulties arose in determining how to incorporate it into regulatory decision-making processes (Colacci *et al.*, 2023).

3. Integrated Approaches to Non-Genotoxic Carcinogens

Non-genotoxic carcinogens increase cancer risk through various mechanisms that are not currently being assessed by international regulatory approaches. In April 2014, the OECD Working Group of the National Coordinators of the Test Guideline Program (WNT) meeting recognized that the Carcinogenicity Testing Assay (CTA) alone was insufficient to address non-genotoxic carcinogenicity. A more comprehensive set of tests addressing the different non-genotoxic mechanisms of carcinogenicity is needed in the future. This prompted the development of an Integrated Approach to Testing and Assessment (IATA) to properly address the issue of non-genotoxic carcinogenicity, in which CTA, along with other relevant assays, could be incorporated. In recent years, the IATA has been created for simpler endpoints, such as eye irritation and skin sensitization. It was the first time that a IATA approach used for such a complex endpoint. Under the guidance of the OECD, an expert working group was established to examine the current international regulatory requirements and limitations regarding non-genotoxic carcinogenicity. The group aimed to develop an IATA to assist regulators in assessing non-genotoxic carcinogenicity. Additionally, the working group reviewed, described, and evaluated the relevant in vitro assays. The goal was to organize these assays into testing levels according to the adverse outcome pathway (AOP). This approach facilitated the creation of potential structures for future IATA. Various in vitro methods have been used as research tools to study potential non-genotoxic mechanisms, such as oxidative stress or inhibition of gap junction intercellular communication. However, these methods cannot reliably predict the carcinogenic potential of substances. Instead, they contribute to improving our understanding of the mechanistic basis of the effects caused by a compound within a weight-of-evidence assessment strategy, such as the IATA (Jacobs *et al.*, 2020).

4. Toxicogenomics-Based Methods for Carcinogenicity.

Toxicogenomics has been applied in various in vitro and short-term in vivo test systems to study carcinogenicity. For instance, the EU Framework Project called CarcinoGENOMICS aims to develop toxicogenomic tests in liver, lung, and kidney cells to detect potential genotoxicants and carcinogens. This project also assessed the reproducibility of the assay using different bioinformatic approaches. The potential applications of toxicogenomics-based assays include clarifying the Mode of Action (MoA), hazard classification, deriving points of departure, and prioritization. Among these applications, the use of transcriptomic tests to determine the MoA appears to be the preferred approach. However, the incorporation of transcriptomics into regulatory decision-making remains limited. This was discussed during a recent workshop organized by HESI, Health Canada, and McGill University in 2017. Although companies use transcriptomics method tests for internal decision-making, the major obstacle to submitting data is the uncertainty surrounding how regulators would interpret these findings. Furthermore, the lack of validation and regulatory guidance are also considered challenges (Hernández *et al.*, 2010; Yauk *et al.*, 2020) .

Alternative Approach of Reproductive and Developmental Toxicity Evaluation

1. Zebrafish Embryo Assays

Due to the high expenses and prolonged evaluations associated with developmental toxicity testing in mammals, the vertebrate organism such as zebrafish (*Danio rerio*) and African clawed frog (*Xenopus, laevis*), have emerged as valuable substitute for conducting high-throughput assessments of developmental toxicity. Techniques such as dynamic cell imaging or the use of frog eggs (FETAX assay) have been employed to study zebrafish embryos in detail. The evaluation of FETAX assay by the Interagency Coordinating Committee on the Validation of Alternative Methods (ICCVAM) has been quite critical. Presently, the Evidence-Based Toxicology Collaboration is conducting a systematic review of existing protocols and data. This retrospective analysis is also investigating whether such systematic reviews can serve as substitutes for traditional validation methods (Hoke and Ankley, 2005). Since of the advantages such as rapid development, optical clarity, and genetic malleability, zebrafish embryos appear to provide the most comprehensive representation of embryonic development.

Zebrafish are extensively utilized in ecotoxicology to explore the impact of chemicals and environmental contaminants on fish population. Several fish species, including zebrafish and Japanese Medaka (*Oryzia latipes*), are incorporated into internationally accepted OECD guidelines for assessing systemic toxicity in fish, such as the Fish Acute Toxicity Test (OECD TG No.203) and the Fish Embryo Acute Toxicity Test (OECD TG No.236). Under the current European Commission Directive 2010/63/EU, experimentation on fish embryos during their

earliest life stages is permitted without being regulated as animal experiments, including zebrafish embryos and early larval stages until they reach free-swimming and independent feeding, corresponding to 5 days post-fertilization (dpf) after raising at 28.5°C (Scholz *et al.*, 2008; Strähle *et al.*, 2012). These regulations allow toxicological studies in zebrafish at these early developmental stages as an alternative model to animal testing in other vertebrates, such as rodents. In alignment with the principles of 3Rs in toxicology experiments involving small fish species at all developmental stages, researchers should prioritize methods that avoid or replace the use of animals. However, such investigations are often limited to developmental and acute toxic effects.

Although not adopted by the OECD test guidelines, zebrafish embryos have long been considered as an alternative method for evaluating developmental toxicity. Zebrafish shares similar to all other vertebrate species a conserved basic body plan. While *in vitro* models can be suitable replacements for some applications, living organisms are necessary for investigating systemic toxic effects, whole animal development, or organ function. Whole organism models that can bridge the gap between the high-throughput, low-cost, cell-line testing models and the low-throughput, costly, mammalian models are thus still required. Zebrafish is an established alternative model for toxicity testing that can provide a medium-throughput, cost-effective model that can also provide more information than can be obtained from cell line testing alone. To minimize the number of animals used, researchers can employ reduction methods, obtaining comparable information from fewer animals or maximizing information from the same number of animals. Examples relevant to fish tests include non-invasive imaging, intravital time-lapse investigations, and the careful selection or combination of fluorescent transgenic animals. Refinement methods should also be considered to alleviate or minimize potential pain, suffering, or distress, enhancing animal welfare. Although general pain scoring methods and analgesics in zebrafish are currently limited, ongoing developments are underway.

On the other hand, systems toxicology involves understanding how exposure to xenobiotic compounds induces molecular changes, potentially leading to cellular and organism-level effects. Transcriptomics, particularly gene-expression profiling, is a key method in systems toxicology, providing insights into perturbed biological networks. In zebrafish, transcriptomic analyses have identified commonly and selectively expressed genes in response to developmental toxicants, suggesting shared and unique modes of action. High-content assays using transgenic zebrafish embryos, with endpoints like morphology and behavior, are gaining popularity for toxicity screening. Zebrafish serves as an excellent model in the systems toxicological approach for developmental toxicity testing, integrating traditional and advanced assays. Systems toxicology aims to elucidate molecular mechanisms and functional changes induced by xenobiotic exposure, ultimately developing mathematical models for predicting

developmental toxicity in humans (Achenbach *et al.*, 2020).

2. *In vitro* Embryotoxicity Tests

Since 1970, reproductive toxicologists have developed *in vitro* assays for studying the mammalian reproductive cycle. Many *in vitro* methods are currently being developed, and the embryonic stem cell test (EST) is an assay that uses embryonic stem cells, which was developed to meet the needs of the 3Rs in 1997 by Dr. Horst Spielmann's group. Mouse EST (mEST) has been found to be more predictive and reproducible than other tests, and has undergone a formal validation study sponsored by ECVAM. This study validated two other *in vitro* embryotoxicity tests: the micromass test and the whole embryo culture test. The validation process involved assessing these tests against a set of chemicals with well-documented *in vivo* embryotoxicity data from both laboratory animals and humans. However, these tests have not reached the status of official OECD test guidelines and have not yet received regulatory acceptance (Hareng *et al.*, 2005). Efforts are being made to involve regulators early in the validation process and to apply integrated approaches to testing and assessment. Sumitomo Chemical Co. Ltd has developed Hand-1 Luc EST to improve the original EST. Hand-1 (heart and neural crest derivative expressed 1) is a key gene in the development of the heart and other organs (e.g., craniofacial bones and limbs). The Hand-1 Luc EST was validated and sponsored by JaCVAM from 2013 to 2016 (Nagahori *et al.*, 2016). Although it was concluded that the reproducibility and predictivity of this assay were sufficient, the lack of a mechanistic explanation for this assay still limits its ability to predict unknown teratogens. For negative results in this assay, further approaches, such as IATA and *in vitro* or *in vivo* embryotoxicity testing, are required. In addition, a variant of EST using human stem cells and metabolite measurements has shown promising results and is currently being validated. Discussions regarding the use of these assays for regulatory evaluations are ongoing. The FDA has proposed a streamlined qualification process for new models or assays, allowing their use without reviewing the underlying data. The current revision of the ICH S5 Guidelines includes provisions for *in vitro* tests in pharmaceutical registration (Piersma *et al.*, 2022).

3. Endocrine Disruptor Screening Assays

Endocrine disruption is a crucial aspect of developmental and reproductive toxicology. Endocrine-disrupting chemicals (EDSs) are generally defined as substances that can disrupt the hormonal balance in humans and result in adverse health effects. Endocrine disruption is considered a critical endpoint in DART evaluation. The OECD has issued an updated version of Guidance Document 150, which provides standardized test guidelines for assessing chemicals for endocrine disruption. Additionally, it considers scientific advancements in test methods, including several *in vitro* assays (e.g., OECD TG No. 173 and 174), and the assessment of the endocrine activity of chemicals.

Nonetheless, all these assay developments serve as essential components in an integrated testing approach for carcinogenicity and reproductive/developmental toxicity.

Chapter 3: Understanding Adverse Outcome Pathways (AOPs)

3.1 Overview of AOPs

Adverse Outcome Pathways (AOPs) provide a structured framework for understanding the sequence of events that leads from exposure to a stressor, such as a chemical or environmental factor, to an adverse outcome in a biological system. This chapter discusses the foundational principles of AOPs and emphasizes their significance in the field of toxicology.

An AOP is a detailed account of the sequence of events triggered by a molecular initiating event (MIE), which is the direct interaction between a chemical and it's molecular target. This sequence of events ultimately leads to an adverse outcome at the individual or population level. The AOP includes a series of intermediate key events (KE) occurring at various biological levels (Knapen *et al.*, 2015; D. L. Villeneuve *et al.*, 2014). In the context of AOPs, KEs help identify specific areas where assays require improvement or development. A KE is typically defined as an observable change in a biological state that is necessary, although not necessarily sufficient on its own, for progression towards a particular adverse outcome (D. Villeneuve *et al.*, 2014). Examples of KEs include alterations in the expression and function of genes, proteins, and metabolites; changes in cellular or tissue morphology; and disruptions in physiological functions. Collectively, these KEs form a causal pathway that leads to an adverse outcome relevant for risk assessment. KEs need to be measurable, a direct linkage exists between the AOP framework and the design of assays, especially when exploring substitutes for conventional whole-organism tests that depend on the direct observation of endpoint results.

The foundations for AOP research were laid through an understanding of the toxicological mechanisms. In the late 20th century, researchers began to explore the relationship between the molecular-initiating events of toxicity and adverse outcomes. Early studies often focused on specific toxicological pathways without a formalized AOP framework. The Organization for Economic Co-operation and Development (OECD) has played a significant role in advancing AOP research. In 2007, the OECD initiated the development of AOPs as a tool for improving chemical safety assessments and established the AOP Development Program to facilitate collaboration among experts from various fields, leading to the formation of AOP knowledge networks. AOPs can facilitate the creation of non-animal testing methods. Nonetheless, recently developed AOPs and their associated assays necessitate validation before their regulatory application. Despite the validation process often incorporating animal models, AOP development should not be perceived as a mechanism for augmenting animal testing. AOPs can function as valuable instruments guiding research endeavors toward the validation of alternative tests. In practical terms, subsequent assessments grounded in validated AOPs will only sporadically demand comprehensive validation experiments, such as when transitioning to a

different species (Groh *et al.*, 2015).

In 2010, the OECD published the "Users' Handbook Supplement to the Guidance Document for Developing and Assessing AOPs," providing guidance for the development and assessment of AOPs. This was followed by other studies that further detailed the AOP development. In 2013, the OECD launched the AOP-Wiki (https://aopwiki.org/) in collaboration with various stakeholders. The AOP-Wiki is an online platform designed to compile, review, and share information. It serves as a central repository of AOP-related knowledge and has played a crucial role in facilitating the exchange of AOP information within the global scientific community. AOPs have been increasingly integrated into regulatory frameworks for chemical safety assessments, and regulatory agencies, such as the EPA and European Chemicals Agency (ECHA), have recognized the value of AOPs in hazard and risk assessments. AOP research has seen a growing emphasis on collaboration among researchers, toxicologists, regulators, and other stakeholders. International conferences, workshops, and working groups have helped to advance the development and application of AOPs. This research continues to evolve with ongoing efforts to improve the development and applications of AOPs, and is expanding to address various areas of toxicology, including human health and environmental risk assessments.

AOPs are important in toxicology for several reasons:

1. Mechanistic understanding AOPs provide a mechanistic understanding of how exposure to chemicals or stressors can lead to adverse health effects. They offer a structured framework for linking an initial interaction with a stressor to the outcome of a biological system.

2. Hazard evaluation and risk assessment: AOPs aid in risk assessment by helping toxicologists and regulators evaluate the hazards associated with specific compounds. This knowledge allows the development of exposure limits, helps set safe exposure limits, and makes regulatory decisions.

3. Reduction in animal testing: AOPs support the development of alternative testing methods that reduce the reliance on animal experimentation. They align with the 3R principles (reduction, replacement, and refinement) for animal welfare and ethical considerations.

4. Data integration: AOPs help integrate various data sources such as *in vitro* studies, omics data, and epidemiological research into a cohesive framework to assess the potential risks of chemicals and environmental factors.

3.2 Identifying AOPs for Carcinogenicity

AOPs for carcinogenicity encompass both genotoxic and non-genotoxic mechanisms, offering a comprehensive framework for understanding the diverse pathways that lead to carcinogenic effects. Cancer is widely recognized as a complex process involving multiple

stages including initiation, promotion, and progression. Chemical carcinogens can disrupt these processes and trigger cancer-induced effects. A distinguishing characteristic of cancer cells is the presence of numerous mutations in crucial genes, underscoring the theory that cancer results from irreversible DNA damage (Basu, 2018; Barnes *et al.*, 2018; Hernández *et al.*, 2009; Huang and Zhou, 2021). In most cases, chemical carcinogens induce DNA damage either directly or following xenobiotic metabolism, and are described as genotoxic. Non-genotoxic carcinogens induce cancer through mechanisms that do not involve direct DNA damage and have been observed to function as tumor promoters, endocrine modifiers, receptor mediators, and initiators of tissue-specific toxicity and inflammatory responses (Benigni *et al.*, 2013; Hernández *et al.*, 2009; Shaw and Jones, 1994).

Unlike genotoxic carcinogens, which share a common mechanism of inducing DNA damage and can be identified using various *in vitro* genotoxicity assays, non-genotoxic carcinogens exhibit various mechanisms that do not directly cause cellular damage. Consequently, they are often undetectable in short-term assays and require a two-year rodent cancer bioassay. Peroxisome proliferators are among the most widespread non-genotoxic carcinogens. Chronic administration of peroxisome proliferators in rodents results in the development of hepatocellular carcinomas (Cattley, 2004). However, the implications of these findings in human populations have sparked intense debate. Notable variations in the response to peroxisome proliferators have been observed among different species, with rats and mice demonstrating high susceptibility; hamsters showing weak responsiveness; and humans, primates, dogs, and guinea pigs largely resistant to the short-term effects of peroxisome proliferator exposure (Bentley *et al.*, 1993). While humans possess a functional PPARα, the exact mechanism behind their resistance to peroxisome proliferation remains incompletely understood. Discrepancies in the expression or activation of PPARα are plausible explanations for species-specific effects of peroxisome proliferators (Tugwood *et al.*, 1996). Considering the available evidence, some expert panels contend that the likelihood of peroxisome proliferators acting as human liver carcinogens at expected levels of human exposure is extremely low. However, the significance of PPARα-mediated rodent hepatocarcinogenesis under various conditions of peroxisome proliferator exposure cannot be entirely dismissed.

Another famous non-genotoxic mechanism is aryl hydrocarbon receptor (AhR)-induced carcinogenicity. While evidence supports AhR and the activation of the AhR signaling pathway by endogenous physiological ligands, no definitive high-affinity endogenous agonists have been identified thus far. Although AhR plays a crucial role in mediating these effects, the molecular mechanisms underlying most aspects of these toxic responses, as well as the biological functions of AhR, remain unknown. In contrast to PPARα, AhR-mediated hepatocarcinogenesis is considered highly relevant to humans. Exposure to enduring agonists

like 2,3,7,8-tetrachlorodibenzo-p-dioxin (TCDD) and its analogs can result in a range of toxic and biological effects that vary among species and tissues. These effects encompass teratogenicity, promotion of liver tumors, and carcinogenicity.

Other mechanisms, such as the induction of oxidative stress and disruption of hormonal imbalance, have also been reported as non-genotoxic carcinogenic mechanisms. This study focused on hepatic carcinogens that often trigger liver cancer via nuclear receptor like PPAR-α and AhR -medicated mechanisms. In many cases, the initial effect of these carcinogens is liver hypertrophy. However, differentiating hypertrophy, which ultimately leads to carcinogenesis, is not a complex process. Consequently, the assessment of the carcinogenic potential during liver hypertrophy is a formidable task, often necessitating a comprehensive two-year carcinogenicity evaluation. Chapter 4 discusses the mechanisms underlying adaptive liver hypertrophy and carcinogenesis-associated hypertrophy. This study focused on identifying the key event in the AOP of non-genotoxic carcinogenicity that distinguishes between the two forms of hypertrophy. The goal of this study was to elucidate the specific pathways and biological processes that lead to liver cancer in response to these non-genotoxic carcinogens.

3.3 Identifying AOPs for Reproductive and Developmental Toxicity

Reproductive and developmental toxicity assessments play a vital role in understanding the potential risks of chemical exposure to humans and the environment. Traditional toxicity evaluation methods often rely on animal testing, which is resource-intensive, time-consuming, and raises ethical concerns. To address these challenges, the scientific community has increasingly turned to the concept of AOPs as a framework for enhancing our understanding of the mechanisms underlying reproductive and developmental toxicity. The development of comprehensive AOPs for these toxicities is an ongoing endeavor that requires thorough validation before they can be used for regulatory purposes and may involve animal testing. However, AOP development is not viewed as an additional source of animal testing but rather as a means of prioritizing research efforts for alternative tests.

A PubMed search using the keywords "AOP" and "reproductive toxicity" resulted in more than 100 references in 2023. In a comprehensive analysis, the distinct relevance of the human placenta to the AOP concept was suggested, highlighting its significance as a physiological barrier that offers essential insights into human organ functions across various levels of biological organization (Gundacker and Ellinger, 2020). However, a few studies are available on AOPs related to developmental toxicity, particularly in the context of craniofacial malformations.

Developmental toxicity is characterized by any reversible or irreversible structural or functional alteration that disrupts homeostasis, normal growth, differentiation, development, or

behavior. It is induced by environmental insults, including drugs, alcohol, environmentally toxic chemicals, and physical factors. These insults may affect various developmental stages, including pre-fertilization (involving parental gametes), embryonic stages (both pre- and post-implantation), fetal development, and postnatal phases. The AOP framework is an exceptionally valuable tool for consolidating the knowledge related to developmental toxicity pathways and networks. This approach facilitates evidence-based toxicology rather than relying solely on empirical animal-based studies. Several examples of AOPs associated with developmental toxicity are summarized below.

One of the initial AOPs for developmental toxicity is disruption of embryonic vascular development (Knudsen and Kleinstreuer, 2011). Drawing on a comprehensive review of vascular development biology and utilizing US EPA ToxCast HTS data, they delineated the key events (KEs) triggered by embryonic vascular disruption, potentially leading to low birth weight, functional deficits, malformations, and mortality. KEs included altered angiogenesis mediated by vascular endothelial growth factor (VEGF) (AOP-Wiki: AOP43). Another research for developing the AOPs is focused on congenital axial malformations, including skeletal defects and cleft palate, occur in one in every 500–1,000 live births. Many of these malformations are linked to genetic syndromes or intrauterine exposure to antiepileptic drugs (Knudsen *et al.*, 2021). A potential shared Key Event (KE) in such malformations is the altered homeostasis of retinoic acid, a metabolite of vitamin A. Data on *in vitro* profiling of the retinoid system, sourced from the ToxCast/Tox21 datasets, and information on *in silico* models predicting skeletal dysmorphogenesis, gathered from the literature and the ToxRefDB_v2 databases, are currently available. However, systematic collation of this information is scarce, and only a few AOPs have been documented in the literature or in the AOPWiki. For instance, computational modeling and data mining approaches using HTS data and chemical structural descriptors have been used to derive putative MIEs leading to an AOP for cleft palate. However, no clear KEs of cleft palate have been reported.

A notable challenge in using the AOP framework to increase the regulatory uptake is the assessment of developmental neurotoxicity (DNT). The OECD has taken the lead in fostering international collaboration to consider the integration of alternative approaches to improve chemical DNT testing. Recently, a sequence of workshops has been conducted, culminating in a consensus that emphasizes the need to develop a testing battery for DNT. This battery is based on in vitro assays that are intricately linked to crucial neurodevelopmental processes (Sachana *et al.*, 2021). The molecular and cellular mechanisms underlying many neurodevelopmental disorders are largely unknown, and in some cases, the features and symptoms of these diseases overlap because they are not specific to a particular disease. Therefore, the complex etiology and limited mechanistic understanding of neurodevelopmental disorders make the identification

of KEs extremely difficult.

The consideration of life stages plays a crucial role in formulating AOPs for reproductive and developmental toxicity. Some KEs and AOs may be specifically related to adult phase reproductive toxicity. The IATA approach involves a comprehensive analysis of existing information combined with the generation of new data to characterize chemical hazards. It has also been acknowledged that integrated analysis relies on AOP-based ontologies, but there is a recognized need for more information on toxicokinetic and *in vitro/in vivo* extrapolation (IVIVE) modeling. Although there is a wealth of literature on reproductive and developmental toxicants, it is often fragmented, posing challenges for regulatory assessments. Regulators require well-documented causal links between experimental findings and disease outcomes. The use of AOPs provides a means to integrate diverse data types for robust assessments. However, the current scope of AOPs is limited, covering only a narrow range of disorders and hampering the creation of comprehensive networks.

Efforts to expand AOPs, particularly for prevalent outcomes with hypothesized chemical links, are essential. This expansion is crucial for enhancing the development of accurate AOP networks and serves as a vital resource for the regulatory evaluation of reproductive and developmental toxicity.

Chapter 4: Investigation and Technological Development in Chemical-Induced Hepatic Carcinogenicity

4.1 Introduction

4.1.1 Critical issue in assessing liver hypertrophy caused by chemicals.

The evaluation of hepatotoxicity is particularly important in repeated-dose toxicity studies because the liver plays a central role in the clearance and metabolism of chemicals. Among the hepatotoxicity findings observed in toxicological studies, liver hypertrophy, which is characterized as an increase in liver weight, hepatocellular hypertrophy, and/or hepatocellular cell proliferation, is well known as one of the most frequent effects.

The toxicological relevance of liver hypertrophy has been debated for more than 50 years and has become a critical issue in chemical safety assessment (Gilbert and Goldberg, 1965; Rowe *et al.*, 1959; Weil and McCollister, 1963). In 2000s, the United States Environmental Protection Agency (U.S. EPA) (2002) and the Joint Food and Agriculture Organization of the United Nations/World Health Organization (FAO/WHO) (2006) presented a similar conclusion that liver hypertrophy in the absence of histopathological and relevant clinical changes should not be considered as an adverse effect. However, some research data appears to contradict this assessment. For example, a survey of agrochemicals found that a 50% increase in liver weight was correlated with liver tumors in mice even in the absence of clinical or histopathological changes(Carmichael *et al.*, 1997). Moreover, liver hypertrophy has been identified as the best predictor for murine liver tumors (Allen *et al.*, 2004). Thus, in 2012, the European Society of Toxicologic Pathology (ESTP) convened an expert panel to reach consensus on the role of liver hypertrophy in toxicology. After all, although ESTP also lead to a similar conclusion with FAO/WHO and U.S. EPA, they mentioned some uncertainty that the correlation between liver hypertrophy and carcinogenesis has not been fully investigated, and continuous hypertrophy occasionally results in tumors(Hall *et al.*, 2012).

In general, a hepatocellular hypertrophy that is accompanied by enzyme induction is regarded as an adaptive response(Maronpot *et al.*, 2010; Thoolen *et al.*, 2010). However, liver hypertrophy with certain changes, such as necrosis, inflammation, and cell proliferation have been considered to be adverse effects related to carcinogenesis(Butler, 1996; Peters *et al.*, 1997; Schulte-Hermann *et al.*, 1980). Furthermore, adaptive hypertrophy with enzyme induction and adverse hypertrophy with a proliferative response share common upstream regulators such as aryl hydrocarbon receptor (AhR), constitutive androstane receptor (CAR), and peroxisome proliferator-activated receptor alpha (PPARα) (Budinsky *et al.*, 2014; Corton *et al.*, 2014; Elcombe *et al.*, 2014; Plant and Aouabdi, 2009). Therefore, there is room for further clarification regarding the involvement of liver hypertrophy in carcinogenesis in terms of

molecular mechanism. Previous studies on the mechanism of liver hypertrophy have mainly focused on the induction of the phase I and II drug-metabolizing enzymes, which is generally considered to trigger adaptive responses.

4.1.2 Application of toxicogenomics analysis techniques the assessment of liver hypertrophy.

On the other hand, Nagata et al. employed a toxicogenomic approach using a DNA microarray to identify genes related to increases in liver weight, and reported several hypertrophy-related genes that are not drug-metabolizing enzymes (Nagata *et al.*, 2014). However, since there are no studies focused on the molecular mechanism of hypertrophic hepatocarcinogenesis, exhaustive analyses would be required to decipher what mode of action in liver hypertrophy should be considered for assessing the risk of cancer.

Toxicogenomic analysis has been shown to suitable for analyzing the molecular mechanisms and predicting the toxicity (Matsumoto *et al.*, 2009; Suter *et al.*, 2004; Watanabe *et al.*, 2012). Computational techniques, such as discriminate analysis (e.g. support vector machine (SVM)) are extensively used in toxicogenomics research (Rätsch *et al.*, 2006). Although machine learning makes it possible to build a high-performance predictive model, it sometimes leads to over-fitting. Furthermore, machine learning does little to facilitate interpretation of the mechanism of action, because it does not give added weight to each gene. Therefore, I have applied a logistic ridge regression model, which helps identify epidemiological risk factors, in order to identify genes important for liver hypertrophy and hypertrophic hepatocarcinogenesis, and to develop a predictive model for discriminating carcinogenic liver hypertrophy from adaptive one.

4.2 Materials and Methods

4.2.1 Data selection and compound classification.

Data resources.

DNA microarray data (Affymetrix Rat Genome 230 2.0 Arrays) for all compounds were gathered from the Toxicogenomics Project-Genomics Assisted Toxicity Evaluation System (TG-GATEs), a toxicogenomic database developed in Japan. This database contains microarray data of *in vitro* and *in vivo* experiments, clinical and pathological examination results for rat single- and repeated-dose toxicity tests of 170 compounds (Igarashi *et al.*, 2015). The repeated-dose toxicity test data consists of 4 time points (days 4, 8, 15 and 29) and 3 administration doses (low, middle and high). In the present study microarray data of 134 compounds at high dose which were obtained from 28-day repeated-dose toxicity tests was used.

Classification of selected TG-GATEs compounds.

The compounds used in the present study are summarized in Table 4.1. Using data on liver

weight and liver hypertrophy histopathological examination from TG-GATEs and Open TG-GATEs (http://toxico.nibiohn.go.jp/english/index.html), the compounds were categorized as liver hypertrophic if they met either of the following criteria: (1) The increase in the weight of the liver compared to the total body weight was greater than 1.2-fold, with a p value of < 0.05 in the Student's t-test for at least one dose at one time point, and (2) Centrilobular hypertrophy or hepatocyte hypertrophy was observed for liver histopathology in more than 3 animals at the same time point and dose. The 62 compounds that satisfied either of these criteria were classified as liver hypertrophic compounds (HC), and the remaining 72 compounds were classified as liver non-hypertrophic compounds (NHC). Compounds known to be liver hypertrophic, such as omeprazole, phenobarbital, and clofibrate (Hall *et al.*, 2012; Maronpot *et al.*, 2010) were correctly classified using this method.

To investigate the mechanism of hypertrophic hepatocarcinogenesis, HC were further classified according to their carcinogenicity in rodent livers and their mutagenicity status, which were obtained from the Carcinogenic Potency Database (CPDB), the Toxicology Data Network (TOXNET), and relevant studies (Gusenleitner *et al.*, 2014; Römer *et al.*, 2014; Uehara *et al.*, 2011). Compounds lacking carcinogenicity information were categorized as unknown. Thus, 27 hypertrophic non-carcinogens (HNCCs) and the 15 hypertrophic carcinogens (HCCs)) were selected from 62 HC for the analysis of hypertrophic carcinogenesis–related genes. In order to focus on the mechanism of non-genotoxic carcinogenesis, compounds known as genotoxic carcinogens (coumarin, isoniazid and methylene dianiline) were excluded from HCC (Table 4.1).

Table 4.1. Compounds used in this study.

Data obtained from Japan's Toxicogenomics Project-Genomics Assisted Toxicity Evaluation System database.

Liver hypertrophic compounds (HC)* (62)	
Carcinogens (18)	
Genotoxic carcinogens	Coumarin (CMA), Isoniazid (INAH), Methylene Dianiline (DAPM)
Non-genotoxic Carcinogens* (HCC) (15)	Acetaminophen (APAP), Carbamazepine (CBZ), Carbon Tetrachloride (CCL4), Clofibrate (CFB), Ethinylestradiol (EE), Fenofibrate (FFB), Gemfibrozil (GFZ), Hexachlorobenzene (HCB), Methapyrilene (MP), Omeprazole (OPZ), Phenobarbital

	(PB), Rifampicin (RIF), Simvastatin (SST), Thioacetamide (TAA), Wy-14643 (WY)
Non-carcinogens* (HNCC) (27)	Amiodarone (AM), Aspirin (ASA), Bendazac (BDZ), Benzbromarone (BBr), Benziodarone (BZD), Bromoethylamine (BEA), Butylated Hydroxyanisole (BHA), Caffeine (CAF), Chloramphenicol (CMP), Chlorpropamide (CPP), Danazol (DNZ), Diazepam (DZP), Diltiazem (DIL), Disulfiram (DSF), Erythromycin Ethylsuccinate (EME), Ethambutol (EBU), Ketoconazole (KC), Methimazole (MTZ), Methyltestosterone (MTS), Mexile tine (MEX), Phenacetin (PCT), Phenylbutazone (PhB), Phenytoin (PHE), Propylthiouracil (PTU), Quinidine (QND), Tolbutamide (TLB), Trimethadione (TMD)
Unknown (17)	1% Cholesterol + 0.25% Sodium Cholate (CH+DS-Na)†, 2,4-Dinitrophenol (DNP), Amitriptyline (AMT), Bromobenzene (BBZ), Chlormezanone (CMN), Chlorpheniramine (CHL), Dantrolene (DTL), Fluoxetine Hydrochloride (FLX), Flutamide (FT), Hydroxyzine (HYZ), Imipramine (IMI), Nimesulide (NIM), Papaverine (PAP), Promethazine (PMZ), Tamoxifen (TMX), Terbinafine (TBF), Ticlopidine (TCP)

Liver non-hypertrophic compounds* (NHC) (72)	
Carcinogens (5)	
Genotoxic carcinogens	Acetamidofluorene (AAF), Lomustine (LS)
Non-genotoxic carcinogens	Acetamide (AAA), Ethanol (ETN), Ethionine (ET)
Non-carcinogens (57)	Acarbose (ACA), Acetazolamide (ACZ), Allopurinol (APL), Allyl alcohol (AA), Azathioprine (AZP), Captopril (CAP), Cephalothin (CLT), Chlormadinone (CLM), Chlorpromazine (CPZ), Cimetidine (CIM), Ciprofloxacin (CPX), Cisplatin (CSP), Clomipramine (CPM), Colchicine (COL), Cyclophosphamide (CPA), Cyclosporine A (CSA), Diclofenac (DFNa), Disopyramide (DIS), Doxorubicin (DOX), Enalapril (ENA), Famotidine (FAM), Fluphenazine (FP), Furosemide (FUR), Gentamicin (GMC), Glibenclamide (GBC), Griseofulvin (GF), Haloperidol (HPL),

	Ibuprofen (IBU), Iproniazid (IPA), Mefenamic Acid (MEF), Metformin (MFM), Methyldopa (MDP), Moxisylyte (MXS), Naphthyl Isothiocyanate (ANIT), Nicotinic Acid (NIC), Nifedipine (NIF), Nitrofurantoin (NFT), Nitrofurazone (NFZ), Pemoline (PML), Penicillamine (PEN), Perhexiline (PH), Phenylanthranilic Acid (NPAA), Propranolol (PPL), Ranitidine (RAN), Rosiglitazone Maleate (RGZ), Rotenone (ROT), Sulfasalazine (SS), Sulindac (SUL), Sulpiride (SLP),Tannic Acid (TAN), Tetracycline (TC), Theophylline (TEO), Thioridazine (TRZ), Tiopronin (TIO), Triamterene (TRI), Valproic Acid (VPA), Vitamin A (VA)
Unknown (10)	Adapin (ADP), Ajmaline (AJM), Amphotericin B (AMB), Bucetin (BCT), Carboplatin (CBP), Desmopressin Acetate (DDAVP), Etoposide (ETP), Labetalol (LBT), Tacrine (TAC), Triazolam (TZM)

* The microarray data of HC, NHC, HNCC, and HCC were analyzed in the present study.

† This mixture is classified as a chemicals in the present study.

4.2.2 Identification of differentially expressed genes associated with liver hypertrophy and hypertrophic carcinogenesis

A matrix of 134 compounds and 26,468 probes (filtered from the initial 31,099 probes by 50% absolute value and 20% PA (Present/Absent) call filters), was derived using data from TG-GATEs. The value of each cell in the matrix was the fold change on a base 2 logarithmic scale. To identify the liver hypertrophy and hypertrophic hepatocarcinogenesis–related genes, we conducted a two-step screening to identify differentially expressed genes (DEGs). First, the Mann-Whitney *U* test was conducted to extract DEGs for liver hypertrophy to compare the median values of the 72 HCs and the 62 NHCs for each gene probe. Probes that had a *p*-value of less than 0.05 and a median absolute fold change greater than 0.5 were selected as DEGs related to liver hypertrophy. Then DEGs related to hypertrophic hepatocarcinogenesis were selected from the DEGs related to liver hypertrophy in the same manner to compare gene expression between the 27 HNCCs and the 15 HCCs.

4.2.3 Development of a predictive model for liver hypertrophy and hypertrophic hepato-carcinogenesis via the selection of important genes from among the DEGs.

Determination of gene importance using logistic ridge regression analysis

Logistic ridge regression was employed to identify important genes from among the DEGs in order to develop predictive models for hypertrophy and hypertrophic carcinogenicity.

Regression coefficients that are widely used in epidemiology to identify risk factors were used as an indicator of the importance (contribution) of a gene to liver hypertrophy and hypertrophic hepatocarcinogenesis. The independent variables are the fold change of the probes, and the dependent variable was whether the compound was liver hypertrophic or hypertrophic hepatocarcinogenic. To suppress over-learning, L2 regularization was employed and the hyperparameter was optimized with a 5-fold cross-validation.

The importance of a gene (I_g) was evaluated using the following equations:

$$\text{logit}(P) = \sum_g a_g x_g \,, \qquad (1)$$

$$\alpha_g = \text{abs}(a_g)\,, \qquad \sigma_g = std(x_g)\,, \qquad \text{and} \qquad (2)$$

$$I_g = \frac{\alpha_g \sigma_g}{\sum_{g'} \alpha_{g'} \sigma_{g'}}\,. \qquad (3)$$

Equation (1) is the model definition of logistic regression. P is the predicted probability that a particular compound is liver hypertrophic or hypertrophic hepatocarcinogenic, a_g is the regression coefficient, and x_g is the fold change of gene expression. Equation (2) defines some auxiliary variables: α_g is the absolute value of the regression coefficient, and σ_g is the standard deviation of x_g. The regression coefficient can be interpreted as how much the corresponding variable (gene) affects the decision surface. Multiplying with the standard deviation and normalizing as equation (3), the intrinsic volatility of the gene is removed and substantial gene importance is obtained. We will use the word probability to refer P in equation (1) hereafter.

Selection of predictive models and important genes

The DEGs of liver hypertrophy and hypertrophic hepatocarcinogenesis in the selected compounds were sorted by gene importance. Subsequently, the DEG lists were used to select the minimum number of important genes needed to build a predictive model with maximum performance using accuracy (acc), meaning the ratio of correctly predicted results, and the harmonic mean of precision and sensitivity (f1), calculated with a 10-fold cross-validation in logistic ridge regression.

The acc and f1 are defined as

$$\text{acc} = \frac{TP + TN}{TP + TN + FP + FN} \quad and$$

$$\text{f1} = \frac{2TP}{2TP + FP + FN}\,,$$

where *TP*, *TN*, *FP*, and *FN* are true positive, true negative, false positive, and false negative, respectively. Positive and negative means present and absence of chemical characteristics

in toxicology (liver hypertrophy inducible or hypertrophic carcinogenicity). For example, true positive indicate that the number of positive chemicals which correctly evaluated. In theory, the important genes derived from these models should be involved in the core mechanism of liver hypertrophy and hypertrophic hepatocarcinogenesis.

4.2.4 Interpretation and biological relevance of selected important genes.

Pathway analysis

Ingenuity Pathway Analysis (IPA) software (Ingenuity Systems, Redwood City, CA, USA) was used to elucidate the pathways involved in liver hypertrophy and hypertrophic hepatocarcinogenesis for selected genes.

Comparison of the fold changes of genes important for liver hypertrophy and hypertrophic hepatocarcinogenesis

To further elucidate the differences between adaptive liver hypertrophy and hypertrophic hepatocarcinogenesis, we compared the fold changes of selected important genes (35 genes for liver hypertrophy and 13 genes for hypertrophic hepatocarcinogenesis between NHCs and HCs, as well as HNCCs and HCCs. The median fold change ratios of all important genes between NHC and HC were plotted on the Y-axis, and the ratios between HNCCs and HCCs were plotted on the X-axis.

4.2.5 Probability of liver hypertrophy and hypertrophic hepatocarcinogenicity of TG-GATEs compounds.

To examine the usefulness of logistic ridge regression in the identification of important genes and the construction of high-performing predictive models, we analyzed whether these scores reflect the magnitude of liver hypertrophy and tumors observed in repeated-dose toxicity studies with rodents.

4.3 Results

4.3.1 Selection of important genes and development of predictive models for liver hypertrophy and hypertrophic hepatocarcinogenesis

A total of 193 DEGs related to liver hypertrophy and 29 DEGs related to hypertrophic hepatocarcinogenesis were identified using Mann-Whitney *U* test. These DEGs were used to build liver hypertrophy and hypertrophic hepatocarcinogenesis predictive models with different gene numbers (Figure 4.1). We found that 50 probes, sorted by an importance order, were needed to achieve maximum performance for the prediction of liver hypertrophy. A similar pattern was observed for the prediction of hypertrophic hepatocarcinogenesis, requiring fewer

probes (15 probes) and achieving better performance. Furthermore, among the 50 probes from our optimal liver hypertrophy prediction model, 35 identified were known genes. The coefficient, importance, p value, and median fold change for these genes are summarized in Table 2. Metabolism-related genes including *Acot1*, *Abcc3*, *Cyp2b1/2*, non-metabolism-related genes including *Gpr155*, and *Stac3* were identified as the important liver hypertrophy-related genes with higher importance. Thirteen known genes were identified from the 15 probes used in the hypertrophic hepatocarcinogenesis model (Table 4.3). Amino acid synthesis–related genes *Asns*, *Oat*, and *Phgdh*, oxidative stress-related gene *Gpx2*, and cell death and proliferation related genes *Cgref1*, *Cidea*, *Esm1* were included.

4.3.2 Mechanisms of liver hypertrophy and hypertrophic hepatocarcinogenesis using pathway analysis of important genes

The major pathways involved in liver hypertrophy and hypertrophic hepatocarcinogenesis were identified by canonical and upstream-regulator pathway analysis of the 35 genes identified as important genes in the liver hypertrophy model (Table 4.2) and the 13 genes derived as important from the hypertrophic hepatocarcinogenesis model (Table 4.3). Xenobiotic metabolism and degradation, LPS/IL-1 mediated inhibition of RXR function, and nuclear receptor activation were identified as major canonical pathways of liver hypertrophy (Table 4.4). Similarly, amino acid biosynthesis and degradation (metabolism), and glutathione redox reactions were indicated for hypertrophic hepatocarcinogenesis (Table 4.4). With regard to the oxidative stress response, HIF1α signaling and the NRF-2 mediated pathway were also suggested. In the upstream-regulator pathway analysis, the well-known nuclear receptors and inflammatory cytokines were suggested as the common upstream regulators of liver hypertrophy and hypertrophic hepatocarcinogenesis (liver hypertrophy: AHR, CAR, PXR, PPAR, IFNG (interferon-γ), and IL (interleukin)-1 and IL-6; hypertrophic carcinogenesis: PPAR, IFNG and IL-5) (Figure 2).

4.3.3 The features of liver hypertrophy and hypertrophic hepatocarcinogenesis important genes

The median fold change ratios of important genes in liver hypertrophy and hypertrophic hepatocarcinogenesis between NHCs and HCs were compared with those between HNCCs and HCCs (Figure 4.3). The fold changes of most of the liver hypertrophy-important genes (e.g., *Abcc3, Cyp1a1, Cyp1b1* and *Akr7a3*) by HCs were different from those by NHCs, whereas little difference was found between HNCCs and HCCs. In contrast, the fold changes of the hypertrophic carcinogenesis–important genes (e.g., *Stac3, Gpx2*) were

significantly different between HNCCs and HCCs. These results suggest that two kinds of mechanisms are involved in liver hypertrophy. One is for adaptive response that is common to all HCs including HNCCs and HCCs, and the other is for adverse effects associated with carcinogenesis that was observed only with HCCs but not HNCCs.

4.3.4 Probabilities calculated from the identified important genes.

The probabilities of liver hypertrophy and carcinogenicity were calculated for 102 compounds using the best predictive models and data from TG-GATEs (Figure 4.4). The probability values are on a scale ranging from 0 to 1, and the values greater than 0.5 were considered positive. All HCs were predicted correctly with the optimized liver hypertrophy prediction model. For hypertrophic hepatocarcinogenesis, HNCCs and HCCs were well-separated, except for 5 compounds (BBr, PB, APAP, SST and RIF) that had probabilities of approximately 0.5.

4.4 Discussion

The present study is the first to use a toxicogenomic approach to elucidate the relationship between liver hypertrophy and hypertrophic hepatocarcinogenesis. Three major findings have been obtained:

1. Drug-metabolizing enzyme-related genes previously reported as liver hypertrophy-related showed little relevance to carcinogenesis.
2. Thirteen novel genes, including *Asns*, *Gpx2* and *Tox3*, which are considered to be involved in both liver hypertrophy and hypertrophic hepatocarcinogenesis, were identified.
3. The logistic ridge regression approach appears to be useful for identifying toxicity-related genes and developing a mechanism-based, high-performance predictive model.

The identified important genes for liver hypertrophy include drug-metabolizing enzymes that are known to be hepatic hypertrophy–related (e.g. *Cyp1a1, Cyp2b1/2*). However, no significant differences in the fold changes of these genes were observed between HNCs and HCCs, indicating that these genes have little direct association to hepatocarcinogenesis. Interestingly, the other metabolism-related genes, *aldh1b1, akr7a3* and *abcc3,* which have been reported as carcinogenicity-related, (Zúñiga-García *et al.*, 2015; Singh *et al.*, 2015; Ahmed *et al.*, 2011), were not considered as hypertrophic hepatocarcinogenesis related in the present analysis. Thus, as several prior studies indicated (Maronpot *et al.*, 2010; Hall *et al.*, 2012), liver hypertrophy accompanied by enzyme induction do not necessarily have direct relevance to hepatocarcinogenesis.

We newly identified 13 important genes for hypertrophic carcinogenesis (Table 4.3). Canonical pathway analysis of the 13 genes suggested that amino acid biosynthesis and

oxidative responses would be involved in the hypertrophic carcinogenesis. First, amino acid synthesis–related genes, *Asns*, *Oat*, and *Phgdh*, were included as protein metabolism-related genes. *Asns* (asparagine synthetase) is reported to be up-regulated in cancer tissues and cells (Li *et al.*, 2014; Yu *et al.*, 2016) and would be associated with damage to hepatocytes and the proliferation of hepatocellular carcinoma (Zhang et al. 2013). *Phgdh* (phosphoglycerate degydrogenase) and *Oat* (ornithine aminotransferase) were also reported to be associated with hepatocellular carcinoma (Zogg *et al.*, 2014; Zigmond *et al.*, 2015). Therefore, amino acid biosynthesis considered the key mechanism of hypertrophic hepatocarcinogenesis. Second, oxidative stress-related gene identified, *Gpx2* (glutathione peroxidase 2), is known for its role in preventing inflammation-mediated carcinogenesis (Brigelius-Flohé and Kipp, 2012), and is highly expressed in hepatocellular carcinomas with inflammation (Suzuki *et al.*, 2013). Moreover, *Tox3* (TOX high mobility group box family member 3) was included in 13 genes and it is known as immune-related genes. Therefore, oxidative stress accompanied by inflammation would not be irrelevant to hypertrophic hepatocarcinogenesis.

Although it was not suggested in the canonical pathway analysis, 13 genes contained cell death and proliferation related genes, *Cgref1* (cell growth regulator with EF hand domain 1), *Cidea* (cell death-inducing DFFA-like effector A), and *Esm1* (endothelial cell-specific molecule1). Since these genes suggested to be involving the process to carcinogenesis (Deng *et al.*, 2015; Laurencikiene *et al.*, 2008; Sheth *et al.*, 2006), cell death and proliferation may be important mechanism of hepatocarcinogenesis. In the remained genes, whereas *zdhhc2*, *Snx10* (sorting nexin 10), and *egln3* (EGL nine homolog 3) have been reported to be associated with cancer (Peng et al., 2014; Fu and Taubman, 2013; You et al., 2016; Yu and Li, 2015), and *Stac3* (SH3 and cysteine rich domain 3) and *Spin-2* (similar to Spindlin-like protein 2) were the first to be indicated the association with carcinogenesis. Further study is needed to clarify the relevance between these genes and hepatocarcinogenesis.

In terms of the median fold change, the expression levels of *stac3* and *Acot1* (acyl-CoA thioesterase 1) were significantly different between HNCC and HCC (Table 4.3 and Figure 4.3), though *Acot1* was omitted because the p-value was slightly deviated from the criteria (p-value: 0.066). These two genes have been reported to be a common gene in liver hypertrophy (Gusenleitner, Scott S Auerbach, *et al.*, 2014), and also identified to be important for liver hypertrophy in the present study (Table 4.2). Although the relationship between *Stac3* and hepatocarcinogenesis has not been studied, *Acot1* is a target gene of PPARα, which is well known as its rule for liver proliferation and tumorigenesis (Peters *et al.*, 1997; Konstandi *et al.*, 2013). Our results suggest these two genes may play critical roles in hypertrophic hepatocarcinogenesis.

Furthermore, upstream-regulatory pathway analysis suggests that liver hypertrophy and

hypertrophic hepatocarcinogenesis are similarly regulated by nuclear receptors and inflammatory cytokines and that several upstream genes such as those encoding IFN-γ, PPARα, PPARγ and RXRα are involved in both liver hypertrophy and hypertrophic hepatocarcinogenesis (Figure 4.2). Therefore, although the same upstream regulators are activated, downstream target genes are different between adverse (carcinogenic) liver hypertrophy and adaptive hypertrophy, indicating the analysis of the expression levels of the 13 genes identified is important to discriminate these two types of liver hypertrophy. Further investigation on the hepatic expression of these proteins and the reverse genetic approach verification are necessary in future studies.

We used logistic regression analysis to elucidate the relationship between gene expression and toxicity quantitatively. Non-linear algorithms such as kernel SVM and Random Forest gives weight to the achievement of high accuracy for classification rather than the elucidation of explanatory-variable contribution. These algorithms generally do not directly output the relation between objective variables and explanatory variables. On the other hand, logistic regression is a linear classification model which directly gives the relation between objective and explanatory variables in the form of regression coefficient, thus the selected gene markers are considered to have robustness. Furthermore, we employed an L-type regularization method to reduce over-fitting in logistic regression. Recently, several regression models based on sparsity have been developed to improve the disadvantages of the stepwise method using Akaike information criterion (AIC). The lasso regression model using L1 regularization (Tibshirani. R, 1996), which can set more coefficients to “0”, is considered to be a good model to reduce Type I error (false positive rate). However, since important genes with different mechanisms may be excluded by multicollinearity problems when there are highly correlated among the extracted genes, lasso regression has serious limitations in toxicogenomics research for deciphering mode of action. In contrast, the ridge regression model based on the L2 regularization (Hoerl and Kennard, 2000) improves the multicollinearity problem with missing the important genes. It however leads to an increase in Type I error. Therefore, we eliminated irrelevant genes by finding the optimal number of important genes, which gives maximized accuracy for prediction, from the importance-ordered gene list. Thereby, we have achieved a high accuracy model using the minimum number of genes, which might correspond to core mechanisms.

In contrast to other discriminant analyses, logistic regression has an advantage to calculate the probability, which is considered to be useful for risk assessment. Indeed, the degrees of liver-weight increase or hepatocellular hypertrophy for the compounds with low probability in liver hypertrophy analysis were low (data not shown). In the prediction of

hypertrophic hepatocarcinogenesis, 5 compounds (APAP, PB, RIF, SST, and BBr) were not predicted correctly. However, the degrees of the liver tumors of these compounds were weak or not clear. For instance, the liver tumors by RIF was only observed in mice but not in rats, suggesting that it is difficult to correctly predict since the microarray data used was from the experiments with rats. PB has different results in CPDB, positive in phenobarbital sodium but negative in phenobarbital, and the probability in our predictive model is 0.49, approximately to 0.5. Moreover, BBr had controversial information on carcinogenicity in the relevant literatures (Gusenleitner et al., 2014; Römer et al., 2014; Schulte-Hermann et al., 1980). Therefore, the probabilities obtained from the models developed here appear to reflect the results of animal experiments.

The present study showed that the genes that varied significantly between HCs and HCCs were not only associated with adaptive response but also contributed to liver carcinogenesis. These findings are consistent with the consensus that liver hypertrophy accompanied by the induction of drug-metabolizing enzymes is an adaptive reaction (Maronpot *et al.*, 2010), and support the fact mentioned in 3rd ESTP (Hall *et al.*, 2012) that prolonged liver hypertrophy occasionally resulted in liver tumors. In the present study, we succeeded to discriminate adverse liver hypertrophy, which leads to hepatocarcinogenesis, from adaptive hypertrophy, by the characterization of gene expression data in rat 28-day repeated dose toxicity studies. While further investigations are needed, the identified genes could be used as new biomarkers for hypertrophic hepatocarcinogenesis by using quantitative PCR and/or immunohistochemical examination.

4.5 Conclusions

The present study showed that the genes that varied significantly between HCs and HCCs were not only associated with adaptive response but also contributed to liver carcinogenesis. These findings are consistent with the consensus that liver hypertrophy accompanied by the induction of drug-metabolizing enzymes is an adaptive reaction (Maronpot *et al.*, 2010), and support the fact mentioned in 3rd ESTP (Hall *et al.*, 2012) that prolonged liver hypertrophy occasionally resulted in liver tumors. In the present study, we succeeded to discriminate adverse liver hypertrophy, which leads to hepatocarcinogenesis, from adaptive hypertrophy, by the characterization of gene expression data in rat 28-day repeated dose toxicity studies. While further investigations are needed, the identified genes could be used as new biomarkers for hypertrophic hepatocarcinogenesis by using quantitative PCR and/or immunohistochemical examination.

In conclusion, we have applied logistic ridge regression to identify important genes for liver hypertrophy and hypertrophic hepatocarcinogenesis and developed predictive models that can

be used for discriminating adaptive liver hypertrophy from hypertrophic hepatocarcinogenesis. Our findings revealed different modes of action involved in liver hypertrophy, providing a mechanistic explanation for the processes from liver hypertrophy to tumors. Thus, we believe that the identified genes and the constructed predictive models are useful for evaluating the carcinogenicity of liver hypertrophy-inducing compounds.

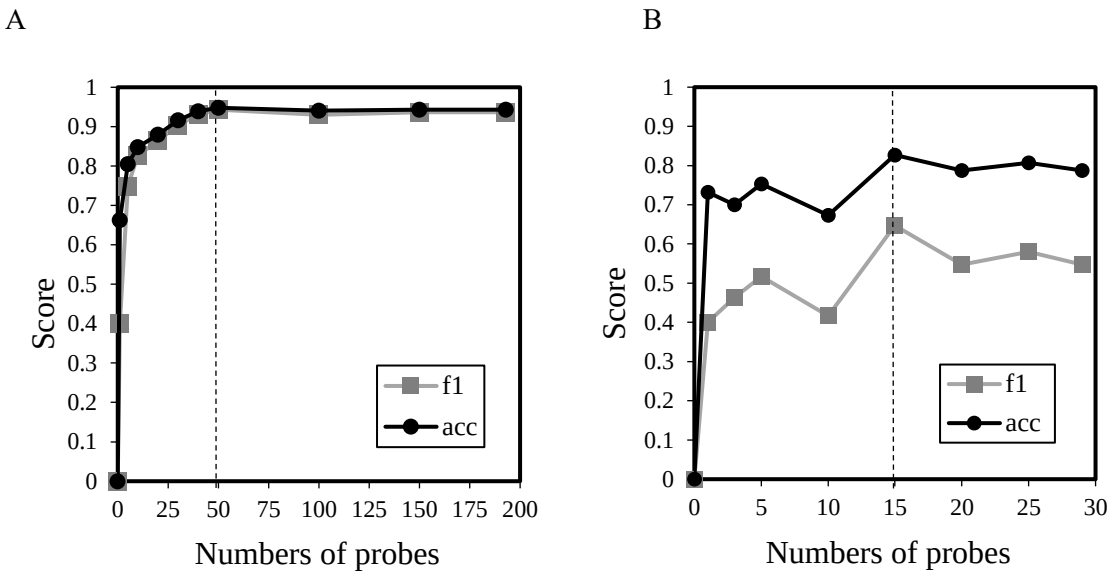

Figure 4.1. Prediction performance for predicting hypertrophy and hypertrophic carcinogenicity with different number of the genes identified. (A) Prediction performance of the extracted 193 differentially expressed genes in liver hypertrophic compounds. (B) Prediction performance of extracted 29 differentially expressed genes in hypertrophic hepatocarcinogens. The prediction accuracy (acc) and the harmonic mean of precision and sensitivity score (f1) in both prediction models were plotted in the different numbers of probes sorted in an importance order. Dashed lines indicate the minimum number of probes that provided the maximum performances.

Table 4.2. List of 35 genes identified as important for liver hypertrophy.

Affymetrix probe IDs, gene symbols, coefficients, and importance of selected genes calculated by logistic regression analysis, *p* values, median fold changes obtained by Mann-Whitney *U* test are summarized.

Probe ID	Gene symbol	Gene name	Coef	Importance	*p* value	Fold change (median)
1398250_at	*Acot1*	acyl-CoA thioesterase 1	0.082	0.020	<0.001	0.906
1369698_at	*Abcc3*	ATP binding cassette subfamily C member 3	0.101	0.018	<0.001	2.695
1385715_at	*Gpr155*	G protein-coupled receptor 155	-0.138	0.015	<0.001	-0.985
1395403_at	*Stac3*	SH3 and cysteine rich domain 3	0.093	0.015	0.001	-0.823
1371076_at	*Cyp2b1/2*	cytochrome P450 family 2 subfamily b, polypetide1/// cytochrome P450 family 2 subfamily b, polypetide2	0.119	0.014	<0.001	1.727
1379034_at	*Loc102554789*	uncharacterized LOC102554789	-0.135	0.014	<0.001	-0.834
1392943_at	*Mboat2*	membrane bound O-acyltransferase domain containing 2	0.111	0.014	0.004	0.962
1370491_a_at	*Hdc*	histidine decarboxylase	0.087	0.013	0.001	0.678
1369509_a_at	*A1bg*	alpha-1-B glycoprotein	-0.096	0.013	0.002	-0.753
1370233_at	*Fgf12*	fibroblast growth factor 12	0.142	0.013	0.001	0.583
1397266_at	*Klf11*	Kruppel-like factor 11	0.121	0.012	0.012	0.702
1397590_at	*Myo1b*	myosin IB	0.122	0.012	0.045	0.559
1379747_at	*Prss35*	protease, serine 35	0.105	0.012	0.026	0.522
1378451_at	*Cyba*	cytochrome b-245 alpha chain	-0.114	0.011	0.002	-0.553
1386047_at	*Galnt13*	polypeptide N-acetylgalactosaminyltransferase 13	0.106	0.011	0.004	0.787
1392041_at	*RGD1565959*	RGD1565959	-0.109	0.011	0.008	-0.539
1396832_at	*Kb15*	keratin 90	-0.117	0.010	0.045	-0.531
1376702_at	*Mlc1*	megalencephalic leukoencephalopathy with subcortical cysts 1	0.061	0.010	0.048	-0.951
1368935_at	*Camk2a*	calcium/calmodulin dependent protein kinase II alpha	0.092	0.010	0.010	0.707
1388272_at	*Igh-6*	immunoglobulin heavy chain 6	-0.099	0.009	0.005	-0.634
1383472_at	*Aldh1b1*	aldehyde dehydrogenase 1 family member B1	-0.100	0.009	<0.001	-0.931
1387902_a_at	*Igkc*	immunoglobulin kappa constant	-0.099	0.009	<0.001	-0.743
1382696_at	*Dscam*	Down syndrome cell adhesion molecule	0.092	0.009	0.029	0.677

1370269_at	*Cyp1a1*	cytochrome P450 family 1 subfamily a member 1	0.041	0.009	0.001	2.068
1394483_at	*Adamts5*	ADAM metallopeptidase with thrombospondin type 1 motif 5	0.075	0.009	<0.001	0.559
1394920_at	*Dapk2*	death-associated protein kinase 2	0.076	0.008	0.033	0.744
1369832_at	*Adam3a*	a disintegrin and metallopeptidase domain 3 (cyritestin)	-0.114	0.008	<0.001	-0.702
1367703_at	*Crygd*	crystallin gamma D	-0.091	0.008	0.042	-0.504
1379928_at	*Cops3*	COP9 signalosome subunit 3	0.109	0.008	0.001	0.514
1396035_at	*Rpesp*	somatomedin B and thrombospondin type 1 domain containing	0.090	0.008	<0.001	1.073
1398651_at	*Loc102551017*	uncharacterized LOC102551017	0.073	0.008	0.014	0.566
1373436_at	*Rgd136739*	chromosome 10 open reading frame 107	0.078	0.008	<0.001	0.878
1389854_at	*Nr1h2*	nuclear receptor subfamily 1 group H member 2	-0.082	0.007	0.009	-0.633
1370394_at	*IgG-2a*	gamma-2a immunoglobulin heavy chain	-0.079	0.007	0.007	-0.561
1368121_at	*Akr7a3*	aldo-keto reductase family 7, member A3 (aflatoxin aldehyde reductase)	0.083	0.007	<0.001	1.247

Table 4.3. List of 13 genes identified as important for hypertrophic hepatocarcinogenesis.

Affymetrix probe IDs, gene symbols, coefficients, and importance of selected genes calculated by logistic regression analysis, *p* values, and median fold changes obtained by Mann-Whitney *U* test are summarized.

Probe ID	Gene symbol	Gene name	Coef	Importance	*p* value	Fold change (median)
1387925_at	*Asns*	asparagine synthetase	-0.223	0.072	0.026	1.668
1374070_at	*Gpx2*	glutathione peroxidase 2	0.176	0.069	0.006	2.111
1382579_at	*Tox3*	TOX high mobility group box family member 3	0.191	0.064	0.041	0.641
1367811_at	*Phgdh*	phosphoglycerate dehydrogenase	0.161	0.056	<0.001	2.008
1370361_at	*Cgref1*	cell growth regulator with EF hand domain 1	0.185	0.050	0.021	1.331
1389179_at	*Cidea*	cell death-inducing DFFA-like effector a	0.192	0.048	0.004	1.225
1368078_at	*Esm1*	endothelial cell-specific molecule 1	0.171	0.044	0.018	0.941
1384274_at	*LOC367746*	similar to Spindlin-like protein 2 (SPIN-2)	-0.107	0.044	0.007	-1.246
1395403_at	*Stac3*	SH3 and cysteine rich domain 3	0.086	0.041	0.004	-3.061
1383585_s_at	*Snx10*	sorting nexin 10	0.158	0.039	<0.001	1.999
1367729_at	*Oat*	ornithine aminotransferase (gyrate atrophy)	-0.185	0.039	0.001	-0.692
1368174_at	*Egln3*	EGL nine homolog 3 (C. elegans)	0.199	0.039	<0.001	1.054
1370828_at	*Zdhhc2*	zinc finger, DHHC-type containing 2	0.241	0.035	<0.001	0.886

Table 4.4. Canonical pathway analysis of liver hypertrophy and hypertrophic hepatocarcinogenesis important genes.

Canonical pathways of 35 genes important for liver hypertrophy and those of 13 genes important for hypertrophic hepatocarcinogenesis, which were suggested by IPA, are summarized. –log (*p* value) represents statistical significance for canonical pathway based on –log (*p* value) > 1.3 (equal to *p* value < 0.05). Genes represent the genes whose expressions were increased or decreased in each pathway.

Ingenuity canonical pathways	-log (*p* value)	Genes
Hypertrophy–important genes		
Xenobiotic metabolism signaling	4.06	*Aldh1b1, Cyp1a1, Camk2a, Cyp2b1, Abcc3*
LPS/IL-1 mediated inhibition of RXR function	3.29	*Aldh1b1, Nr1h2, Cyp2b1, Abcc3*
Bupropion degradation	3.01	*Cyp1a1, Cyp2b1*
Acetone degradation I	2.97	*Cyp1a1, Cyp2b1*
Histamine biosynthesis	2.67	*Hdc*
Estrogen biosynthesis	2.63	*Cyp1a1, Cyp2b1*
Nicotine degradation III	2.49	*Cyp1a1, Cyp2b1*
Melatonin degradation I	2.47	*Cyp1a1, Cyp2b1*
Superpathway of melatonin degradation	2.39	*Cyp1a1, Cyp2b1*
Nicotine degradation II	2.37	*Cyp1a1, Cyp2b1*
PXR/RXR activation	2.17	*Cyp2b1, Abcc3*
LXR/RXR Activation	1.74	*Nr1h2,a1bg*
Methylglyoxal Degradation III	1.64	*Akr7a3*
Aryl Hydrocarbon Receptor Signaling	1.53	*Aldh1b1,Cyp1a1*
CDP-diacylglycerol Biosynthesis I	1.5	*Mboat2*
Hypertrophic carcinogenicity important genes		
Asparagine biosynthesis I	3.01	*Asns*
Arginine degradation I (arginase pathway)	2.40	*Oat*
Arginine biosynthesis IV	2.31	*Oat*
Proline biosynthesis II (from arginine)	2.31	*Oat*
Serine biosynthesis	2.31	*Phgdh*
Arginine degradation VI (arginase 2 pathway)	2.31	*Oat*
Superpathway of serine and glycine biosynthesis I	2.16	*Phgdh*
Citrulline biosynthesis	2.10	*Oat*
Superpathway of Citrulline Metabolism	1.86	*Oat*
Glutathione Redox Reactions I	1.78	*Gpx2*

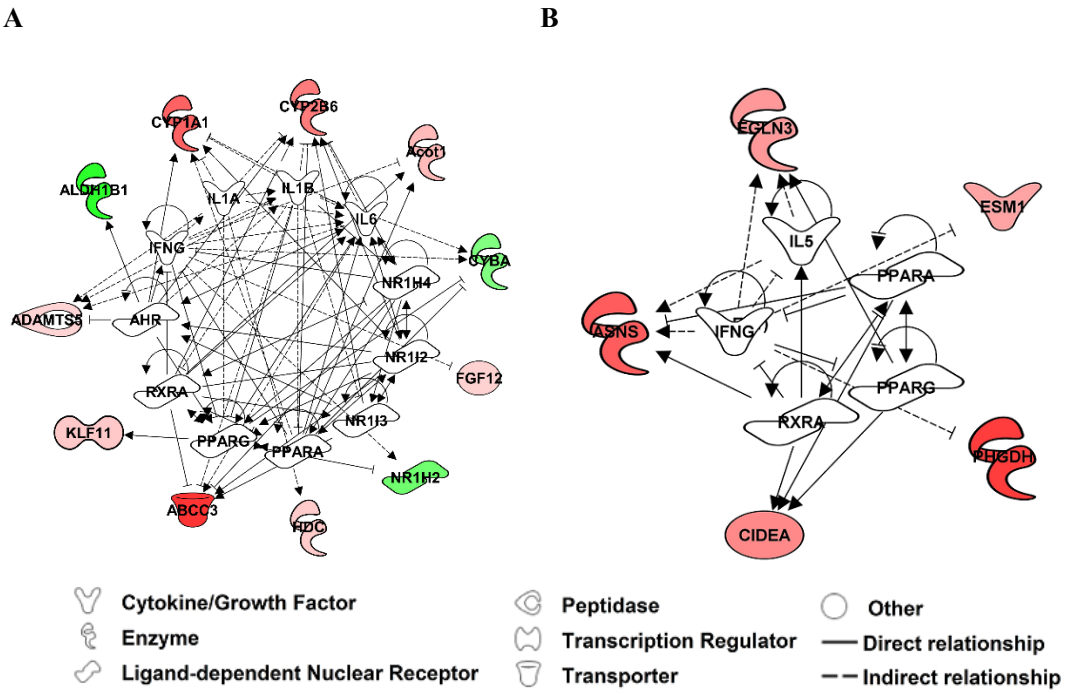

Figure 4. 2. Upstream regulator pathway analysis of liver hypertrophy and hypertrophic hepatocarcinogenesis-important genes. The results of analyses of 35 liver hypertrophy-important genes (A) 35 hypertrophic non-carcinogenic important genes and (B) 13 hypertrophic hepatocarcinogenesis-important genes are shown. Red and green symbols represent up-regulated and down-regulated molecules (genes), respectively. Molecules incorporated into the network are shown in white. Transcription regulators, cytokines, kinases, transporters, and enzymes are shown as different shapes. Arrows and lines indicate the direct interaction between two molecules, and dashed arrows and lines indicated indirect interactions. The gene symbols are described in Tables 4.2 and 4.3.

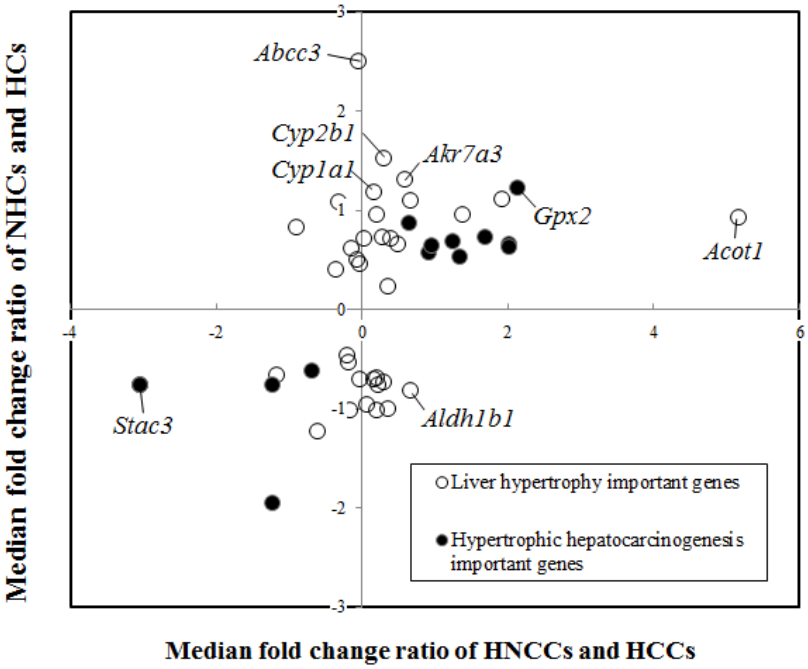

Figure 4. 3. Comparison of the fold changes of liver hypertrophy- and hypertrophic carcinogenesis- important genes. The median fold change ratios of important genes obtained by Mann-Whitney U test between hypertrophic non-carcinogens (HNCCs) and hypertrophic carcinogens (HCCs) and those between non-hypertrophy compounds (NHCs) and hypertrophic compounds (HCs were plotted on the X-axis and Y-axis, respectively. The plots close to the X-axis indicate little difference between NHCs and HCs, and the plots close to the Y-axis indicated little difference between HNCCs and HCCs. The plots in the regions between X- and Y- axes indicate the contribution to both hypertrophy and hypertrophic carcinogenesis. The gene symbols are described in Tables 4.2 and 4.3.

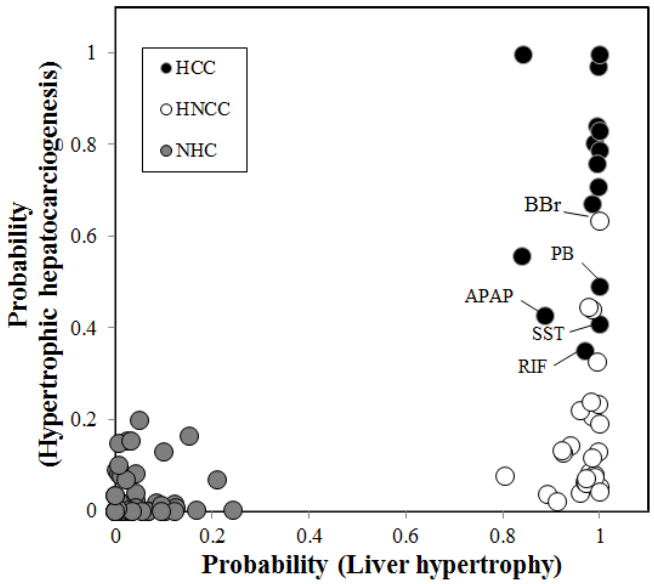

Figure 4. 4. Comparison of the probabilities for non-hypertrophic compounds (NHCs, hypertrophic non-carcinogens (HNCCs) and hypertrophic carcinogens (HCCs). Probabilities were calculated from the logistic regression equation using the prediction model developed in the present study. The probability of liver hypertrophy was calculated by the predictive model based on the 35 hypertrophy-important genes. The probability of carcinogenicity was calculated by the predictive model based on the 13 hypertrophic hepatocarcinogenesis-important genes. The probability values are on a scale ranging from 0 to 1. The compound abbreviations are described in Table 4.1.

Chapter 5: Investigation and Technological Development in Chemical-Induced Reproductive and Developmental Toxicity

5.1 Introduction

The teratogenic potential, or teratogenicity, is evaluated and assessed by developmental toxicity tests. Recently the growing number of produced chemicals demands their evaluation and assessment with high-throughput and greater accuracy. Although mammals such as rodents and rabbits have been traditionally used for the tests, current trends toward the 3R principles (Replacement, Reduction and Refinement) and saving resources have encouraged the development of alternative teratogenicity testing methods (Strähle *et al.*, 2012). To develop an alternative testing strategy for teratogenicity, we definitely need an adverse outcome pathway (AOP) framework which would improve prediction including cross-species extrapolation, and contribute to human health risk assessment. Therefore, a central issue is identification of AOPs that are relays of sequential events with a causal relationship at different levels of biological response leading to a toxic effect (Ankley et al., 2010; Villeneuve *et al.*, 2014; Tollefsen *et al.*, 2014; Burden *et al.*, 2015; Knapen *et al.*, 2015). On the other hand, Craniofacial anomalies comprise over one-third of all congenital birth defects and over 700 disorders are associated with craniofacial features (https://www.ncbi.nlm.nih.gov/omim). These anomalies are thought to be caused by genetic and environmental factors, including pharmaceuticals and chemical agents, during embryonic development (Poswillo, 1988; Edison and Muenke, 2003; Beaty *et al.*, 2016; Yoon *et al.*, 2016). In the present study, we focus on the mechanism of chemical-induced craniofacial anomalies, and aim to develop an AOP based alternative method for developmental toxicity evaluation.

In the last decade, zebrafish has been considered as a promising model of an alternative method of teratogenicity testing (He *et al.*, 2014; Yamashita *et al.*, 2014; Nishimura *et al.*, 2016; Bambino and Chu, 2017; Teixidó *et al.*, 2019). Zebrafish has several experimental advantages for high-throughput genetic and chemical screening, including evolutionarily conserved developmental programs, various tools for genetic manipulation and rapid external development during the embryonic stage. Accumulating evidence has indicated that the zebrafish model has a high predictive ability for teratogenicity (Brannen *et al.*, 2010; Selderslaghs *et al.*, 2012; Augustine-Rauch *et al.*, 2016; Inoue *et al.*, 2016). Thus, the zebrafish model enables us to describe an AOP of developmental anomalies precisely and develop alternative methods for evaluating teratogenicity based on the AOP.

Here we treated zebrafish embryos with 12 pharmaceuticals (retinoic acid, methotrexate, salicylic acid, valproic acid, caffeine, warfarin, hydroxyurea, dexamethasone, phenytoin, imatinib, boric acid, and thalidomide) which are recognized to be teratogens in mammals. We confirmed that the craniofacial anomalies those teratogens are associated with defects in neural crest cells (NCCs) and their derivatives. Furthermore, these craniofacial anomalies phenocopied neurocristopathy which is a pathology in human caused by the defects in development, migration, or differentiation of neural crest

cells (Liu *et al.*, 2020; Narumi *et al.*, 2020). These results strongly suggest that the AOP of craniofacial teratogenicity is conserved between zebrafish and mammals. Thus, we hypothesized that the developmental process of NCCs would include key events for describing the AOP of teratogenicity. To examine the behavior of NCCs, visualization of these cells with a genetic marker is crucial. *sox10* has been characterized as a common neural crest marker in vertebrates, including mammals and fish (Southard-Smith *et al.*, 1998; Aoki *et al.*, 2003; Meulemans and Bronner-Fraser, 2004; McKeown *et al.*, 2005; Carney *et al.*, 2006; Simões-Costa and Bronner, 2015). Thus, we expected that we can monitor NCC development with transgenic zebrafish lines expressing a fluorescent protein driven by the *sox10* promoter.

We next developed a series of transgenic zebrafish lines, *sox10:EGFP*, *sox10:EGFP-CAAX* and *sox10:Dendra2*, which visualize NCCs. In these lines, the fluorescence demarcated cranial neural crest cells (CNCCs), which migrate from the neural tube along the stereotypical pathway to form the first pharyngeal arch (PA1) and differentiate into craniofacial cartilages such as the ethmoid plate (zebrafish palate) and upper and lower jaws. We administered teratogens known to cause craniofacial anomalies in mammals to the transgenic embryos, and examined the teratogenic effect on CNCC development and craniofacial development. All of the teratogens induced craniofacial anomalies such as cleft palate and micrognathia at 96 hpf, as highlighted by the EGFP fluorescence. We further found that impaired migration of CNCCs and PA1 formation during the first 24 hours of development are the early major phenotypes associated these later craniofacial anomalies. Considering that zebrafish embryos around these developmental stages have similar morphological and molecular characteristics compared to mammalian embryos, we postulate that the CNCC migration period is critical for inducing craniofacial anomalies across vertebrates. Based on these results, we propose the AOP of craniofacial anomalies centered by CNCC development. Furthermore, *sox10* transgenic lines are ideal for an AOP-based teratogenicity model for evaluating and predicting craniofacial anomalies.

5.2 Materials and Methods

5.2.1 Zebrafish strain and maintenance

The zebrafish (Danio rerio) strain RIKEN WT (RW), *Tg*(*-5.0sox10:EGFP*), *Tg*(*-5.0sox10:EGFP-CAAX*) and *Tg*(*-5.0sox10:Dendra2*) (RW background) were maintained with a 14-h light/10-h dark cycle. The water temperature was kept at 28°C ± 1°C and water quality conditions were maintained according to the Zebrafish Book (Westerfield, 2000) and the Guide for the Care and Use of Laboratory Animals 8th edition (National Research Council ., 2011).

5.2.2 Transgenesis

The Tol2 transposon system was used for the transgenesis(Suster *et al.*, 2009). The promotor region of *sox10* was isolated from RW strain. The promoter region located in the genome 5.0

kb upstream from the translation initiation site was amplified by PCR. The isolated promoter region and EGFP, EGFP-CAAX or Dendra2 were cloned into pT2AL200R150G by In-Fusion cloning (Takara) to load a transposon cassette according to the manufacturer's protocol. For Tol2 transposase synthesis, pCS-zT2TP was linearized by Not I restriction enzyme (Takara) and Tol2 transposase mRNA was synthesized using the mMESSAGE mMACHINE SP6 Transcription Kit (Invitrogen). Each transposon construct and Tol2 transposase mRNA were co-injected at the one-cell embryo stage.

5.2.3 Test chemicals

The test chemicals used in this study are listed in Table 5.1. Before embryo exposure experiments, a dose range-finding study was performed at the highest concentration of 1 mM in E3 medium or at the highest soluble concentration above which a precipitate was observed. The highest concentration at which embryos were viable was used in the exposure experiments, with a common dilution ratio of a stock solution into E3 medium of 2 or 3.

5.2.4 Egg production and embryo exposure

Adult male and female zebrafish (4–10 months after fertilization) were placed in a breeding tank with a separator in the late afternoon of the day before spawning. The separator was removed in the morning and spawning was stimulated when the light was turned on. Fertilized eggs were collected within 1 h after removal of the separator. The eggs were incubated in E3 medium (5 mM NaCl, 0.17 mM KCl, 0.33 mM $CaCl_2$, 0.33 mM MgSO4, 0.1 mM NaOH) at 28°C and exposed to test compounds at 4 hpf. The exposure medium was replaced daily and samples were collected from the 5-6 somite stage until 96 hpf.

5.2.5 Morphological observation and quantification

Morphological changes in the eyes, otic vesicle, and heart were observed under a stereomicroscope at 96 hpf. To quantify the size of the eyes and otic vesicle, images were captured with a Leica M80 camera equipped with a DFC450C lens (Leica). Then, images were analyzed using ImageJ (National Institutes of Health). Heart rate was analyzed using movies made with bright-field microscopy, and the number of heart beats in a 10-s window were recorded.

5.2.6 Real-time quantitative RT-qPCR analysis

Thirty zebrafish embryos at 48 hpf were homogenized in TRIzol reagent (Invitrogen). Total RNA was purified with an RNeasy Mini Kit (Qiagen) according to the manufacturer's protocol. The purified RNA with an absorbance ratio of 1.8–2.0 at A260/280 was used for further analysis.

Total RNA (1.5 μg) was used for reverse transcription using the SuperScript III first-strand synthesis system (Thermo Fisher Scientific). RT-qPCR was performed with 5-fold diluted complementary DNA, Taqman Master Mix (Thermo Fisher Scientific), TaqMan probes, and gene-specific primers (Bio-Rad) using the 7500 Fast Real-Time PCR System. The housekeeping gene *glyceraldehyde-3-phosphate dehydrogenase* (*GAPDH*) was used as an internal control. The gene-specific primers were as follows: *tfap2a*, *zic2a1*, *pax3a*, *dlx5a*, *sox9a*, *sox10*, *snail2a*, and *col2a1* primers. The expression levels of target genes were normalized by the *GAPDH* expression level, and the normalized relative gene expression was calculated using the comparative Ct ($2^{-\Delta\Delta Ct}$) method. All reactions were performed in triplicate.

5.2.7 Cartilage staining and chondrocyte measurement

Zebrafish embryos were fixed at 96 hpf with 4% paraformaldehyde in phosphate-buffered saline for 2 h. After the samples were washed with 100 mM Tris (pH 7.5), they were treated with 100 mM Tris (pH 7.5) containing 25 mM $MgCl_2$ for 30 min. Then, samples were transferred into a 0.05% Alcian blue (MP Biomedicals) dissolved in 80% ethanol (EtOH), 100 mM Tris (pH 7.5), and 25 mM $MgCl_2$ overnight. Next, the stained samples were placed in 80% EtOH containing 100 mM Tris (pH 7.5) and 25 mM $MgCl_2$ and then gradually rehydrated by incubating with 50% and 25% EtOH in 100 mM Tris (pH 7.5) for 30 min per step. Samples were washed with potassium hydroxide (KOH) for 30 min and processed to remove pigmentation by bleaching in 3% hydrogen peroxide and 0.1% KOH for 30 min. Then, samples were rinsed with 35% saturated sodium borate decahydrate ($NaBO_4$) for 30 min. For clearing, the samples were treated with 1% trypsin (Wako) dissolved in 35% saturated $NaBO_4$ for 30 min and then washed with 0.5% KOH overnight. All procedures were performed at room temperature.

After cartilage staining, samples were transferred into 100% glycerol. The craniofacial structure was disassembled into the neurocranium and viscerocranium using fine forceps. Each structure was mounted on a glass slide, and the mounted samples were covered with glass coverslips and pressed to prepare flat-mount samples. For preparation of flat-mounted samples, the stained samples were placed on a glass slide and were slowly covered with a cover slip placed by using forceps to minimize the generation of air bubbles. Glycerol was added to fill the space between the coverslip and the glass slide. Photographs were then taken using a BZ-710 microscope (Keyence). The number of chondrocytes in the ethmoid plate of the neurocranium and Meckel's cartilage of the viscerocranium was counted. For length and width measurements, more than 60 chondrocytes were measured using ImageJ. All measurements were performed in triplicate.

5.2.8 Immunofluorescence staining and fluorescence imaging

Immunofluorescence staining was performed as described (Narumi *et al.*, 2020), with minor modifications. Zebrafish embryos were fixed with 4% paraformaldehyde in phosphate-buffered saline (PBS) (Wako) at the 10 somite stage (ss), 20 ss, 24 hpf, and 96 hpf, and then treated with 100% ice-cold methanol (Wako) to achieve dehydration and kept at −20°C for longer storage. The fixed embryos except those being sampled at 96 hpf were permeabilized with 1% Triton X-100 (Cayman Chemical) in PBS (Invitrogen) for more than 1 h before blocking with 3% bovine serum albumin (BSA, Wako) in PBS-T (PBS containing 0.1% Triton X-100), while the 96 hpf samples were prepared by following Narumi et al., 2020. After the blocking with 3% BSA in PBS-T for 2 h, the samples were incubated with mouse anti-GFP (1/1000, Invitrogen: AB_221568; or 1/1000, EMD Millipore: MAB3580), mouse anti-dendra2 (1/500, Thermo Fisher Scientific: TA180094), mouse anti-collagen type II (anti-coll2, 1/100, DSHB: AB_528165), rabbit anti-active caspase3 (1/1000, BD Pharmingen: 559565), and rabbit anti-phospho-histone H3 (Ser10) (1/1000, EMD Millipore: 06-570) primary antibody or PNA lectin conjugated with Alexa Fluor 488 (1/1000, Thermo) overnight at 4°C. The samples were washed six times with PBS-T for 15 min, and stained with the following secondary antibodies: Alexa Fluor 488-goat anti-mouse, Alexa Fluor 568-goat anti-mouse or 568-goat anti-rabbit, or Alexa Fluor 647-goat anti-mouse secondary antibodies (1/1000, Life Technologies), and DAPI solution (1/1000, DOJINDO) overnight at 4°C. After the samples were then washed six times with PBS-T for 15 min, they were embedded in 1% low-melting agarose and mounted on a 35-mm non-coated glass-bottom dish (Matsunami). For live imaging, the samples were anesthetized with 0.02% MS-222 (Sigma-Aldrich) and embedded in 1% low-melting agarose (Sigma-Aldrich) containing 0.02% MS-222 on the glass bottom dish. All immunofluorescence images were acquired using a Zeiss LSM880 or LSM800 system equipped with Zeiss ZEN black or blue software. All procedures were performed at room temperature unless otherwise specified.

For time-lapse imaging, samples were pretreated with valproic acid (30 μM) for 30 min. prior to sample embedding. The samples were anesthetized with 0.02% MS-222 and embedded in 1% low-melting agarose containing 0.02% MS-222 and the teratogens on a four-chambered glass bottom dish (Greiner). Subsequently, the E3 medium containing MS-222 and teratogens at the same concentrations as above was additionally applied onto the samples.

5.2.9 Lineage Tracing

For lineage tracing of NCCs, *Tg(-5.0sox10:Dendra2)* was used. The samples were anesthetized with 0.02% MS-222 and embedded in 1% low-melting agarose containing 0.02% MS-222. To photoconvert the frontonasal region, maxillary region and mandibular region in

Tg(-5.0sox10:Dendra2) at 10 ss and 24 hpf, each ROI (region of interest) was selected using ZEN blue software on a Zeiss LSM800 confocal microscope and exposed to 10% UV (405 nm) laser for 30 seconds. Successful photolabeling was confirmed by specific photoconversion of Dendra2 from green to red in each ROI.

5.2.10 Quantification of CNCC migration, proliferation and apoptosis

To quantitatively assess the migration of cranial neural crest cells (CNCCs), we measured the linear distance between the midbrain-hindbrain boundary (MHB) and the anterior border of the CNCC population migrating via the frontonasal pathway at 10 ss (for details, see Figure 5.10) using Fiji measurement plugin (National Institutes of Health). To quantify mitotic CNCCs, we counted the number of the cells that displayed positive signals for both pH3 and EGFP anterior to the MHB at 10 ss (magenta region in Figure 5.12 A A') or within the first pharyngeal arch (PA1) at 24 hpf. Similarly, for quantifying apoptotic CNCCs, we counted the number of the cells that displayed double-positive signals for both active-Caspase 3 and EGFP in the same regions as above. In both experiments, we used z-stack images obtained by confocal microscopy and counted the number of mitotic and apoptotic cells distributed on the left side of the embryos.

5.2.11 Statistical analysis

Statistical analyses were performed using Microsoft Excel, and boxplot graphs were made using RStudio (RStudio Inc.). Multiple comparison tests were performed using Graph Pad Prism version 8 software for Windows (La Jolla). *P*-values were calculated with an unpaired Student's *t*-test with Welch's correction for unequal population standard deviations. P-values < 0.05 were considered statistically significant. For the quantification of the migration distance of the pH3- or Active Cas3-positive cranial neural crest cells, P-values were calculated using a one-way ANOVA followed by Dunnett's multiple comparison tests. P-values < 0.05 were considered statistically significant. All data are presented as the mean ± SD unless otherwise specified.

5.3 Results

5.3.1 Teratogen exposure induced abnormal craniofacial development in zebrafish

To investigate the effects of teratogens on zebrafish craniofacial development, embryos were exposed to the 12 teratogens listed in Table 5.1. These teratogens are known to induce craniofacial defects such as cleft palate, micrognathia, ear anomalies and eye defects in mammals. Morphological changes of the embryos at 96 hpf were examined in the head, eyes and otic vesicles (Figure 5.1). Although embryos treated with five chemicals (RA, MTX, SA,

CAF and HU) displayed gross morphological defects, embryos treated with the other chemicals showed only minor phenotypes due to the embryos' transparency (Figure 5.1B–O). Therefore, for better visualization of the cranial structure and its phenotype, cartilage staining with Alcian blue was performed (Figure 5.2). The cartilaginous head skeleton was clearly visualized at 96 hpf and consisted of two prominent subdivisions, which were the neurocranium composed of the ethmoid plate, trabeculae and parachordal, and the viscerocranium composed of the pharyngeal skeleton, such as Meckel's cartilage, palatoquadrate, ceratobranchial, and ceratohyal (Figure 5.2 A). No phenotypic differences were detected between E3 control and DMSO as vehicle control (Figure 5.2 B, C). Specific defects in the viscerocranium and the neurocranium were clearly detected in embryos treated with each of the teratogens tested (Figure 5.2 D–O). RA-, MTX-, SA-, and VPA-treated embryos displayed severe defects in the neurocranium and the viscerocranium (Figure 5.2 D–G). In these embryos, deformities of the craniofacial skeleton were marked by the absence or shortening of the skeletal elements in the viscerocranium and malformation of the ethmoid plate, which consisted of a fused (RA treatment) or separated (MTX, SA and VPA treatment) ethmoid plate (Figure 5.2 D–G). CAF-, WAF-, HU-, and DEX-treated embryos showed moderate phenotypes, such as shortening of Meckel's cartilage and a separate or short ethmoid plate (Figure 5.2 H–K). PHT-, IM-, BA-, and THA-treated embryos showed slight changes in both the neurocranium and the viscerocranium (Figure 5.2 L–O). In these embryos, the anteroposterior length of the ethmoid plate and trabeculae and the width of the parachordal were shorter than those in the control group. Clear differences in palatoquadrate, hyosymplectic, ceratohyal, and ceratobranchial cartilages were not detected; however, shortened Meckel's cartilage was observed in these embryos (Figure 5.2 L–O). These morphological defects were quantified and summarized in Figure 5.2P. The dimensions of the morphological changes found in the head structure were greater than those of the changes in overall size of the embryos (Figure 5.2Q).

Based on these observations, we speculated that the ethmoid plate and trabeculae in the neurocranium and Meckel's cartilage in the viscerocranium had sensitive responses to the teratogens. To test this, we then performed quantitative analysis of both the neurocranium cartilages and Meckel's cartilage (Figure 5.3). For the neurocranium analyses, the anteroposterior length of the ethmoid plate and trabeculae were measured and the width was measured from one side of the parachordal to the other (Figure 5.3A). The average neurocranium length in the teratogen-treated embryos was significantly decreased compared to that in control embryos (Figure 5.3B). Also, the average width of the neurocranium in the teratogen-treated embryos was significantly decreased (Figure 5.3C). These analyses suggested that all of these teratogens affected neurocranium morphogenesis, resulting in smaller neurocranium phenotypes. Likewise, the length and width of the Meckel's cartilage in the

viscerocranium were quantified (Figure 5.3D–F). The length was measured from the anterior edge of the Meckel's cartilage midline to the tip of the retroarticular, and the width was defined as the distance between the opposing retroarticulars (Figure 5.3D). The average length of the Meckel's cartilage was significantly decreased by treatment with each of the teratogens except HU, IM, BA and THA (Figure 5.3E). The average width of the Meckel's cartilage was decreased significantly by treatment with each of the teratogens (Figure 5.3F).

Thus, the sizes of the neurocranium and viscerocranium were significantly decreased by treatment with the teratogens. All of the teratogens induced small jaw (micrognathia) and small head (microcephaly), and large jaw or head or hyperplasia of the craniofacial skeleton was not observed. Together, our data suggested that the teratogens affected the craniofacial development, leading to craniofacial malformation. The ethmoid plate, trabeculae and Meckel's cartilage consist of chondrocytes, which originate from neural crest cells(Mork and Crump, 2015; Szabo-Rogers *et al.*, 2010), and therefore our findings suggest that the development of neural crest cells was disrupted by these teratogens.

5.3.2 Teratogen-induced craniofacial malformations were caused by decreased chondrocyte proliferation, and by disturbed chondrocyte maturation and differentiation

We next examined at the cellular level how the malformation of the ethmoid plate and Meckel's cartilage was induced by teratogen treatment. Morphogenesis of the ethmoid plate and Meckel's cartilage is mediated by the convergence and integration of facial prominences, followed by elongation with cell proliferation(Dougherty *et al.*, 2012; Kamel *et al.*, 2013) In addition to cell proliferation, chondrocyte shaping and stacking are required for proper formation and function of the craniofacial cartilage. We analyzed which of these steps were influenced by teratogen treatment, focusing on the morphology of the ethmoid plate and Meckel's cartilage, and the number of chondrocytes and their morphology (Figure 5.4, 5.5).

The morphology of the ethmoid plate was disturbed by teratogen treatment (Figure 5.3B, C, Figure 5.4C–N). RA-treated embryos displayed an ethmoid plate with a rod-like shape (Figure 5.4C). MTX-, SA-, VPA-, CAF-, WAF-, HU-, DEX-, PHT-, IM- and THA-treated embryos showed a clefting or rough edge of the anterior ethmoid plate (Figure 5.4 D–L, N). A prominent morphological defect in the ethmoid plate was not observed in BA-treated embryos (Figure 5.4M). Mature chondrocytes showed an elongated shape and stacking on each other to form linear columns at 96 hpf in control embryos (Figure 5.4A', B'). In teratogen-treated embryos, chondrocytes showed atypical morphology and lost the stacked structure (Figure 5.4C' –N'). Rounded chondrocytes were observed in RA-, MTX-, SA-, DEX- and THA-treated embryos (Figure 5.4 C' –E', J', N'). In VPA-, CAF- and IM-treated embryos, chondrocytes showed

decreased size (Figure 5.4F, F', G, G', L, L'). In WAF-treated embryos, chondrocytes showed increased size compared to the control group (Figure 5.4H'). HU-, PHT-, and BA-treated embryos exhibited smaller chondrocytes with rounded morphology (Figure 5.4I, I', K, K', M, M').

To obtain quantitative results, the number of chondrocytes in the anterior half of the neurocranium (the ethmoid plate and the trabeculae) was counted and the length/width ratio and the orientation of each chondrocyte in the ethmoid plate was measured (Figure 5.4 O–R). The number of chondrocytes was significantly decreased by all of the teratogen treatments, whereas no significant changes were observed in the vehicle control (Figure 5.4P). In order to quantify the disturbance of chondrocyte morphology, the length/width ratio and the orientation of the longest cell axis were measured (Figure 5.4Q, R). The average ratio was greater than 2 in the control and vehicle control, while the average ratio in all teratogen-treated groups was significantly decreased (Figure 5.4Q). The chondrocyte stacking was also significantly disturbed by all of the teratogen treatments (Figure 5.4R). Thus, the morphological anomalies of the neurocranium induced by teratogen treatment were caused by both a decreased number of chondrocytes and a morphological defect of the chondrocytes.

The same analyses were performed for the Meckel's cartilage in the viscerocranium (Figure 5.5). The Meckel's cartilage had an inverse U shape in control and vehicle control (Figure 5.5A, B). After teratogen treatment, the morphology of the Meckel's cartilage was changed and its size was decreased (Figure 5.3E, F, Figure 5.5 C–N). Mature chondrocytes were elongated and stacked on each other to form a columnar structure at 96 hpf in control and vehicle control (Figure 5.5A', B'). Rounded chondrocytes and a lack of stacked structure were observed in the teratogen-treated embryos (Figure 5.5 C' –N'). In order to obtain quantitative results, the number of chondrocytes in half of the Meckel's cartilage was counted and the length/width ratio and the orientation of the chondrocytes was measured (Figure 5.5 O–R). The number of chondrocytes in the Meckel's cartilage was significantly decreased in all treatment groups; however no statistical difference was observed between the control and the vehicle control groups (Figure 5.5P). The average length/width ratio was greater than 4 in the control and vehicle control (Figure 5.5Q). The average length/width ratio was significantly decreased in all treatment groups (Figure 5.5Q). The chondrocyte stacking in the Meckel's cartilage was also disturbed significantly by all of the teratogen treatments (Figure 5.5R). Thus, morphological anomalies of the viscerocranium induced by the teratogens were caused by both a decreased number of chondrocytes and morphological defects of the chondrocytes.

Taken together, these results indicated that craniofacial malformation induced by the teratogens was due to defects of not only chondrocyte proliferation (decreased cell number) but also chondrocyte maturation and differentiation (altered chondrocyte shape and stacking).

These results also led us to speculate that the development of the CNCCs) ce was perturbed by teratogen treatment.

5.3.3 The expression of CNC-related genes was perturbed in chemical-induced craniofacial malformation

We next investigated whether the observed phenotypes of craniofacial structures and chondrocytes were due to the disruption of CNC development. The expression of CNC-related genes was analyzed by RT-qPCR. For this, we selected eight genes, which were classified into three categories during CNC development: border specification gene markers (*tfap2a*, *zic2a1*, *pax3a* and *dlx5a*), migrating gene markers (*sox9a*, *sox10* and *snail2a*) and differentiated cell marker (*col2a1*) (Figure 5.6). After teratogen treatment, samples were collected at 48 hpf to examine the effect on the CNC development. The expression level of *tfap2a* was significantly decreased in RA-, MTX-, SA-, VPA-, WAF-, HU-, DEX-, IM- and BA-treated embryos (Figure 5.6A). Other neural crest border specifying genes, *pax3a*, *zic2a1*, and *dlx5a*, also showed similar effects as *tfap2a*. The expression level of *zic2a1* was significantly decreased in RA-, MTX-, SA-, CAF-, WAF-, HU-, DEX-, IM-, and THA-treated embryos (Figure 5.6B). The expression level of *pax3a* was significantly decreased in SA-, VPA-, CAF-, WAF-, HU- and PHT-treated embryos, whereas it was increased 1.8 fold in RA-treated embryos (Figure 5.6C). The expression of *dlx5a* was significantly decreased in RA-, MTA-, SA-, VPA-, CAF-, WAF-, HU-, DEX-, PHT- and BA-treated embryos (Figure 5.6D). We also examined the expression levels of several migrating CNC marker genes, namely, *sox9a*, and *sox10* and *snail2a* (Figure 5.6 E–G). The expression level of *sox9a* was decreased significantly by treatment with all teratogens except PHT and THA (Figure 5.6E). The expression level of *sox10* was also decreased significantly in SA-, VPA-, CAF-, WAF-, HU- and PHT-treated embryos, whereas it was increased significantly in RA- and MTX-treated embryos (Figure 5.6F). The expression level of *snail2a* was significantly decreased in all teratogen-treated embryos (Figure 5.6G). The expression of *col2a1* a chondrocyte differentiation marker, was significantly decreased in RA-, MTX-, SA-, VPA-, CAF-, WAF-, HU-, DEX-, PHT-, IM- and BA-treated embryos (Figure 5.6H). In THA-treated embryos, the expression level of *col2a1* was not significantly decreased, although a tendency to decrease was observed. The strength of the effect on the expression levels of the CNC genes observed corresponded to the severity of the phenotypic defect. RA-, MTX-, SA-, and VPA-treated embryos exhibited absence of cranial structures (Figure 5.2 D–G). In contrast, PHT-, IM-, BA- and THA-treated embryos showed minor phenotypes of the ethmoid plate and the Meckel's cartilage, and weaker disturbances of the gene expression levels (Figure5.2 H–K).

5.3.4 *sox10* reporter lines visualize the developmental process of neural crest cells

Thus, we hypothesized that the developmental process of NCCs would include key events for describing the AOP of teratogenicity, and then we monitor NCC development with transgenic zebrafish lines expressing a fluorescent protein driven by the sox10 promoter. To visualize the developmental process of NCCs in zebrafish, we generated *Tg(-5.0sox10:EGFP), Tg(-5.0sox10:EGFP-CAAX)* and *Tg(-5.0sox10:Dendra2)* (referred to as *sox10:EGFP, sox10:EGFP-CAAX* and *sox10:Dendra2*, respectively) lines using the Tol2 transposon system (Figure 5.7A, Table 5.2). EGFP expression was detected as early as the 5–6 somite stage (ss) in premigratory and migratory NCCs by live imaging (Figure 5.7B, B'). At the 10–21 ss, the fluorescence highlighted cranial NCCs (CNCCs), which migrated from the anterior midbrain and hindbrain to the pharyngeal pouches via the frontonasal pathway (black arrows) and maxillary pathway (blue arrows), respectively (Figure 5.7C–E'). The migratory CNCCs via the frontonasal pathway reached the ventral side of the eye at around the 21 ss (Figure 5.7E' black arrow). The migratory CNCCs expressing EGFP reached the ventral side of the pouches and began to form the pharyngeal arches at 24 hpf (Figure 5.7F, F'). The first pharyngeal arches (PA1), which give rise to a large part of the craniofacial bones, were EGFP-positive at this stage (Figure 5.7F'). The migratory CNCCs via the frontonasal pathway moved toward the PA1 (Figure 5.7F' black arrow). *sox10:EGFP* continuously visualized the developmental process of CNCCs and craniofacial morphogenesis from 48 to 96 hpf (Figure 5.7G–I'). The EGFP-expressing CNCCs were present in the developing craniofacial skeletal primordium; trabeculae (developing lateral part of the ethmoid plate), median element (developing medial part of the ethmoid plate) derived from frontonasal process, and Meckel's cartilage (lower jaw) at 48 hpf (Figure 5.7G, G'). At this stage, the EGFP-expressing CNCCs were also present in olfactory placodes and gonadotropin-releasing hormone cells (Figure 5.7G, G'). The skeletal primordium differentiated into the ethmoid plate (zebrafish palate) consisting of the trabeculae and median elements and Meckel's cartilage at 72 hpf (Figure 5.7H, H'). These structures grew and each skeletal element was firmly formed at 96 hpf (Figure 5.7I, I').

Based on live-imaging observations, the developmental processes of CNCCs can be roughly classified into three periods: the migration period (Figure 5.7B–E), PA1 formation period (Figure 5.7F) and outgrowth period (Figure 5.7G–I). Collectively, these results show that our *sox10:EGFP* line demarcates all the CNCC populations reported so far(Carney *et al.*, 2006) and thus can visualize the entire processes of CNCC development throughout embryogenesis. Other transgenic lines, *sox10:EGFP-CAAX* and *sox10:Dendra2*, labeled the same population of cells as *sox10:EGFP* during development (Table 5.2, Figure S3).

Next, we examined whether these lines are useful for detecting craniofacial anomalies (Figure 5.8). For this, we tested them with five teratogens (valproic acid (VPA), warfarin (WAF), salicylic acid (SA), caffeine (CAF) and methotrexate (MTX)). These teratogens are known to

cause craniofacial defects in mammals and zebrafish(Liu *et al.*, 2020; Narumi *et al.*, 2020). To visualize cartilage, we immuno- stained treated embryos using both an anti-coll2 antibody and PNA lectin, which recapitulates Alcian blue staining (Figure 5.8 A–C), and compared the fluorescence pattern with EGFP expression pattern. All five teratogens induced craniofacial defects in cartilage at 96 hpf, such as cleft palate and small jaws (micrognathia), as reported in our previous studies (Figure 5.8 D–I; Liu *et al.*, 2020; Narumi *et al.*, 2020). The craniofacial anomalies showed similar patterns among the teratogens; however, the phenotypic severity was dependent on the teratogen. Importantly, the EGFP patterns mostly overlapped with the cartilage staining in treated embryos, and thus these defects were also detected by EGFP expression (Figure 5.8 D'–I").

Taken together, our results show that *sox10:EGFP* can visualize the anomalies of the craniofacial structure as precisely as the conventional cartilage staining. The same craniofacial defects were observed in *sox10:EGFP-CAAX* and *sox10:Dendra2* embryos (Figure S4, S5). Remarkably, the transgenic lines have a great advantage that every key event of CNCC development in an individual embryo can be traced by live imaging, starting from the emergence of CNCCs, which is essential to identify AOPs. Using these transgenic lines, we will describe possible key events for the CNCC-related AOP.

5.3.5 Inhibitory effect of the teratogens on neural crest cell migration

Our previous study suggested that craniofacial defects induced by teratogens are consequences of their adverse effects on CNCC development (Liu et al., 2020; Narumi et al., 2020). To elucidate the key events that trigger craniofacial malformation, we focused on the earliest phase of CNCC development, when the cartilages are yet to be formed. We focused on the migration period and analyzed the effects of the teratogens on migratory CNCCs by live imaging of *sox10:EGFP* embryos at 10 ss. In control embryos, CNCCs migrated from the midbrain and anterior hindbrain region at 10 ss toward the dorsal side to the eye along the frontonasal pathway or toward the pharyngeal region along the maxillary pathway. However, CNCC migration via both pathways was inhibited by all five teratogens tested (Figure 5.9 B–F'). To quantify inhibition of cell migration, we focused on the CNCCs migrating via the frontonasal pathway and measured the distance between the midbrain-hindbrain boundary (MHB, yellow arrowheads in Figure 5.9) and the anterior border of the migratory CNCCs (white arrowheads in Figure 5.9). The migration distance of migratory CNCCs was significantly reduced in the teratogen-treated groups (Figure 5.9G). Furthermore, all teratogens exhibited dose-dependency in their inhibitory effects on CNCC migration (Figure S6 A–E). Indeed, time-lapse imaging of zebrafish embryos treated with a higher dose of VPA, as an example, revealed a pronounced inhibition of CNCC migration (Liu et al 2023, supplementary). Interestingly,

there was a correlation between the extent of the inhibitory effect on migration and the morphological severity of craniofacial anomalies, i.e. cleft palate and micrognathia, at 96 hpf (Figure 5.8 D–I''). Regarding MTX treatment, however, the migration phenotype was milder compared to the morphological phenotype, especially for micrognathia, at 96 hpf (Figure 5.8 I–I'') (Liu et al., 2020).

We have previously reported that the expression level of *sox10* was disturbed by teratogen exposure, as determined by RT-PCR analysis (Liu et al., 2020). Consistently, as shown in Appendix figure S6, the EGFP signal tends to decrease as the concentration of teratogens increase. In spite of this, the intensity of the fluorescence signals at high-dose concentrations was sufficient enough for us to investigate CNCC behavior. These results suggest that a defect in CNCC migration is the earliest key event caused by the teratogens and that this inhibitory effect on CNCC migration account for disruption of or abnormal CNCC development in the later events.

5.3.6 Developmental fate of the CNCCs in the PA1 and frontonasal prominence

Most of the above affected migratory CNCCs are known to colonize the PA1 under normal conditions. To relate the migratory defects with late craniofacial anomalies, we examined the fate of CNCCs in the PA1 NCCs at later stages by lineage tracing. For this, we utilized a *sox10:Dendra2* transgenic line (Figure 5.10A, Figure S3 C–D'). The photoconvertible fluorescent protein Dendra2 irreversibly changes color from green to red upon photoactivation by UV light (405 nm), and thus a specific CNCC population can be labeled and traced chronologically (Figure 5.10A).

We first labeled the maxillary prominence of the PA1 at 24 hpf and analyzed their descendants at 48 and 72 hpf (Figure 5.10 B–B'''). The maxillary prominence eventually became the lateral part of the palate (trabeculae) and pterygoid process (upper jaw) (Figure 5.10B'''). Next, we performed the same analysis for the mandibular prominence of the PA1 (Figure 5.10 C–C'''). The mandibular prominence differentiated into the Meckel's cartilage (lower jaw) (Figure 5.10 C'''). Furthermore, when we labeled the frontonasal prominence at 24 hpf (Figure 5.10D), the labeled cells gradually occupied the medial part of the palate at 48 and 72 hpf (Figure 5.10D'', D'''). Thus, the transgenic lines were able to identify the morphological changes that lead to the craniofacial anomalies (Figure 5.10 E–E''), and revealed the lineage-relationship between CNCCs in the PA1 and later craniofacial skeletons.

5.3.7 Morphological changes in the PA1 are correlated with craniofacial anomalies in *sox10:EGFP* embryos

To obtain the direct relationship between PA1 and teratogen-induced craniofacial phenotypes,

we examined how craniofacial anomalies emerge by focusing on the PA1 formation period and outgrowth period. We treated *sox10:EGFP* embryos with the teratogens and performed live-imaging analysis of the PA1 morphology at 24 hpf, craniofacial placode formation at 48 hpf and craniofacial morphology at 72 hpf (Figure 5.11 A–R). Teratogen-exposed *sox10:EGFP* embryos displayed PA1 defects such as truncated maxillary and mandibular prominences at 24 hpf (Figure 5.11 A–F'). At 48 hpf, the primitive palate (white arrowhead) and lower jaw (yellow arrowhead) were disrupted by the teratogens, leading to hypoplasia or aplasia of the structures (Figure 5.11 G–L). At 72 hpf, the treated embryos exhibited the palate hypoplasia with a cleft (cleft palate) and shortening in Meckel's cartilage (micrognathia) (Figure 5.11 M–R). WA-, SA-, and CAF-treated embryos showed mild phenotypes, namely, hypoplasia of the palate and mandible, while VPA- and MTX-treated embryos showed more severe phenotypes, namely, aplasia of the palate and mandible. These results are in agreement with the severity of craniofacial defects in each teratogen (Figure 5.8, 5.9).

5.3.8 Altered cell proliferation and apoptosis in the CNCCs during the migration period

What cellular defects underlined teratogen-induced craniofacial anomalies? Proper regulation of cell proliferation and death is crucial in neural crest development during vertebrate embryogenesis (Kulesa *et al.*, 2004; Kee and Bronner-Fraser, 2005). Thus, we hypothesized that teratogen-induced disruption of cell proliferation and apoptosis partially account for the observed migration defects of CNCCs during the migration period. These defects could be key events for the PA1 dysplasia, finally leading to craniofacial anomalies as an adverse outcome. We thus examined cell proliferation and apoptosis in premigratory and migratory CNCCs during the first 24 hours of development.

To precisely locate premigratory and migratory CNCCs at 10 ss which are to populate the PA1, we again performed the lineage tracing experiments using *sox10:Dendra2* embryos. Since the CNCCs positioned anterior to the MHB migrated to the craniofacial regions by 24 hpf (Figure 5.9), we reasoned that the CNCCs anterior to the MHB constitute the PA1 derivatives in later stages. To test this, we photoconverted CNCCs in the region of embryos at 10 ss and analyzed the distribution of labeled cells at 48 hpf (Figure 5.12 A–B'). The photoconverted CNCCs differentiated into the primordium of the palate (trabeculae) and lower jaw (Meckel's cartilage) as well as a cell population derived from the frontonasal prominence at 48 hpf (Figure 5.12 B, B'), indicating that these premigratory and migratory CNCCs at 10 ss are destined to constitute the PA1.

The above CNCC populations at 10 ss and in the PA1 at 24 hpf were subjected to cell proliferation assay, i.e. immunofluorescence staining against phospho-Histone H3 (pH3) as a mitotic marker (Figure 5.12 C–N'). Quantification of the number of the pH3-positive

premigratory and migratory CNCCs revealed that the mitotic activity was significantly decreased by treatment with any of the teratogens at 10 ss (Figure 5.12 O). Moreover, the mitotic activity at 10 ss exhibited dose-dependent decrease following treatment with all the teratogens (Figure 5.12 Q-U). These defects in migration behavior and mitotic activity account for the subsequent key event, PA1 formation Figure 5.12 P).

Next, we examined apoptosis by active Caspase-3 (Cas-3) antibody staining (Figure 5.13 A–L'). Quantification of the number of active Cas-3-positive CNCCs indicated that apoptotic cells significantly increased at 10 ss (Figure 5.13M). Moreover, the number of apoptotic cells exhibited a dose-dependent increase following treatment of all teratogens at 10 ss (Figure 5.13 O–S). However, at the highest dose of VPA and WA, embryos did not show a significant increase in apoptotic cells (Figure 5.13O, P). One reason for this result could be that excessive cell death was induced at earlier stages by the high-dosage teratogen treatment. In contrast, apoptosis of CNCCs in the PA1 at 24 hpf was not significantly induced by the teratogen exposure (Figure 5.13N). Thus, the number of apoptotic CNCCs in premigratory and migratory CNCCs was in agreement with the phenotypic severity at later stages.

Collectively, the data indicated that decreased mitotic ability and increased apoptosis in CNCCs during the migration period could be major key events for teratogen-indued craniofacial anomalies via PA1 dysplasia.

5.4 Discussion

In the present study, we first addressed two questions as follows: 1) Do teratogens which induce craniofacial anomalies in mammals cause the same anomalies in zebrafish? 2) Do teratogens target the development of cranial neural crest (CNC) cells, leading to craniofacial anomalies in zebrafish? Our findings provided three novel messages. (1) Twelve teratogens that cause craniofacial abnormalities in mammals were also found to disturb craniofacial development in zebrafish. (2) The craniofacial anomalies occurred due to a decrease in the number of chondrocytes and to disturbing the differentiation and maturation of chondrocytes, as well as disrupting the CNC development-related signaling pathways. (3) Our results showed an association between craniofacial defects induced by teratogens and craniofacial anomalies. Then we established transgenic lines driven by the *sox10* promoter to visualize CNCCs and examined their cellular behaviors in detail to identify an AOP for chemical-induced craniofacial anomalies. Teratogens affected CNCC migration, mitotic ability and apoptosis, leading to the PA1 morphological defect. These defects finally resulted in craniofacial anomalies such as cleft palate and micrognathia as adverse outcomes. Our lineage tracing experiments showed that, like in mammals, CNCCs in the zebrafish PA1 differentiated into craniofacial skeletal elements.

Craniofacial morphogenesis involves a complex series of developmental events that

ultimately create diverse facial morphologies in vertebrates. Despite the differences of vertebrates' craniofacial structures, the neural crest cell and its roles in craniofacial development are conserved across vertebrates (Bronner and LeDouarin, 2012; Rada-Iglesias *et al.*, 2012; Simões-Costa and Bronner, 2015). The etiology of craniofacial anomalies involves the interplay between genetic factors and environmental factors(Dixon *et al.*, 2011). Extensive knowledge about various teratogens that induce craniofacial defects in mammals, including humans, has been reported (Table 5.1). The teratogens used in our experiments are well known to induce multiple craniofacial disorders, such as micrognathia, cleft palate, microcephaly, eye defects and ear abnormalities based on epidemiological data and experiments in mammals (Abbott *et al.*, 1989; Bermas and Hill, 1995; El Gendy *et al.*, 2015; Fujii *et al.*, 1969; HILL and KLEINBERG, 1984a; Hyoun *et al.*, 2012; Jentink *et al.*, 2010; Price *et al.*, 1996; Smithells and Newman, 1992). However, there is limited information about the cellular and molecular mechanisms of craniofacial malformations caused by teratogens.

Here, we exposed zebrafish embryos to specific teratogens. In accord with reports of studies in mammals, our results showed that the teratogens tested here clearly induced malformation of the neurocranium and viscerocranium in a dose-dependent manner (Figure. 5.2, 5.3). These results led us to speculate that CNC development in zebrafish is severely impaired by these chemicals. In accord with this possibility, RA, MTX, VPA, CAF, and DEX have been reported to affect CNC development in mammals and other vertebrates (Berenguer *et al.*, 2018; Li *et al.*, 2011; Ma *et al.*, 2014; Rao and LaBonne, 2018; Ruberte *et al.*, 1991). The other chemicals that we tested, namely SA, WAF, HU, PHT, IM, BA and THA, have been reported to induce craniofacial malformations in mammals, but there have been no reports about the cellular and molecular mechanisms of these malformations (El Gendy *et al.*, 2015; Habib, 1978; HILL and KLEINBERG, 1984b; Liebelt *et al.*, 2007; Price *et al.*, 1996; Smithells and Newman, 1992). In the present study, we showed that all of these teratogens affected craniofacial morphogenesis as well as CNC development at the cellular and molecular level (Figure 5.4, Figure.5.5, Figure. 5.6). This is the first report of a large-scale analysis of numerous teratogens that disturb CNC development and lead to craniofacial malformation. Thus, zebrafish and mammals share conserved responses to various chemicals regarding the chemically induced craniofacial anomalies.

Furthermore, we found that the teratogens also targeted chondrocyte differentiation and maturation. During the process of chondrocyte differentiation and maturation, the cellular features of chondrocytes progressively change within the growth plate in craniofacial cartilages. Small, round chondrocytes need to undergo proliferation and elongation to give rise to long, flattened chondrocytes, and finally become stacked in longitudinal columns in mammals (Kozhemyakina *et al.*, 2015). Zebrafish cartilage formation occurs through the same process,

which is thought to be evolutionally conserved among vertebrates (Shwartz *et al.*, 2012). Most of the craniofacial cartilage elements are formed by 96 hpf in zebrafish, and the chondrocytes of the neurocranium and viscerocranium, such as those in the ethmoid plate and Meckel's cartilage, show characteristic stacking and organization of thin, elongated chondrocytes that are assembled on their respective cartilage element (Kimmel *et al.*, 1998; Sisson *et al.*, 2015). Craniofacial malformation can also be caused by genetic mutations in neural crest-derived chondrocytes in mammals and zebrafish (Clément *et al.*, 2008; Leung *et al.*, 2011). Round-shaped chondrocytes and loss of columnar structure are typical phenotypes caused by such mutations (Ling *et al.*, 2017; Rochard *et al.*, 2016; Sisson *et al.*, 2015).

Intriguingly, the defects caused by genetic mutations were phenocopied by teratogen treatments in our experiments. We focused on the ethmoid plate and Meckel's cartilage because these two structures are derived from the cranial neural crest population, as proven by lineage tracing experiments(Mork and Crump, 2015; Szabo-Rogers *et al.*, 2010; Wada *et al.*, 2005) . As we expected, the number of cartilage cells in the ethmoid plate and Meckel's cartilage was decreased by the teratogen treatment. This suggests that chondrocytes in both of these cranial structures probably cease proliferation or increase apoptosis. Such a defect was confirmed by the decreased expression level of *col2al*, which is a differentiation marker of chondrocytes (Figure. 5.6H). Therefore, our results indicate that the teratogens tested here block the development of cranial neural crest cells and chondrocytes at the molecular and cellular levels, leading to craniofacial malformation. These findings also demonstrate that mammals and fish share conserved responses to these teratogens.

A few teratogens were reported to have a possible influence on CNC development; however, no results direct demonstrating this have been reported. Our results demonstrate for the first time that chemical-induced craniofacial abnormalities share a conserved cellular and molecular mechanism via disruption of CNC development in zebrafish and mammals. Our results demonstrate a conserved response to the teratogens at the cellular and molecular levels; however, the key signaling pathways disrupted by these teratogens will need to be elucidated to clarify the basis of our findings.

In the present study, we established transgenic lines driven by the *sox10* promoter to visualize CNCCs and examined their cellular behaviors in detail to identify an AOP for chemical-induced craniofacial anomalies. Teratogens affected CNCC migration, mitotic ability and apoptosis, leading to the PA1 morphological defect. These defects finally resulted in craniofacial anomalies such as cleft palate and micrognathia as adverse outcomes. Our lineage tracing experiments showed that, like in mammals, CNCCs in the zebrafish PA1 differentiated into craniofacial skeletal elements. Thus, the AOP of craniofacial anomalies could be conserved between fish and mammal.

The craniofacial morphology of mammals is apparently different from that of zebrafish at the late embryonic (fetal) stages; however, the pharyngeal period (24 hpf for zebrafish and E9.5 for mouse), when pharyngeal arches are being formed, is conserved at the morphological and transcriptome level among vertebrates (Kuratani, 2005; Irie and Kuratani, 2011). During this period, one of the crucial events is the development of NCCs (Simões-Costa and Bronner, 2013; Etchevers *et al.*, 2019; Hockman *et al.*, 2019). CNCCs originate from the midbrain and anterior hindbrain region during neurulation (Chai *et al*., 2000; Rocha *et al.*, 2020, Figure. 5.13A, A'). CNCCs migrate stereotypically along the frontonasal or maxillary pathways and form the frontonasal prominence and the PA1 (the maxillary and mandibular prominence), respectively (Serbedzija *et al.*, 1992; Chai et al., 2000; Rocha *et al.*, 2020; Figure.510E–10E", Figigure5.14A). The frontonasal prominence forms the facial midline, while the PA1 forms the mandibular region (lower jaw including Meckel's cartilage) and the maxillary region (palate) in both mouse and zebrafish (Figure. 5.14A) (Graham, 2001; Knight and Schilling 2006; Clouthier *et al.*, 2010; Graham and Richardson, 2012). Thus, key events constituting AOPs of craniofacial anomalies should be conserved during this period between fish and mammals.

Similarities between fish and mammalian craniofacial development are also observed even after the pharyngeal period. In mammals, one of the critical events causing craniofacial anomalies is a failure of the primary and secondary palate formation (palatogenesis) during late craniofacial morphogenesis (E11.5 for mouse embryos). The primary palate develops from the frontonasal prominence and is transiently formed anterior to the secondary plate (Figure. 5.14A). The secondary palate develops from the maxillary prominence and is finally fused with the primary palate to complete the process of craniofacial morphogenesis (Bush and Jiang, 2012). Any disturbance of this process in mammals can cause orofacial clefts (Lan *et al.*, 2015; Hammond and Dixon, 2022). In zebrafish, in spite of the absence of the secondary palate, the palate is also formed in the anterior neurocranium and is composed of the ethmoid plate and trabeculae, which originate from the frontonasal and maxillary prominences, respectively (Figure. 14A). Clefting, shortening, or the absence of these structures represent prototypical orofacial abnormalities in zebrafish (Wada *et al.*, 2005; Eberhart *et al.*, 2008; Swartz *et al.*, 2011; Dougherty *et al.*, 2012). Thus, palatogenesis following the PA1 formation in zebrafish and mammals is thought to progress in similar manners.

In addition to the morphological similarity, zebrafish and mammals share similar teratogenic responses (Liu *et al.*, 2020). Furthermore, they utilize the same molecular signaling pathways, including Fgf, Pdgfr, Bmp, Tgfb, Wnt, and Shh pathways, in palatogenesis, and disruption of any of these pathways could result in craniofacial defects in both zebrafish and mammals (Schilling and Kimmel, 1997; Bush and Jiang, 2012). Indeed, in our previous research, cleft palate in zebrafish induced by teratogens was triggered by canonical Wnt pathway inhibition,

which is the same etiology of cleft palate as that found in mammals (Narumi *et al.*, 2020). These lines of evidence support the idea that zebrafish share conserved craniofacial morphogenesis and teratogenic responses with mammals. Therefore, zebrafish is considered to be a useful model for evaluating and predicting chemical-induced craniofacial anomalies across vertebrates.

Identification of an AOP has been essential for developmental toxicity evaluation as well as cross-species extrapolations (Ankley *et al.*, 2010; Knapen *et al.*, 2015). Recently, an AOP of developmental vascular toxicity was identified (Saili *et al.*, 2017); however, there is no report of an AOP causing craniofacial anomalies. Developmental toxicity manifests during morphogenesis, and thus teratogenicity should be monitored and evaluated in a chronological manner. Craniofacial anomalies have been investigated mainly by observation of gross external morphology or the pattern of Alcian blue cartilage staining (Brannen *et al.*, 2010, 2013; Liu *et al.*, 2020). Although these strategies have been successful in detecting the readout of teratogenicity, the developmental process for the craniofacial anomalies could not be traced with these methods. To solve this problem, we established a series of *sox10*-reporter transgenic lines in zebrafish, which enables us to monitor for CNCC-based chronological teratogenic response and thereby to elucidate key events along with the causal relationship inducing craniofacial anomalies (Table 5.2, Figure S3). Several genes including *foxd3* have been identified as markers for CNCCs (Drerup *et al.*, 2009). Among these markers, *sox10* is the most suitable in that it continues to be expressed in craniofacial cartilage after 48 hpf (Carroll *et al.*, 2020), and thus can monitor both CNCC development and craniofacial morphogenesis.

Our *sox10:EGFP* zebrafish line enables us to monitor the gross morphology of CNCC populations during craniofacial morphogenesis (Figure. S3A, S3A'). The *sox10:EGFP-CAAX* line demarks the cell membrane of each CNCC (Figure. S3B, S3B') so that phenotypes can be examined at a cellular level. Finally, the *sox10:Dendra2* line enables tracing of the developmental origin and differentiation fate of CNCCs (Figure S3C, S3C'). These lines can also detect cartilage anomalies at later stages (Figure 5.8, S4, S5). The expression patterns of these fluorescent reporter genes are in agreement with the previously reported *sox10* reporter lines (Dougherty *et al.*, 2012; Askary *et al.*, 2015). Therefore, our lines are suitable for examining the early events of teratogenicity such as migration and apoptosis through live imaging and monitoring the development of CNCCs. Gene expression analysis will be needed to further confirm the usefulness of this system, but it will be a next step to be done in the near future. Taken together, these transgenic lines provide the powerful platform with which to analyze the early events causing craniofacial anomalies and to evaluate AOP-based teratogenicity chronologically.

CNCC development is classified into three periods: CNCC migration, PA1 formation and outgrowth of craniofacial placodes. Live imaging with *sox10:EGFP* lines detected defects in

CNCC migration, PA1 formation and craniofacial morphology as an adverse outcome. When exposed to teratogens, premigratory and migratory CNCCs at 10 ss exhibited decreased proliferation and increased apoptosis, but CNCCs in the PA1during the pharyngeal only showed decreased proliferation at 24 hpf. These results suggest that migratory CNCCs are more vulnerable and/or sensitive to teratogens. Consistent with these results, when zebrafish embryos were treated with the teratogens for 4–24 hpf or 24–96 hpf, craniofacial anomalies occurred more frequently in the 4–24 hpf treatment than in the 24–96 hpf treatment embryos (Figure S7). Taken together, we conclude that the migration period is critical for chemical-induced craniofacial anomalies and that the resulting PA1 morphology at the pharyngeal period 24 hpf is a reliable endpoint for predicting chemical-induced craniofacial anomalies.

Finally, we provide the following AOP for chemical-induced craniofacial anomalies (Figure 5.14B):

(1) Molecular response: Disturbance of gene expression during CNCC development
Our previous study showed that teratogen-exposed embryos showed disturbance of the expression of genes involved in CNCC development (*tfap2a*, *zic2a, pax3*, *snail2*, *sox10* and *sox9a*)(Liu *et al.*, 2020). Genetic manipulation of some of these genes also induces defects in CNCCs leading to craniofacial anomalies in zebrafish (Knight *et al.*, 2003; TeSlaa *et al.*, 2013; Minchin and Hughes, 2008; Yan *et al.*, 2005; McKeown *et al.*, 2005).

(2) Cellular response: Inhibition of CNCC migration, decreased mitotic ability and increased apoptosis in premigratory and migratory CNCCs

(3) Tissue response: Disturbance of PA1 morphogenesis at the pharyngeal stage

(4) Adverse outcomes: Craniofacial anomalies such as cleft palate and micrognathia
Taken together, we propose a method for an alternative teratogenicity assay using transgenic zebrafish lines (Figure. 5.13 C). Teratogens are administered to *sox10* transgenic lines at 4 hpf. The first endpoint is the PA1 formation at the pharyngeal period. This deformity predicts later craniofacial anomalies. The second endpoint is craniofacial morphology at 96 hpf, which is a readout of the PA1 defect.

In sum, we have revealed the AOP for craniofacial anomalies caused by teratogens using zebrafish transgenic lines and identified cellular key events. Based on highly conserved developmental mechanisms and teratogenic responses between mammals and fish, we assume that our findings can be directly applicable to mammalian embryos. Zebrafish is thus a promising model for evaluating cross-species chemical-induced developmental toxicity.

5.5 Conclusions

Based on these findings, we propose that our *sox10-EGFP* reporter lines represent a valuable model for detecting craniofacial anomalies during various developmental stages, from early to

late. Our results demonstrate that chemical-induced craniofacial malformation is caused by aberrant development of the CNCCs during the migration period, leading to impaired PA1 formation, a process considered conserved among vertebrates. Furthermore, given the highly conserved CNCC developmental processes around this stage in both zebrafish and mammals, our findings can be extrapolated to mammalian craniofacial development. These also suggest that zebrafish provide a platform for investigating contributions of environmental factors as causative agents of craniofacial anomalies in human.

Table 5.1

Compounds used in the present study. References cited in the reference section or supplemental reference list.

Category	Test compound	Abbreviation	CAS No.	Supplier	Solvent	Concentration range (μM)	Craniofacial defects in mammals
Antineoplastic agents, immunomodulating agents	Hydroxyurea	HU	127-07-1	Sigma-Aldrich	Distilled water	1-1000	Craniofacial dysgenesis, micrognathia, cleft palate, and eye defects (Aliverti et al., 1980; Asano and Okaniwa, 1987; Liebelt et al., 2007)
	Imatinib	IM	152459-95-5	Tokyo Chemical Industry	DMSO	1-250†	Micrognathia, cleft palate, misshapen snouts, eye defects (El Gendy et al., 2015; Pye et al., 2008)
	Methotrexate	MTX	59-05-2	Wako	DMSO	0.1-200*	Micrognathia, cleft lip and palate, prominent eyes, low-set ears, and microphthalmia (Hyoun et al., 2012; Lloyd et al., 1999; Weber-Schoendorfer et al., 2014)
	Thalidomide	THA	50-35-1	Tocris Bioscience	DMSO	1-400†	Micrognathia, retrognathia and cleft palate, mild low set ears, and eye deformities (Smithells and Newman, 1992; Vargesson, 2015)
Cardiovascular agents antithrombotic agents, anticoagulants	Warfarin	WAF	129-06-6	Wako	DMSO	0.1-60*	Microcephaly, short palpebral fissures, maxillary hypoplasia, micrognathia, and cleft palate (Hill and Kleinberg, 1984a; Hill and Kleinberg, 1984b; Howe and Webster, 1990; Starling et al., 2012)
Antiepileptic agents, anticonvulsants	Phenytoin	PHT	57-41-0	Wako	DMSO	1-200†	Micrognathia, agnathia, and cleft palate (Goldman et al., 1982; Nulman et al., 1997; Webster et al., 2006)
	Valproic acid	VPA	99-66-1	Wako	Distilled water	0.1-30*	Micrognathia, cleft palate, flattened nasal bridge, eye and ear abnormalities (Alsdorf and Wyszynski, 2005; Ardinger et al., 1988; Vajda et al., 2004)
Nonsteroidal anti-inflammatory drugs	Salicylic acid	SA	54-21-7	Wako	Distilled water	1-400*	Micrognathia, cleft palate, and microcephaly (Fujii and Nishimura, 1969; Habib, 1978; Saxen, 1975)
Corticosteroids, immunosuppressive agents	Dexamethasone	DEX	59-05-2	Wako	DMSO	1-200†	Micrognathia and cleft palate (Bermas and Hill, 1995; Greene and Kochhar, 1975)
Ophthalmic agents, insecticide	Boric acid	BA	10043-35-3	Wako	Distilled water	1-1000	Micrognathia and low-set ears (Heindel et al., 1994; Price et al., 1996)
Psychostimulants, agents used for ADHD	Caffeine	CAF	58-08-2	Wako	Distilled water	1-500*	Micrognathia, agnathia, cleft lip and palate (Collier et al., 2009; Fujii et al., 1969; Johansen et al., 2009)
Vitamin A, topical use in acne	Retinoic acid	RA	302-79-4	Tokyo Chemical Industry	DMSO	$1x10^{-6}$-$5x10^{-5}$*	Micrognathia, agnathia, cleft lip and palate, ear and eye defects (Emmanouil-Nikoloussi et al., 2000; Lammer et al., 1985; Okano et al., 2007; Padmanabhan and Ahmed, 1997)

*: Highest viable concentration, †: Highest soluble concentration.

Table 5.2. Established transgenic lines

Three transgenic lines were established. Each line showed distinct fluorescence localization and utility for a specific purpose.

Transgenic line	Fluorescent protein localization	Purpose
sox10:EGFP	Cytoplasm	Cell morphology
sox10:EGFP-CAAX	Endomenbrane	Cell morphology
sox10:Dendra2	Cytoplasm	Lineage tracing

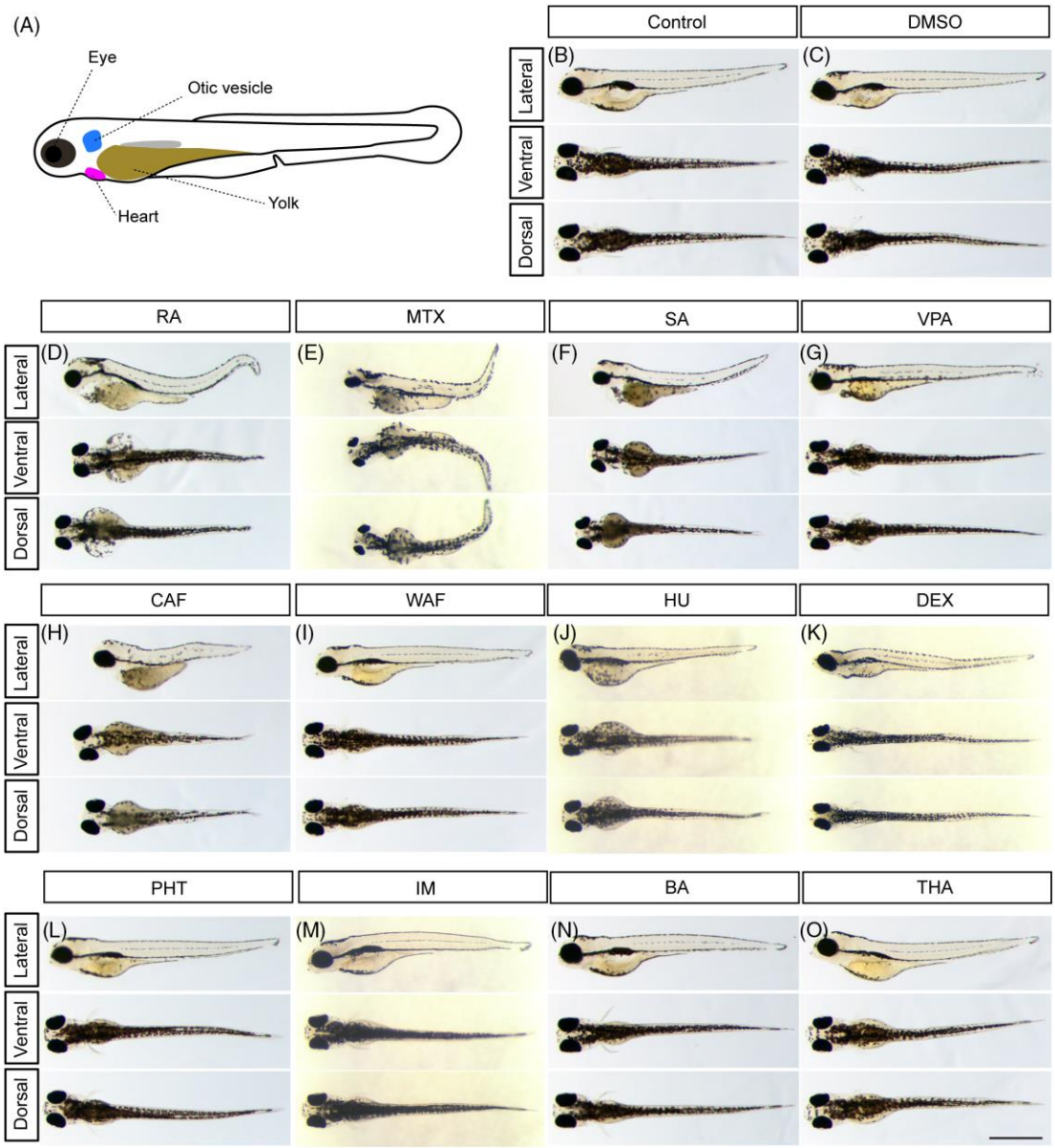

Figure 5. 1. Gross morphological anomalies of teratogen-treated zebrafish embryos at 96 hpf. A, **(**A) Schematic diagram of zebrafish embryo at 96 hpf. (B) E3 control. (C) DMSO control. (D) RA, retinoic acid. (E) MTX, methotrexate. (F) SA, salicylic acid. (G) VPA, valproic acid. (H) CAF, caffeine. (I) WAF, warfarin. (J) HU, hydroxyurea. (K) DEX, dexamethasone. (L) PHT, phenytoin. (M) IM, imatinib. (N) BA, boric acid. (O) THA, thalidomide. Scale bar: 1 mm.

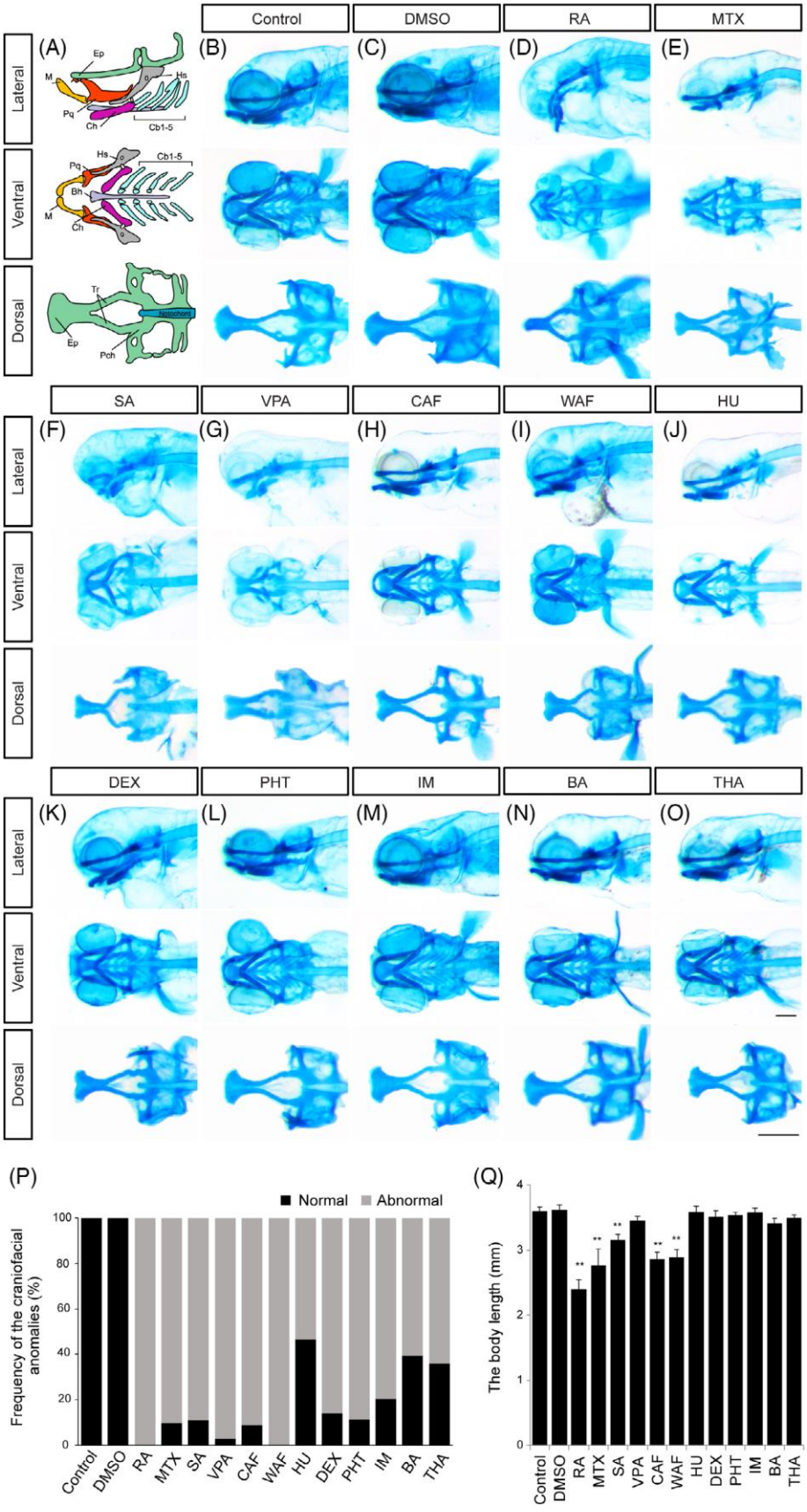
Control
DMSO
RA
MTX
SA
VPA
CAF
WAF
HU
DEX
PHT
IM
BA
THA
Lateral
Ventral
Dorsal
(A)
(B)
(C)
(D)
(E)
(F)
(G)
(H)
(I)
(J)
(K)
(L)
(M)
(N)
(O)
Ep
M
Hs
Pq
Ch
Cb1-5
Bh
Tr
Notochord
Pch
(P)
Normal
Abnormal
Frequency of the craniofacial anomalies (%)
(Q)
The body length (mm)

Figure 5. 2 Alcian blue-stained zebrafish embryos at 96 hpf displayed abnormal cranial development. (A) Craniofacial atlas of the lateral view, the viscerocranium (ventral view) and the neurocranium (dorsal view): Bh, Basihyal; Cb, Ceratobranchial; Ch, Ceratohyal; Hm, Hyomandibula; Hs, Hyosymplectic; Ih, Interhyal; M, Meckel's; OP, Opercle (bone); Pq, Palatoquadrate; Ep, Ethmoid plate; Tr, Trabeculae; Pch, Parachordal of craniofacial structures. (B-O) Zebrafish treated with the following teratogens showed cranial malformations: (B) Control, E3; (C) DMSO, vehicle control; (D) RA, retinoic acid; (E) MTX, methotrexate; (F) SA, salicylic acid; (G) VPA, valproic acid; (H) CAF, caffeine; (I) WAF, warfarin; (J) HU, hydroxyurea; (K) DEX, dexamethasone; (L) PHT, phenytoin; (M) IM, imatinib; (N) BA, boric acid; (O) THA, thalidomide. (P) The summary of craniofacial anomalies (Control: n = 45, DMSO: n = 40, RA: n = 35, MTX: n = 31, SA: n = 27, VPA: n = 36, CAF: n = 34, WAF: n = 32, HU: n = 28, DEX: n = 36, PHT: n = 35, IM: n = 27, BA: n = 33, THA: n = 39). (Q) The body length analysis. Scale bars: 200 μm.

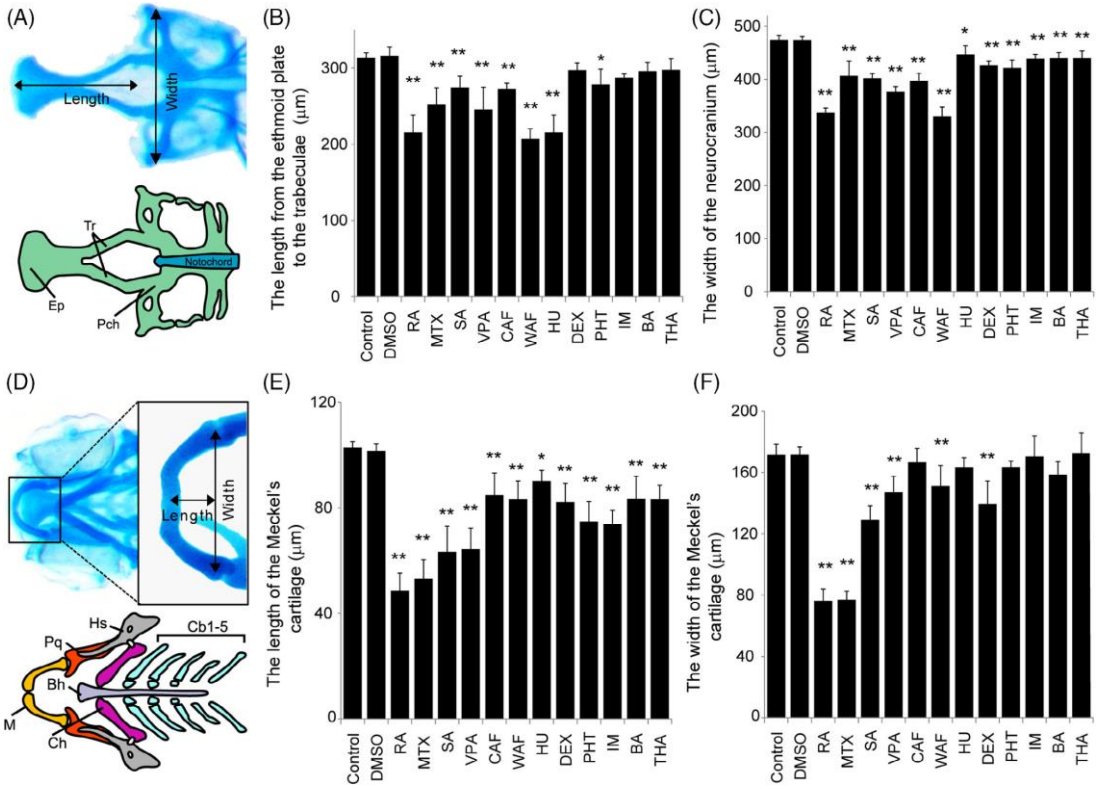

Figure 5. 3 Quantitative measurement of craniofacial malformations. (A) The definitions of the length and width in neurocranium measurements. (B, C) the length and width of the neurocranium were quantified. (D) The definition of the length and width of the Meckel's cartilage in viscerocranium measurement. (E, F) the length and width of the Meckel's cartilage were quantified. The one-way ANOVA followed by Dunnett's multiple comparison tests was used to compare the values between the control and the chemical-treated group (*P < 0.05, **P < 0.01, n = 5).

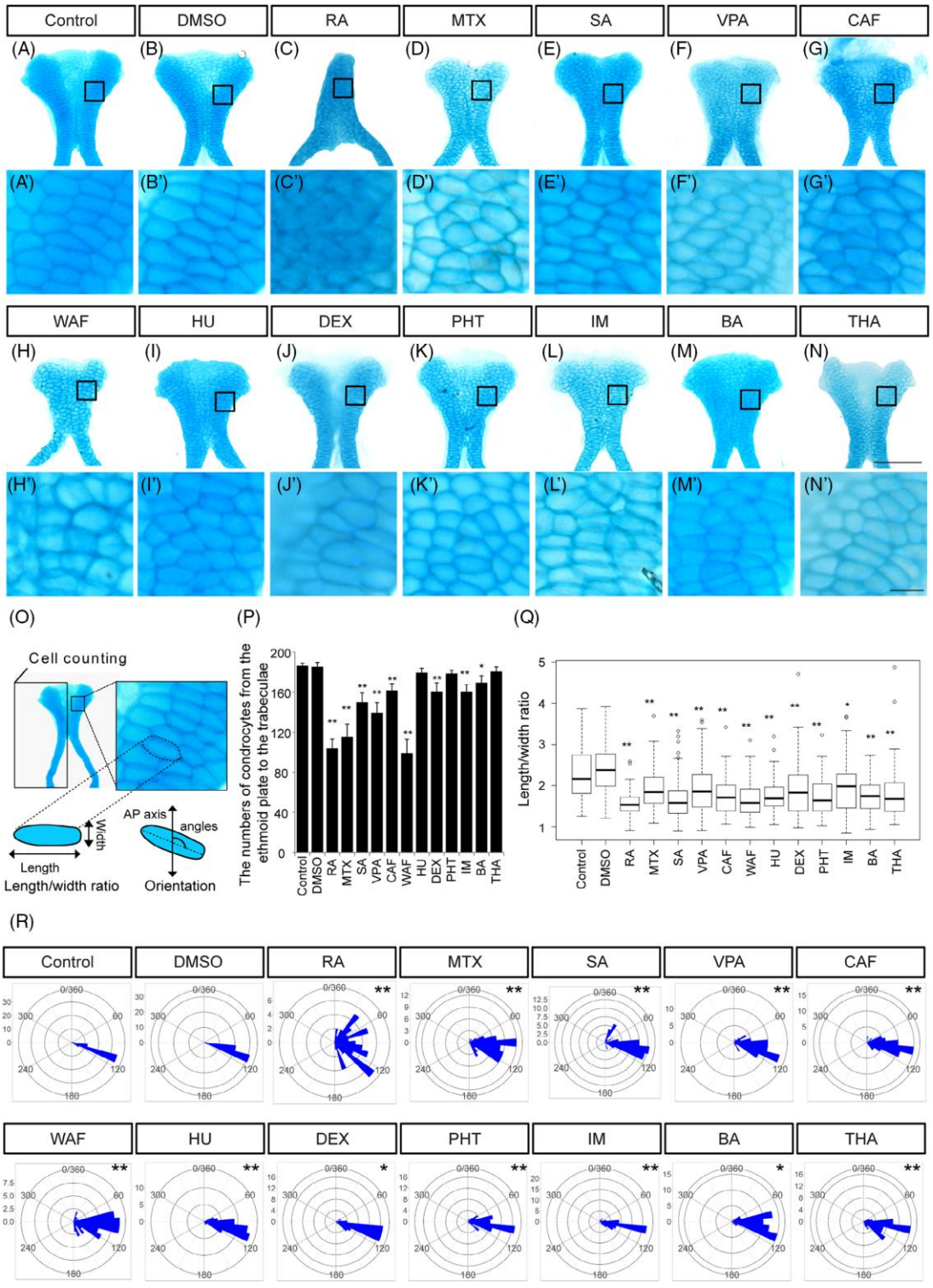
Control
DMSO
RA
MTX
SA
VPA
CAF
WAF
HU
DEX
PHT
IM
BA
THA
(A)
(B)
(C)
(D)
(E)
(F)
(G)
(H)
(I)
(J)
(K)
(L)
(M)
(N)
(A')
(B')
(C')
(D')
(E')
(F')
(G')
(H')
(I')
(J')
(K')
(L')
(M')
(N')
(O)
(P)
(Q)
(R)
Cell counting
Length
Width
Length/width ratio
AP axis
angles
Orientation
The numbers of condrocytes from the ethmoid plate to the trabeculae
Length/width ratio

Figure 5. 4 The number of chondrocytes and their shape in ethmoid plate were affected by teratogen treatment. (A–N) The ethmoid plate was dissected from Alcian blue-stained samples and was flat-mounted. Anterior is to the top. (A'–N') Magnified view of chondrocytes in the ethmoid plate in the region indicated by the boxed area in A–N. (O) The region in which cell counts were determined in the ethmoid plate and the definitions of the length and width of the chondrocytes used for the cell shape analysis. The orientation of longest cell axis was measured to quantify chondrocyte stacking. (P) The number of chondrocytes in half of the ethmoid plate was counted (n = 5). (Q) The length/width ratio of the chondrocytes in Figure 5A'–N' was measured (at least 60 cells were measured per group, n = 3). (R) The chondrocyte orientation was indicated by rose plot (at least 60 cells were measured per group, n = 3). Orientation was significantly differed from that of control and vehicle control (Watson's U2 test; *P < 0.05, **P < 0.01). One-way ANOVA followed by Dunnett's multiple comparison tests were performed for statistical analysis of chondrocyte number and shape (*P < 0.05, **P < 0.01). Scale bars: 50 μm in A–N, 5 μm in A'–N'.

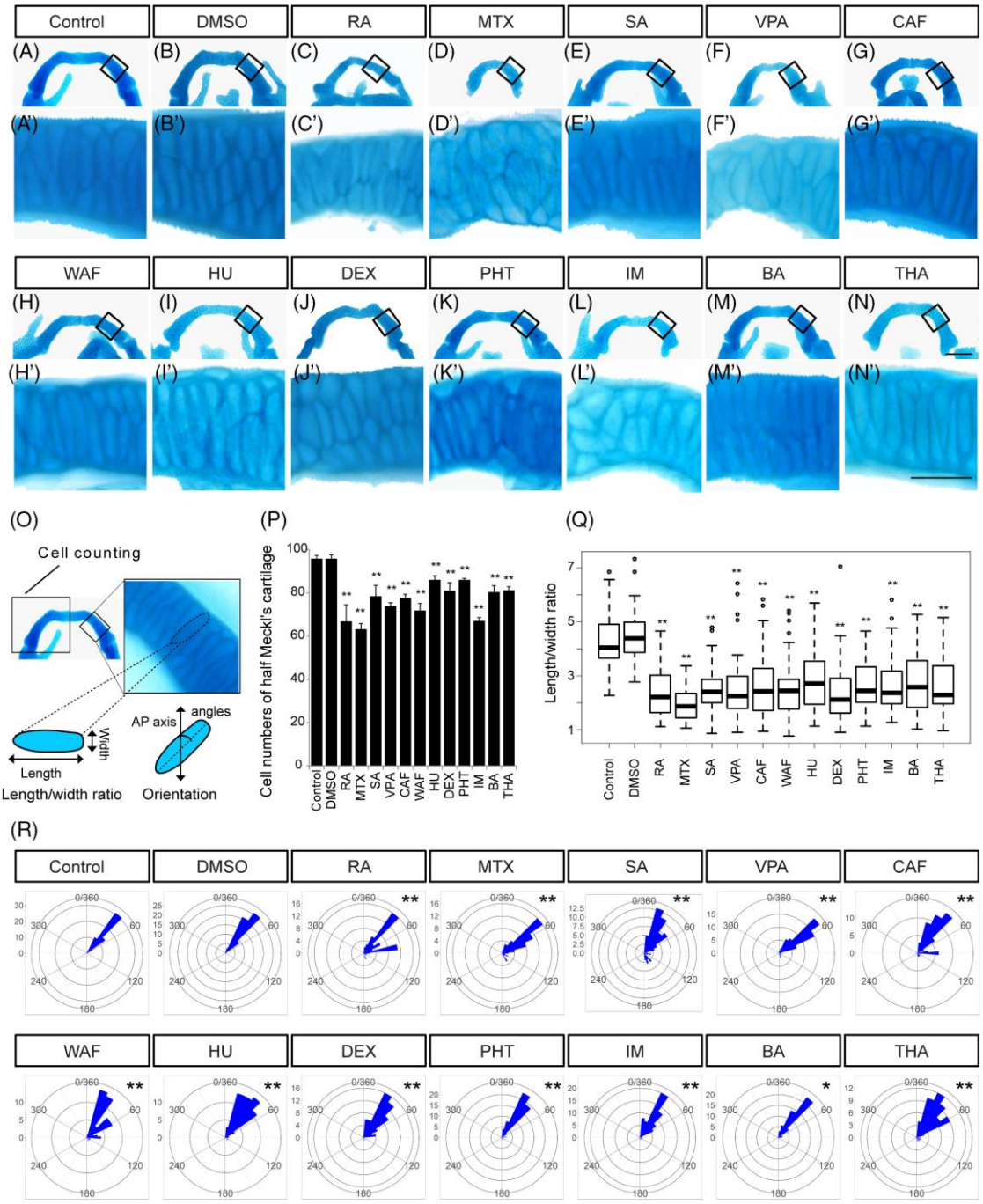
Control
DMSO
RA
MTX
SA
VPA
CAF
WAF
HU
DEX
PHT
IM
BA
THA
(A)
(B)
(C)
(D)
(E)
(F)
(G)
(H)
(I)
(J)
(K)
(L)
(M)
(N)
(A')
(B')
(C')
(D')
(E')
(F')
(G')
(H')
(I')
(J')
(K')
(L')
(M')
(N')
(O)
Cell counting
AP axis
angles
Width
Length
Length/width ratio
Orientation
(P)
Cell numbers of half Meckl's cartilage
(Q)
Length/width ratio
(R)

Figure 5. 5 The number of chondrocytes and their shape in the Meckel's cartilage were affected by teratogen treatment. (A–N) The Meckel's cartilage was dissected from Alcian blue-stained samples and was flat-mounted. Anterior is to the top. (A'–N') Magnified view of chondrocytes in the Meckel's cartilage indicated by the boxed area in A–N. Anterior is to the top. (O) the area used for cell counting in the Meckel's cartilage and the definition of the length and width of the chondrocytes used for the cell shape analysis. The orientation of the longest cell axis was measured to quantify chondrocyte stacking. (P) The number of chondrocytes in half of the Meckel's cartilage was measured (n = 5). (Q) The length/width ratio of the chondrocytes in A'–N' was measured (at least 60 cells were measured per group, n = 3). (R) The chondrocyte orientation was indicated by rose plot (at least 60 cells were measured per group, n = 3). Orientation was significantly different from those of control and vehicle control (Watson's U2 test; *P < 0.05, **P < 0.01). One-way ANOVA followed by Dunnett's multiple comparison tests were performed for statistical analysis of chondrocyte number and shape (*P < 0.05, **P <0 .01). Scale bars: 50 μm in A–N, 20 μm in A'–N'.

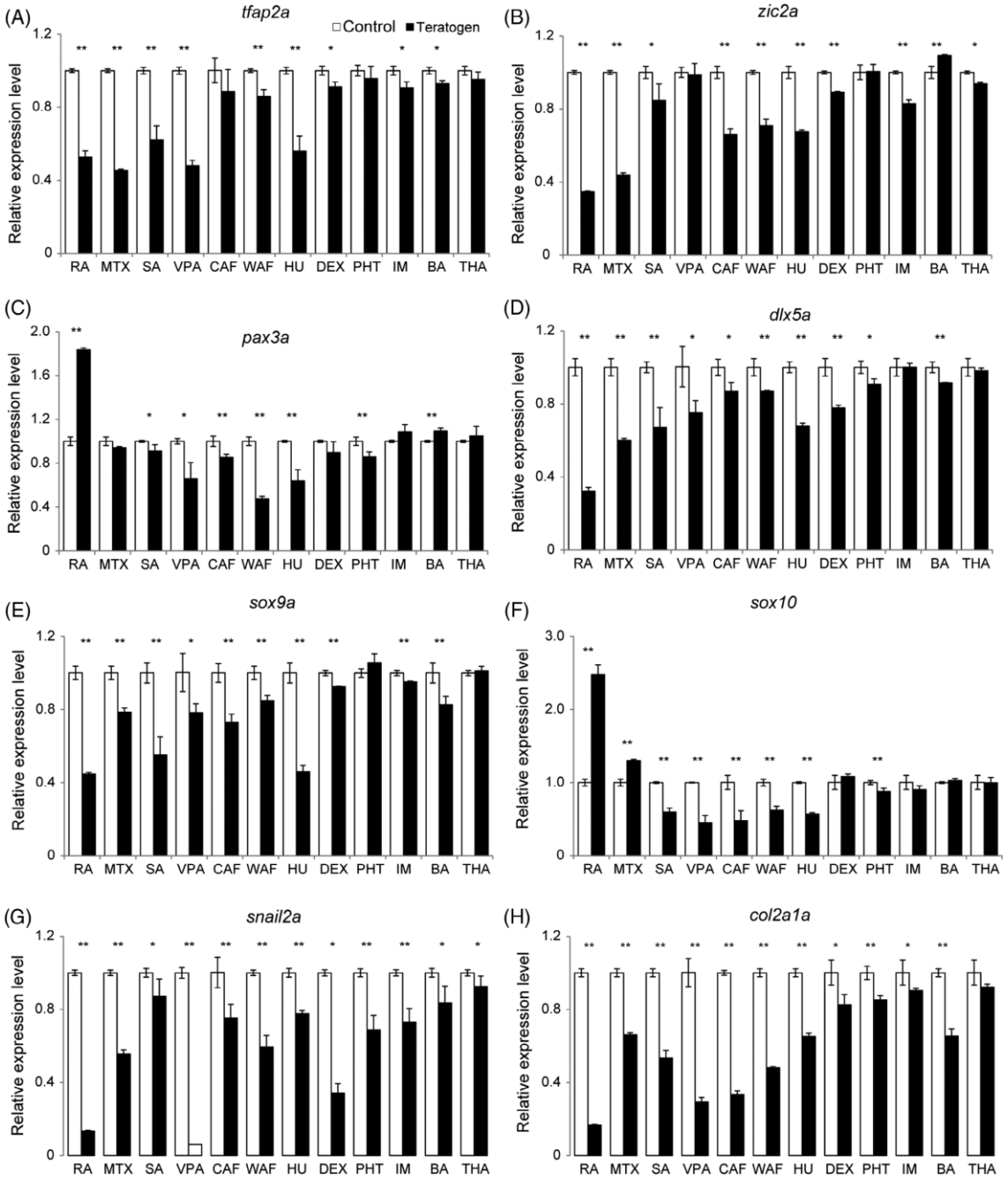

Figure 5. 6 The expression levels of neural crest cell-related genes were perturbed in teratogen-treated embryos. Relative expression levels were examined by RT-qPCR at 48 hpf. The examined genes were as follows: *tfap2a*, A; *zic2a*, B; *pax3a*, C; *dlx5a*, D; *sox9a*, E; *sox10*, F; *snail2a*, G; and *col2a1a*, H. Data are shown as mean ± SD of triplicate samples. Asterisks indicate statistically significant differences between groups (*P < 0.05, **P < 0.01, n = 3).

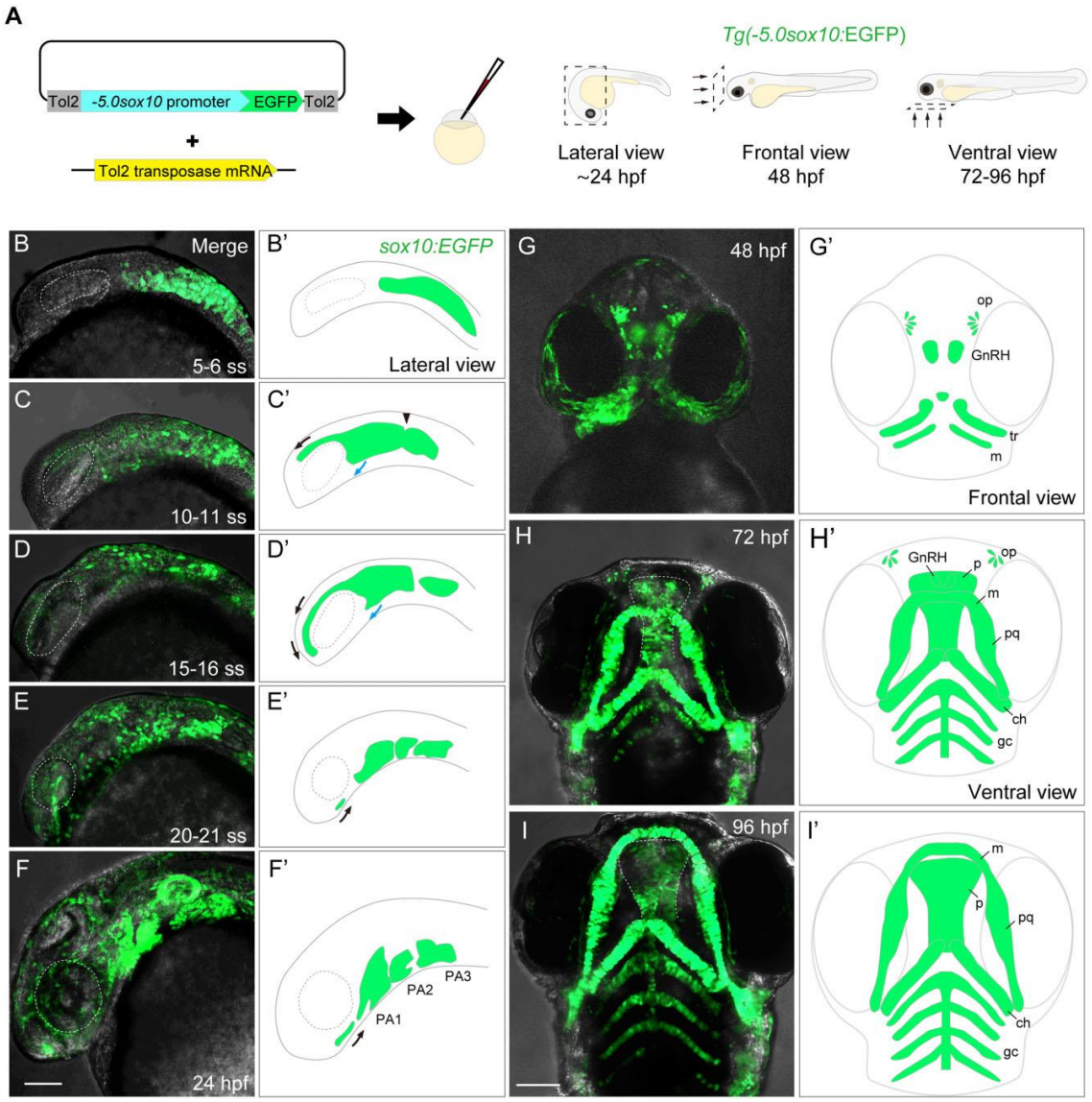
A
Tol2
-5.0sox10 promoter
EGFP
Tol2
+
Tol2 transposase mRNA
Tg(-5.0sox10:EGFP)
Lateral view
~24 hpf
Frontal view
48 hpf
Ventral view
72-96 hpf
B
Merge
5-6 ss
B'
sox10:EGFP
Lateral view
C
10-11 ss
C'
D
15-16 ss
D'
E
20-21 ss
E'
F
24 hpf
F'
PA1
PA2
PA3
G
48 hpf
G'
op
GnRH
tr
m
Frontal view
H
72 hpf
H'
GnRH
op
p
m
pq
ch
gc
Ventral view
I
96 hpf
I'
m
p
pq
ch
gc

Figure 5. 7 Generation and characterization of the *sox10:EGFP* transgenic zebrafish. (A) Schematic diagram for generating *Tg(-5.0sox10:EGFP)* (left) and directions of view for imaging embryos shown in (B)–(I) (right). (B–I') Live imaging of *sox10:EGFP* embryos (B–I) and schematic diagram of the EGFP distribution (B–I'). (B, B') EGFP expression was detected at the 5–6 ss in premigratory and migratory neural crest cells. (C–E') EGFP expression was detected in CNCCs which migrated from the anterior-most midbrain and the hindbrain to the pharyngeal pouch via frontonasal (black arrows) and maxillary (blue arrows) pathways at 10–11 ss (C, C'), 15–16 ss (D, D') and 20–21 ss (E, E'). The arrowhead in C' shows the midbrain-hindbrain boundary (MHB). (F, F') EGFP-positive CNCCs formed pharyngeal arches (PAs) at 24 hpf. (G, G') EGFP-positive CNCCs formed the primordium of craniofacial skeletal elements (the palate and lower jaw) and placodes (olfactory neurons and GnRH neurons) at 48 hpf. (H, H') EGFP-positive CNCCs were observed in the craniofacial skeletal elements and sensory neurons at 72 hpf. (I, I') EGFP-positive skeletal elements grew and eventually composed the face at 96 hpf. ch, ceratohyal; gc, gill cartilages; GnRH, gonadotropin-releasing hormone neuron; m, Meckel's cartilage; op, olfactory placode; p, palate; PA, pharyngeal arch; pq, palatoquadrate; tr, trabeculae. Scale bar: 100 μm.

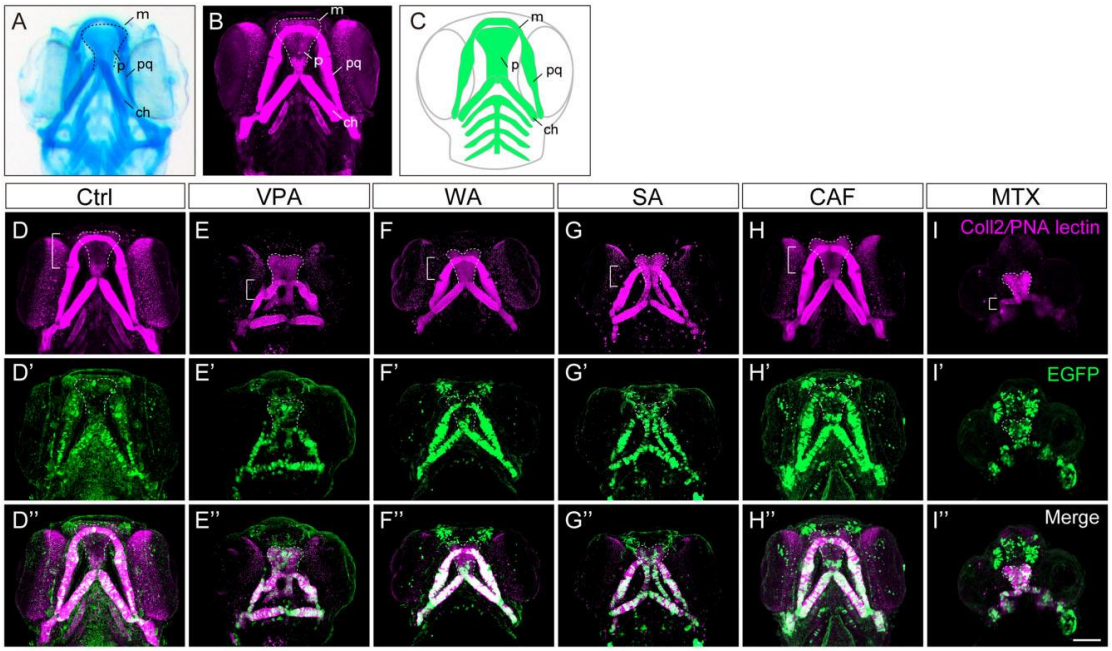

Figure 5. 8 Craniofacial anomalies were identified in teratogen-treated *sox10:EGFP* zebrafish embryos at 96 hpf. (A, B) Craniofacial cartilage stained with Alcian blue (A) and anti-coll2 antibody and PNA lectin (B). (C) Schematic illustration of craniofacial cartilage elements. m, Meckel's cartilage; p, palate; pq, palatoquadrate; ch, ceratohyal. (D–I'') *sox10:EGFP* embryos were treated with the following teratogens and displayed craniofacial anomalies. (D-D'') Ctrl, E3 control. (E-E'') VPA , valproic acid (15 µM). (F-F'') WAF, warfarin (30 µM). (G-G'') SA, salicylic acid (300 µM). (H-H'') CAF, caffeine (500 µM). (I-I'') MTX, methotrexate (200 µM). Immunohistochemical staining of craniofacial cartilage was performed with anti-coll2 antibody and PNA lectin (D–I), and anti-GFP antibody (D'–I') following the teratogen exposure. Anti-GFP staining was co-merged with the cartilage staining (D''–I''). Control: n = 25, VPA: n = 18, WAF: n = 23, SA: n = 16, CAF: n = 31, MTX: n = 26. Bracket indicates the lower jaw of zebrafish. Dashed lines indicate outline of the palate. All images were taken from ventral view. m, Meckel's cartilage; p, palate; pq, palatoquadrate. Scale bar: 100 µm.

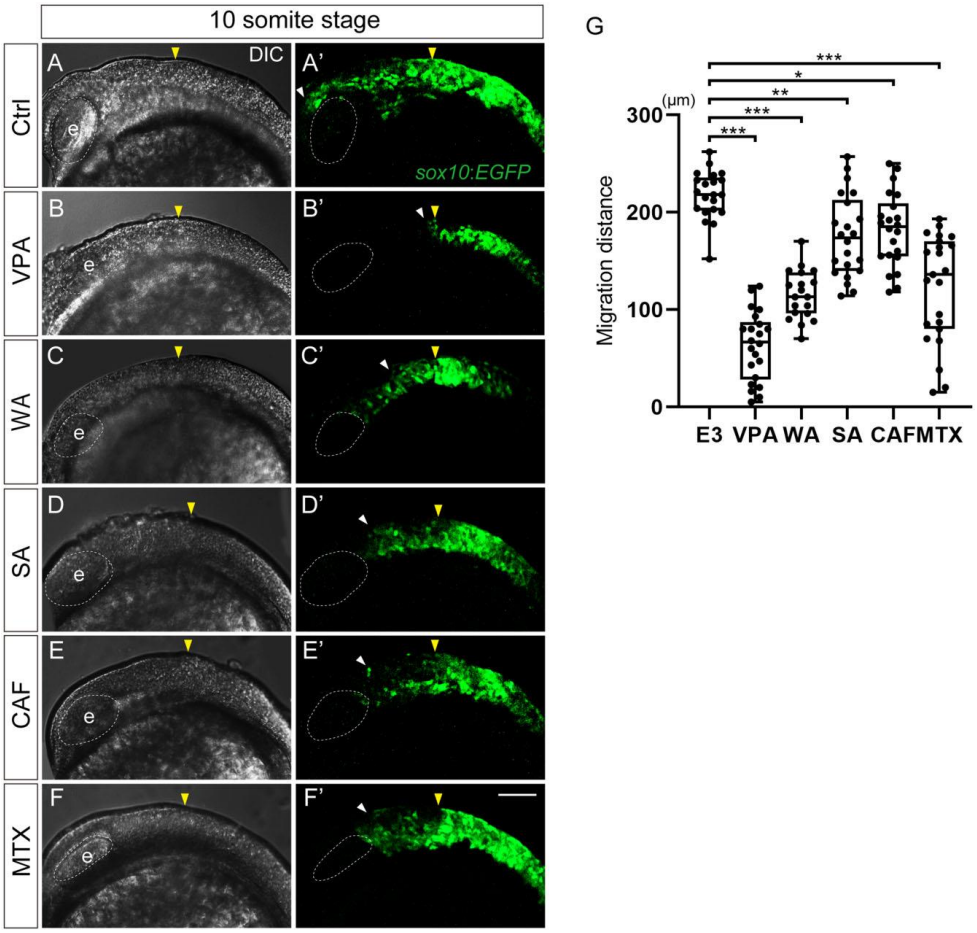

Figure 5. 9 CNCC migration was inhibited in teratogen-treated *sox10:EGFP* embryos.
(A–F') Migratory CNCCs were visualized in *sox10:EGFP* embryos at 10 ss. The yellow arrowheads show the position of the midbrain-hindbrain boundary (MBH). The white arrowheads represent the anterior border of the migratory CNCCs. All teratogens inhibited CNCC migration. (G) Quantification of the distance between the MHB (yellow arrowheads) and the anterior border of the migratory CNCCs via the frontonasal pathway (white arrowheads). Control: n = 21, VPA: n = 22 , WA: n = 19, SA: n = 22, CAF: n = 22, MTX: n = 23. *P < 0.05, **P < 0.01, ***P < 0.001 (one-way ANOVA followed by Dunnett's multiple comparison test) e: eye. Scale bars: 100 μm.

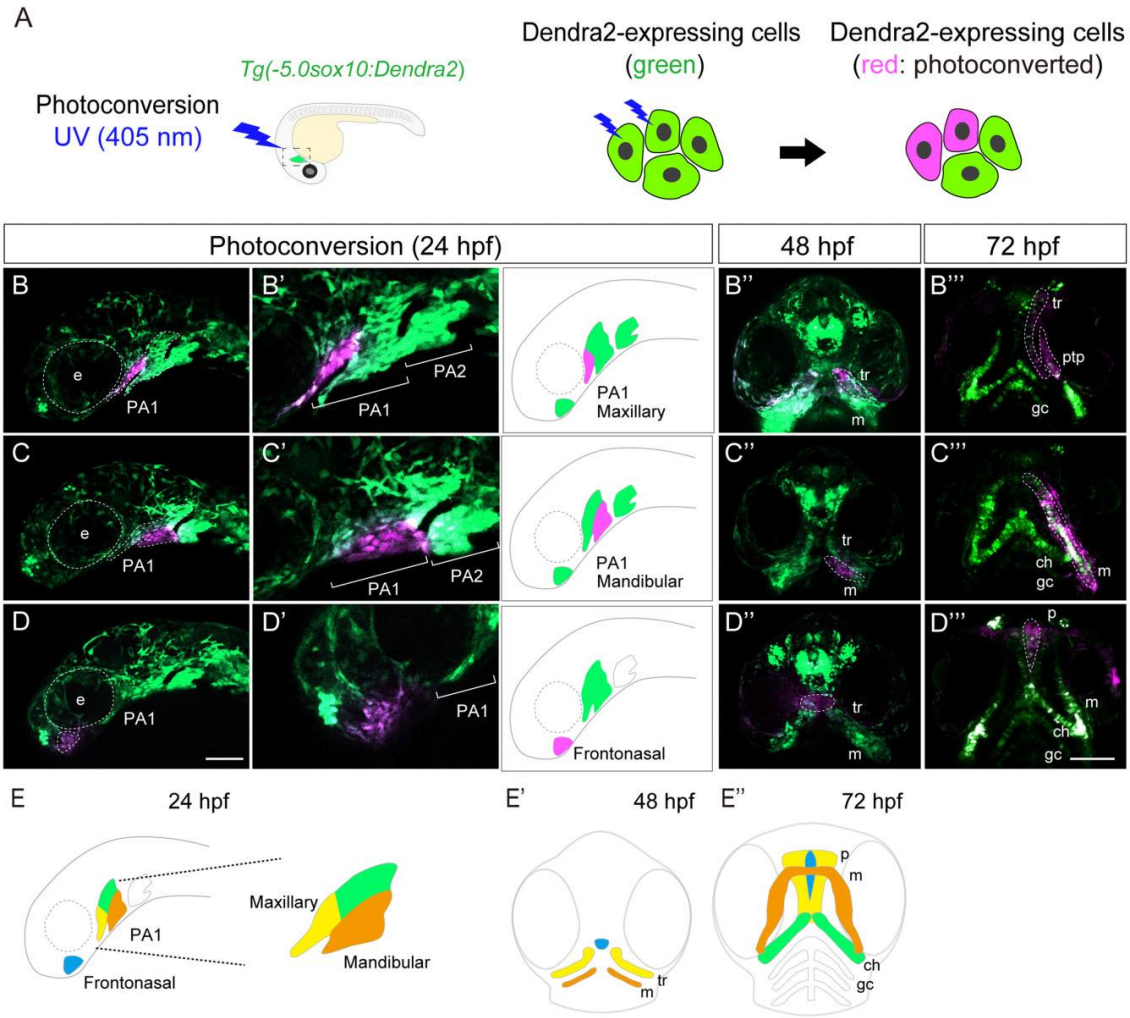
A
Tg(-5.0sox10:Dendra2)
Photoconversion
UV (405 nm)
Dendra2-expressing cells
(green)
Dendra2-expressing cells
(red: photoconverted)
Photoconversion (24 hpf)
48 hpf
72 hpf
B
B'
B''
B'''
C
C'
C''
C'''
D
D'
D''
D'''
e
PA1
PA2
tr
ptp
gc
m
ch
p
PA1
Maxillary
PA1
Mandibular
Frontonasal
E
24 hpf
E'
48 hpf
E''
72 hpf
Maxillary
Mandibular
Frontonasal

Figure 5. 10 Lineage tracing of CNCCs in PA1 and frontonasal prominence using *sox10:Dendra2*. (A) Photoconversion was performed in *sox10:Dendra2* transgenic zebrafish. Photoconvertible fluorescent protein Dendra2 is photoactivated by UV light (405 nm) from green to red. Specific Dendra2-expressing cells were labeled irreversibly and traced. (B–D’’’) Lineage tracing of the PA1 components: maxillary prominence (B, B’), mandibular prominence (C, C’), and frontonasal prominence (D, D’). Magnified view of the photoconverted each prominence was displayed in panel B’, C’ and D’. (B–B’’’) The maxillary prominence was labeled at 24 hpf and differentiated into lateral part of the ethmoid plate (zebrafish palate) and the pterygoid process (ptp), which is the upper jaw at 72 hpf. (C–C’’’) The mandibular prominence was labeled at 24 hpf and differentiated into Meckel’s cartilage of the lower jaw. (D–D’’’) The frontonasal prominence was labeled at 24 hpf and differentiated into the medial part of the palate at 72 hpf. (E–E’’) The schematic diagram of the lineage tracing of the PA1 and frontonasal prominence. Each color in the panel E represents the following: yellow indicates the photoconverted region of the maxillary prominence, orange indicates the photoconverted region of the mandibular prominence, and blue indicates the photoconverted region of the frontonasal prominence. ch, ceratohyal; e, eye; gc, gill cartilages; m, Meckel’s cartilage; mx, maxillary; p, palate; ptp, pterygoid process; tr, trabeculae. Scale bars: 100 μm.

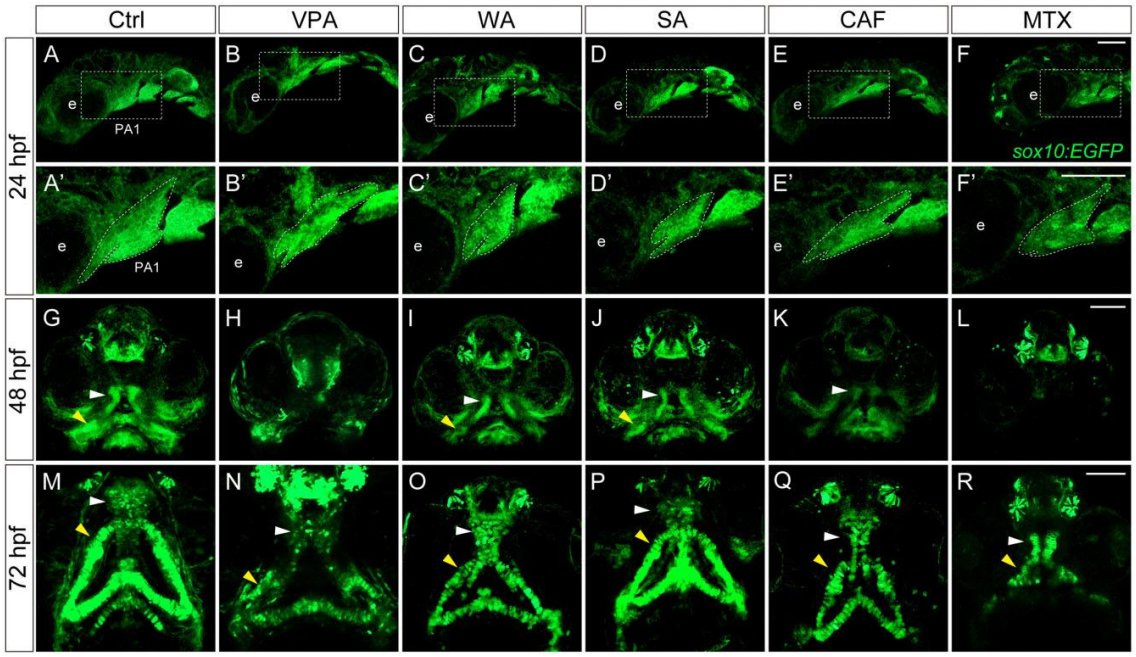

Figure 5. 11 Changes in the morphology of craniofacial anomalies in teratogen-treated *sox10:EGFP* embryos. (A–F) Lateral live view of the first pharyngal arch (PA1) at 24 hpf. (A'–F') Enlarged view of the white rectangle in panel A–F. Abnormal morphology of the PA1 was observed in the teratogen-treated embryos. (G–L) The developing palates (white arrowheads) and mandibles (yellow arrowheads) were disrupted in the teratogen-treated embryos at 48 hpf. (M–R) The PA1 defects resulted in a small-sized palate with clefting (cleft palate) and shortening in the Meckel's cartilage at 72 hpf. e: eye. Scale bars: 100 μm.

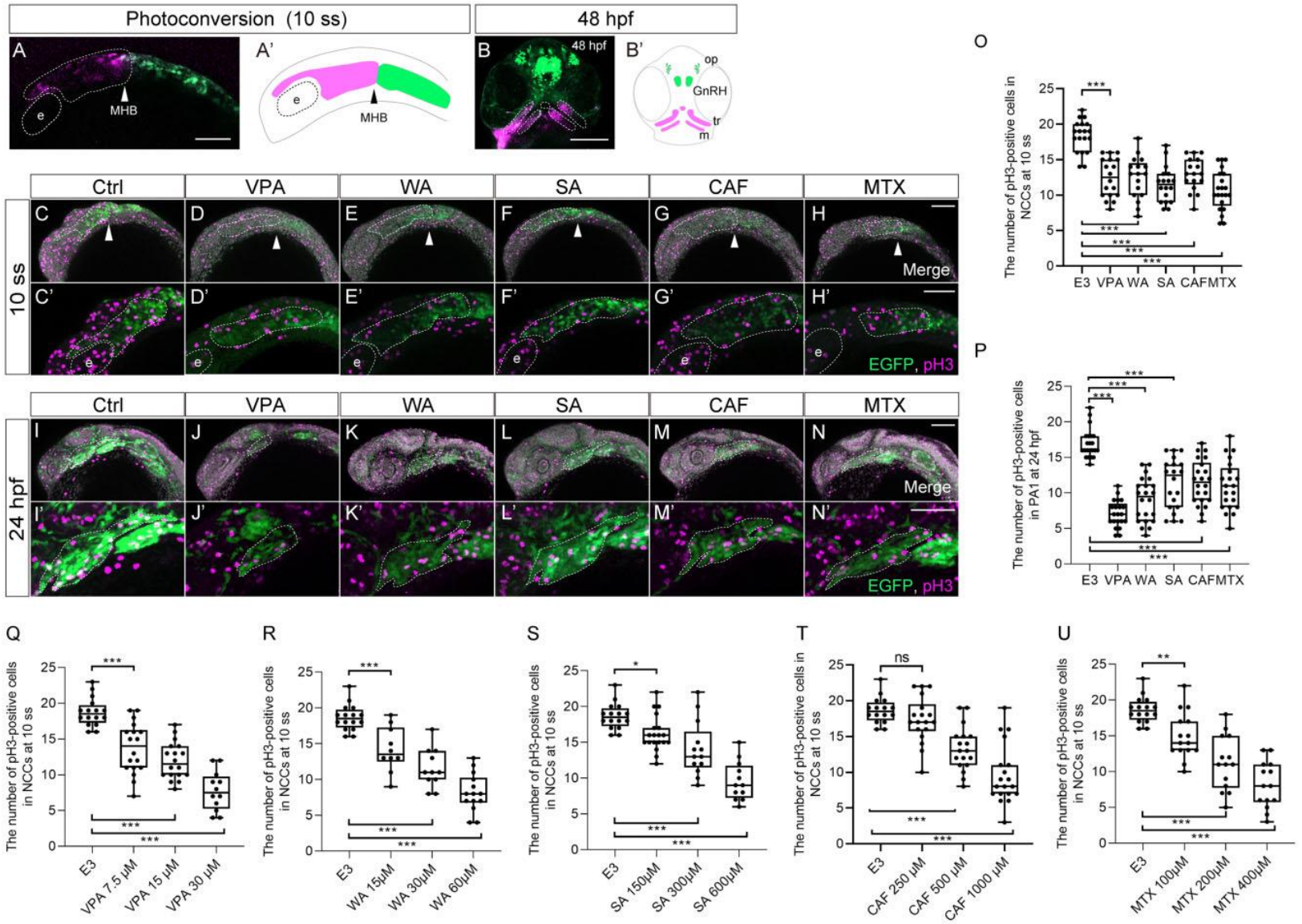
Photoconversion (10 ss)
48 hpf
A
MHB
e
A'
MHB
e
B
48 hpf
B'
op
GnRH
tr
m
Ctrl
VPA
WA
SA
CAF
MTX
10 ss
C
D
E
F
G
H
Merge
C'
D'
E'
F'
G'
H'
EGFP, pH3
24 hpf
I
J
K
L
M
N
Merge
I'
J'
K'
L'
M'
N'
EGFP, pH3
O
The number of pH3-positive cells in NCCs at 10 ss
E3 VPA WA SA CAF MTX
P
The number of pH3-positive cells in PA1 at 24 hpf
E3 VPA WA SA CAF MTX
Q
The number of pH3-positive cells in NCCs at 10 ss
E3
VPA 7.5 μM
VPA 15 μM
VPA 30 μM
R
The number of pH3-positive cells in NCCs at 10 ss
E3
WA 15μM
WA 30μM
WA 60μM
S
The number of pH3-positive cells in NCCs at 10 ss
E3
SA 150μM
SA 300μM
SA 600μM
T
The number of pH3-positive cells in NCCs at 10 ss
ns
E3
CAF 250 μM
CAF 500 μM
CAF 1000 μM
U
The number of pH3-positive cells in NCCs at 10 ss
E3
MTX 100μM
MTX 200μM
MTX 400μM

Figure 5. 12 Cell proliferation was decreased in the migratory and premigratory CNCCs and CNCCs in the PA1 by teratogen treatment. (A, B) The anterior CNCCs (magenta in panel A) were labeled at 10 ss and subsequently differentiated into maxillary (trabeculae), mandibular (Meckel's cartilage) and frontonasal prominence at 48 hpf (magenta in panel B). (A', B') A schematic diagram of the lineage tracing of the anterior CNCCs. Magenta and green indicate the photoconverted region and intact region, respectively. White and black arrowheads in panels A and A' represent the position of the midbrain-hindbrain boundary (MHB). (C–N') Immunofluorescence images of mitotic premigratory and migratory CNCCs at 10 ss (C–H') and 24 hpf (I–N'). VPA-, WA-, SA-, CAF-, and MTX-treated embryos were stained with anti-GFP and anti-phospho-histone H3 (pH3) antibodies. Mitotic premigratory and migratory CNCCs were decreased by teratogen treatment (C–H'). (C'–H') Magnified view of the panels C–H. Mitotic CNCCs in the PA1 were decreased by teratogen treatment. (I'–N') Magnified view of the panels I–N. Green represents the CNCCs at 10 ss and the CNCCs in the PA1 at 24 hpf. Magenta indicates the mitotic cells stained with anti-pH3 antibody. White dotted lines trace the eye, the region of the anterior CNCCs at 10 ss and PA1 at 24 hpf. (O, P) Quantification of the number of pH3-positive CNCCs in the area at 10 ss (O) and PA1 at 24 hpf (P). n = 19 (control), 18 (VPA), 17 (WA), 18 (SA), 17 (CAF), 21 (MTX) in (O). n = 24 (control), 22 (VPA), 23 (WA), 24 (SA), 23 (CAF), 20 (MTX) in (P). (Q-U) Dose-dependent decrease of the mitotic activity. Control: n = 16, VPA (7.5 μM): n = 18, VPA (15 μM): n =18, VPA (30 μM): n = 12, WA (15 μM): n = 10, WA (30 μM): n = 11, WA (60 μM): n = 14, SA (150 μM): n = 19, SA (300 μM): n = 13, SA (600 μM): n = 12, CAF (250 μM): n = 18, CAF (500 μM): n = 18, CAF (1000 μM): n = 19, MTX (100 μM): n = 15, MTX (200 μM): n = 14, MTX (400 μM): n = 14. ***P < 0.001 (one-way ANOVA followed by Dunnett's multiple comparison test). e; eye, GnRH, gonadotropin-releasing hormone neuron; m, Meckel's cartilage; op, olfactory placode, tr; trabeculae. Scale bars: 100 μm.

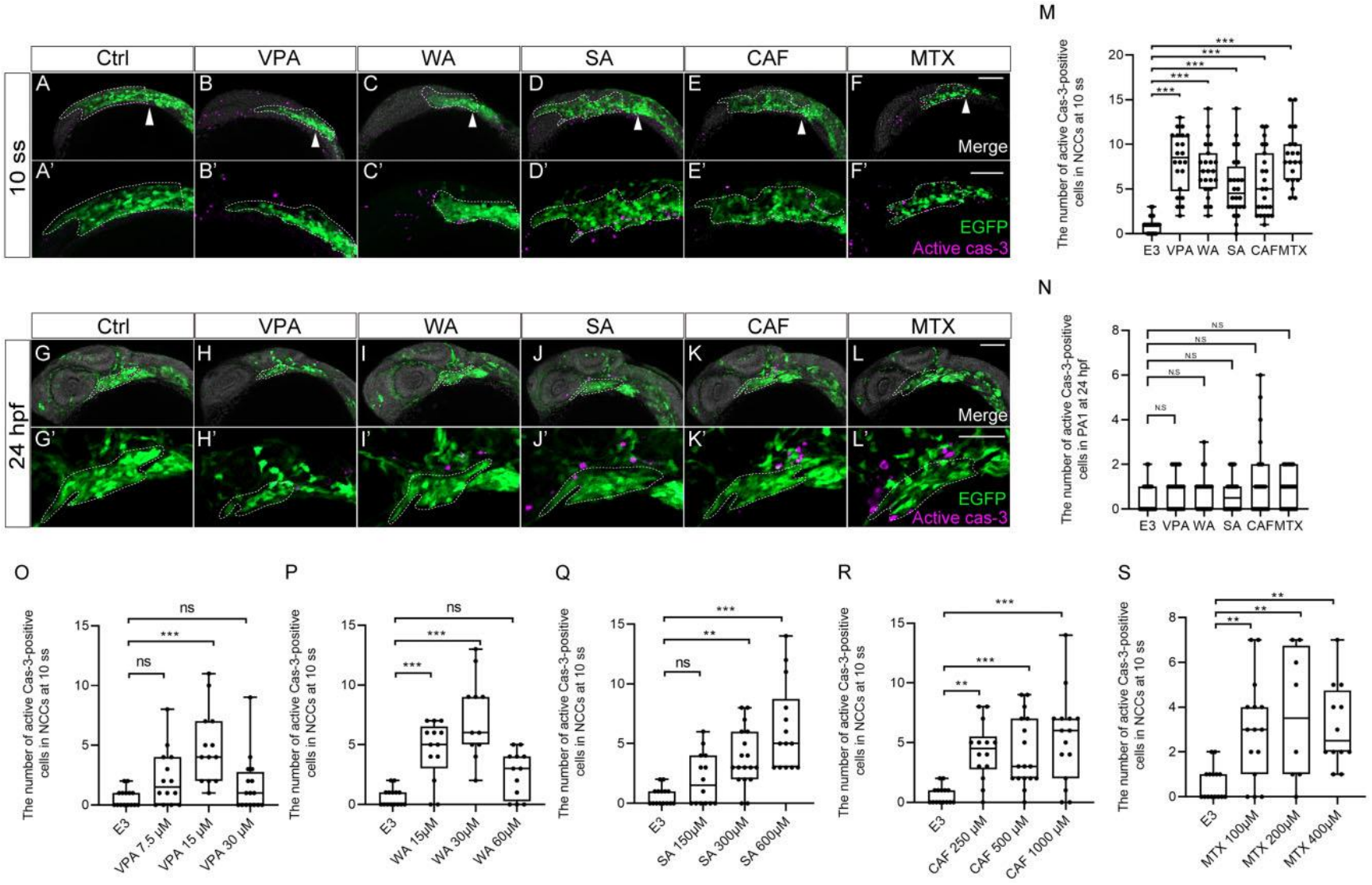
Ctrl
VPA
WA
SA
CAF
MTX
10 ss
24 hpf
Merge
EGFP
Active cas-3
M
N
The number of active Cas-3-positive cells in NCCs at 10 ss
The number of active Cas-3-positive cells in PA1 at 24 hpf
E3 VPA WA SA CAF MTX
O
P
Q
R
S
E3
VPA 7.5 μM
VPA 15 μM
VPA 30 μM
WA 15μM
WA 30μM
WA 60μM
SA 150μM
SA 300μM
SA 600μM
CAF 250 μM
CAF 500 μM
CAF 1000 μM
MTX 100μM
MTX 200μM
MTX 400μM
ns
N.S

Figure 5. 13 Apoptosis was increased in premigratory and migratory CNCCs , but not in CNCCs in PA1. (A–L') Immunofluorescence images of VPA, WA, SA, CAF, and MTX-treated embryos that were stained with anti-active caspase 3 (Active cas-3) and anti-GFP antibody at 10 ss (A–F') and 24 hpf (G–L'). (A–F') Apoptosis in premigratory and migratory CNCCs was increased by teratogen treatment. White arrowheads indicate the midbrain-hindbrain boundary. (A'–F') Magnified view of the panels A–F. (G–L) Apoptotic CNCCs in PA1 were not significantly increased by teratogen treatment. (G'–L') Magnified view of the panels G–L. Green represents the premigratory and migratory CNCCs at 10 ss and the CNCCs in the PA1 at 24 hpf. Magenta indicates the apoptotic CNCCs stained with anti-Active cas-3 antibody. White dotted lines trace the eye and the region of the anterior CNCCs at 10 ss and PA1 at 24 hpf. (M, N) Quantitation of the number of active cas-3-positive CNCCs at 10 ss (M) and PA1 at 24 hpf (N). n = 22 (control), 21 (VPA), 22 (WA), 20 (SA), 22 (CAF), 21 (MTX) in (M). n = 25 (control), 23 (VPA), 20 (WA), 23 (SA), 22 (CAF), 23 (MTX) in (N). (O-S) Dose-dependent increase of apoptotic cells. Control: n = 15, VPA (7.5 μM): n = 14, VPA (15 μM): n =13, VPA (30 μM): n = 16, WA (15 μM): n = 13, WA (30 μM): n = 11, WA (60 μM): n = 12, SA (150 μM): n = 14, SA (300 μM): n = 18, SA (600 μM): n = 14, CAF (250 μM): n = 14, CAF (500 μM): n = 17, CAF (1000 μM): n = 15, MTX (100 μM): n = 15, MTX (200 μM): n = 8, MTX (400 μM): n = 12. ***P < 0.001 (one-way ANOVA followed by Dunnett's multiple comparison test). e: eye. Scale bars: 100 μm.

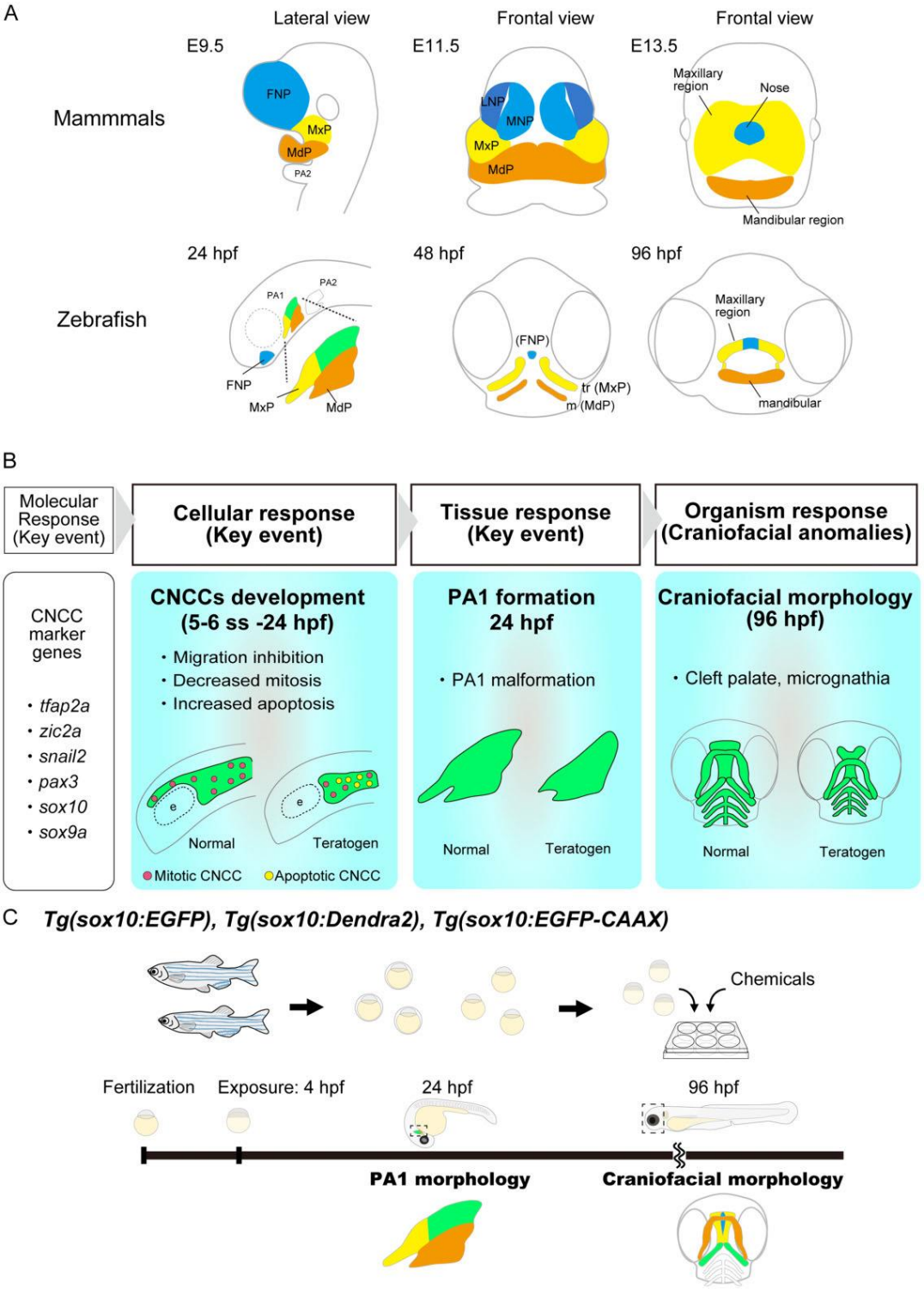
A
Lateral view
Frontal view
Frontal view
E9.5
E11.5
E13.5
Mammmals
FNP
MxP
MdP
PA2
LNP
MNP
MxP
MdP
Maxillary region
Nose
Mandibular region
24 hpf
48 hpf
96 hpf
Zebrafish
PA1
PA2
FNP
MxP
MdP
(FNP)
tr (MxP)
m (MdP)
Maxillary region
mandibular
B
Molecular Response (Key event)
Cellular response (Key event)
Tissue response (Key event)
Organism response (Craniofacial anomalies)
CNCC marker genes
• tfap2a
• zic2a
• snail2
• pax3
• sox10
• sox9a
CNCCs development (5-6 ss -24 hpf)
• Migration inhibition
• Decreased mitosis
• Increased apoptosis
e
e
Normal
Teratogen
Mitotic CNCC
Apoptotic CNCC
PA1 formation 24 hpf
• PA1 malformation
Normal
Teratogen
Craniofacial morphology (96 hpf)
• Cleft palate, micrognathia
Normal
Teratogen
C
Tg(sox10:EGFP), Tg(sox10:Dendra2), Tg(sox10:EGFP-CAAX)
Chemicals
Fertilization
Exposure: 4 hpf
24 hpf
96 hpf
PA1 morphology
Craniofacial morphology

Figure 5. 14 Conserved craniofacial morphogenesis during the pharyngeal stage and the AOP of craniofacial anomalies identified in the present study. (A) Schematic comparison of craniofacial morphogenesis between mammals (mouse) and zebrafish. Zebrafish and mammals share conserved craniofacial morphogenesis. At the pharyngeal stage, the frontonasal prominence (FNP), maxillary prominence (MxP) and mandibular prominence (MdP) are formed in both species. FNP and each region in the PA1 differentiate into craniofacial elements. (B) Identified AOP of chemical-induced craniofacial anomalies. (C) AOP-based teratogenicity assay utilizing the sox10 transgenic lines. PA1 morphology at 24 hpf and craniofacial morphology at 96 hpf are practical endpoints of teratogenicity evaluation and prediction.

Chapter 6: Conclusion and Future Directions

6.1 Summary of Research Findings

In the present study, our primary focus was on advancing our understanding of carcinogenicity and developmental toxicity, with the ultimate goal of developing alternative evaluation methods rooted in AOPs. We made significant progress in elucidating the mechanisms behind these critical aspects of safety assessment.

6.1.1 Carcinogenicity Investigation and Technological Development.

Carcinogenic mechanisms are influenced by both genetic and nongenetic factors. Importantly, we addressed a gap in our understanding of nongenetic carcinogenicity by focusing on liver hypertrophy, a common initial change observed in hepatic carcinogenesis. Through toxicogenomic analysis, we identified oxidative stress and factors related to lipid metabolism as key contributors to carcinogenic liver hypertrophy. Genes such as *Gpx2* and *Acot1* emerged as valuable markers for distinguishing between adaptive liver hypertrophy and hypertrophic liver carcinogenesis, offering insights into the molecular events underpinning hepatic carcinogenesis.

6.1.2 Reproductive and Developmental Toxicity Investigation and Technological Development.

Reproductive and developmental toxicity assessment faces challenges in standardizing alternative test methods. To address these challenges, we concentrated on craniofacial malformations, a major target of teratogenic substances. We discovered a conserved AOPs across mammals and zebrafish, linking teratogenic exposure to craniofacial abnormalities. In alignment with animal welfare principles, we developed an alternative test method using zebrafish embryos. Our findings highlighted that abnormal development and differentiation of neural crest cells are the fundamental causes of craniofacial abnormalities due to teratogenic substances. We also developed the transgenic zebrafish to visualize neural crest cells, providing a means to predict and assess craniofacial abnormalities. This approach offers a valuable tool for evaluating teratogenic potential.

6.2 Limitations and Challenges of the Study

Despite our significant findings, our research does have limitations and challenges. One limitation is that our focus has primarily been on specific aspects of carcinogenicity and reproductive and developmental toxicity. The AOPs identified may not cover the entire spectrum of toxicities and mechanisms. Additionally, AOPs for nongenetic carcinogenicity and developmental toxicity are still evolving, and more comprehensive AOPs is needed to be identified.

6.3 Future Research Directions

The research presented in this study opens the door to several promising avenues for the future investigation:

Identifying AOPs: Expanding the scope of AOPs for both carcinogenicity and reproductive and developmental toxicity, especially nongenetic mechanisms, will contribute to a more comprehensive understanding of toxicological processes.

Alternative Testing Methods: The development and refinement of alternative testing methods that align with the 3R principles (Reduction, Replacement, Refinement) should remain a key focus to reduce reliance on animal experiments.

Integrated Assessment: Future research could explore the integration of multiple AOPs and their interactions, offering a more holistic view of toxicity outcomes.

Validation and Implementation: It is essential to validate AOPs and alternative testing methods rigorously to ensure their practical use in safety assessment and regulatory contexts.

Continuous Improvement: Continuous improvement and adaptation of AOPs and alternative methods will be required in dependent according to science and technology advance.

In conclusion, our research has contributed to advancing the field of toxicology by shedding light on AOPs and alternative testing methods. These findings are instrumental in enhancing human health, animal welfare, and the efficiency of safety assessments. The future holds opportunities for further discoveries and improvements, making the field of toxicology ever more impactful in safeguarding public and environmental health.

References

Abbott, B.D., Harris, M.W., and Birnbaum, L.S. (1989) Etiology of retinoic acid-induced cleft palate varies with the embryonic stage. *Teratology*, **40**, 533–553.

Achenbach, J.C., Leggiadro, C., Sperker, S.A., Woodland, C., and Ellis, L.D. (2020) Comparison of the zebrafish embryo toxicity assay and the general and behavioral embryo toxicity assay as new approach methods for chemical screening. *Toxics*, **8**, 1–13.

Achilleos, A. and Trainor, P.A. (2015) Mouse Models of Rare Craniofacial Disorders. *Curr. Top. Dev. Biol.*, **115**, 413–458.

Adler, S. *et al.* (2011) Alternative (non-animal) methods for cosmetics testing: current status and future prospects-2010. *Arch Toxicol*, **85**, 367–485.

Ahmed, M.M.E., Wang, T., Luo, Y., Ye, S., Wu, Q., Guo, Z., Roebuck, B.D., Sutter, T.R., and Yang, J.Y. (2011) Aldo-keto reductase-7A protects liver cells and tissues from acetaminophen-induced oxidative stress and hepatotoxicity. *Hepatology*, **54**, 1322–32.

Allen, D.G., Pearse, G., Haseman, J.K., and Maronpot, R.R. (2004) Prediction of rodent carcinogenesis: an evaluation of prechronic liver lesions as forecasters of liver tumors in NTP carcinogenicity studies. *Toxicol. Pathol.*, **32**, 393–401.

Ankley, G.T. *et al.* (2010) Adverse outcome pathways: A conceptual framework to support ecotoxicology research and risk assessment. *Environ. Toxicol. Chem.*, **29**, 730–741.

Aoki, Y., Saint-Germain, N., Gyda, M., Magner-Fink, E., Lee, Y.H., Credidio, C., and Saint-Jeannet, J.P. (2003) Sox10 regulates the development of neural crest-derived melanocytes in Xenopus. *Dev. Biol.*, **259**, 19–33.

Askary, A., Mork, L., Paul, S., Dale, R., Mariani, F. V, Gage, J., and Correspondence, C. (2015) Iroquois Proteins Promote Skeletal Joint Formation by Maintaining Chondrocytes in an Immature State. *Dev. Cell*, **35**, 358–365.

Augustine-Rauch, K., Zhang, C.X., and Panzica-Kelly, J.M. (2016) A Developmental Toxicology Assay Platform for Screening Teratogenic Liability of Pharmaceutical Compounds. *Birth Defects Res. Part B Dev. Reprod. Toxicol.*, **107**, 4–20.

Bambino, K. and Chu, J. (2017) Zebrafish in Toxicology and Environmental Health. *Curr. Top. Dev. Biol.*, **124**, 331–367.

Barnes, J.L., Zubair, M., John, K., Poirier, M.C., and Martin, F.L. (2018) Carcinogens and DNA damage. *Biochem. Soc. Trans.*, **46**, 1213.

Basu, A.K. (2018) DNA Damage, Mutagenesis and Cancer. *Int. J. Mol. Sci. 2018, Vol. 19, Page 970*, **19**, 970.

Beaty, T.H., Marazita, M.L., and Leslie, E.J. (2016) Genetic factors influencing risk to orofacial clefts: Today's challenges and tomorrow's opportunities. *F1000Research*, **5**.

Benigni, R., Bossa, C., and Tcheremenskaia, O. (2013) Nongenotoxic carcinogenicity of chemicals: Mechanisms of action and early recognition through a new set of structural alerts. *Chem. Rev.*, **113**, 2940–2957.

Bentley, P., Calder, I., Elcombe, C., Grasso, P., Stringer, D., and Wiegand, H.J. (1993) Hepatic peroxisome proliferation in rodents and its significance for humans. *Food Chem. Toxicol.*, **31**, 857–907.

Berenguer, M., Darnaudery, M., Claverol, S., Bonneu, M., Lacombe, D., and Rooryck, C. (2018) Prenatal retinoic acid exposure reveals candidate genes for craniofacial disorders. *Sci. Rep.*, **8**, 1–17.

Bermas, B.L. and Hill, J.A. (1995) Effects of immunosuppressive drugs during pregnancy. *Arthritis Rheum.*, **38**, 1722–1732.

Brannen, K.C., Panzica-Kelly, J.M., Danberry, T.L., and Augustine-Rauch, K.A. (2010) Development of a zebrafish embryo teratogenicity assay and quantitative prediction model. *Birth Defects Res. Part B Dev. Reprod. Toxicol.*, **89**, 66–77.

Brannen, K.C., Charlap, J.H., and Lewis, E.M. (2013) Zebrafish teratogenicity testing. *Methods Mol. Biol.*, **947**, 383–401.

Brigelius-Flohé, R. and Kipp, A.P. (2012) Physiological functions of GPx2 and its role in inflammation-triggered carcinogenesis. *Ann. N. Y. Acad. Sci.*, **1259**, 19–25.

Bronner, M.E. and LeDouarin, N.M. (2012) Development and evolution of the neural crest: An overview. *Dev. Biol.*, **366**, 2–9.

Budinsky, R.A. *et al.* (2014) Mode of action and dose-response framework analysis for receptor-mediated toxicity: the aryl hydrocarbon receptor as a case study. *Crit. Rev. Toxicol.*, **44**, 83–119.

Burden, N., Sewell, F., Andersen, M.E., Boobis, A., Chipman, J.K., Cronin, M.T.D., Hutchinson, T.H., Kimber, I., and Whelan, M. (2015) Adverse Outcome Pathways can drive non-animal approaches for safety assessment. *J. Appl. Toxicol.*, **35**, 971.

Bush, J.O. and Jiang, R. (2012) Palatogenesis: morphogenetic and molecular mechanisms of secondary palate development. *Development*, **139**, 231–243.

Bushita, H., Liu, S., Ohta, T., Ito, Y., Saito, K., Nukada, Y., Ikeda, N., and Morita, O. (2018) Effects of dietary alpha-linolenic acid-enriched diacylglycerol oil on embryo/fetal development in rats. *Regul. Toxicol. Pharmacol.*, **98**, 108–114.

Butler, W.H. (1996) A review of the hepatic tumors related to mixed-function oxidase induction in the mouse. *Toxicol. Pathol.*, **24**, 484–492.

Carmichael, N.G., Enzmann, H., Pate, I., and Waechter, F. (1997) The significance of mouse liver tumor formation for carcinogenic risk assement: results and conclusions from a survey of ten years testing by the agrochemical industry. *Environ. Health Perspect.*, **105**, 1196–1203.

Carney, T.J., Dutton, K.A., Greenhill, E., Delfino-Machín, M., Dufourcq, P., Blader, P., and Kelsh, R.N. (2006) A direct role for Sox10 in specification of neural crest-derived sensory neurons. *Development*, **133**, 4619–4630.

Carroll, S.H. *et al.* (2020) An Irf6-Esrp1/2 regulatory axis controls midface morphogenesis in vertebrates. *Dev.*, **147**.

Cattley, R.C. (2004) Peroxisome Proliferators and Receptor-Mediated Hepatic Carcinogenesis. *http://dx.doi.org/10.1080/01926230490451680*, **32**, 6–11.

Clément, A., Wiweger, M., Von Der Hardt, S., Rusch, M.A., Selleck, S.B., Chien, C. Bin, and Roehl, H.H. (2008) Regulation of Zebrafish Skeletogenesis by ext2/dackel and papst1/pinscher. *PLOS Genet.*, **4**, e1000136.

Clouthier, D.E., Garcia, E., and Schilling, T.F. (2010) Regulation of facial morphogenesis by endothelin signaling: Insights from mice and fish. *Am. J. Med. Genet. Part A*, **152 A**, 2962–2973.

Colacci, A., Corvi, R., Ohmori, K., Paparella, M., Serra, S., Da Rocha Carrico, I., Vasseur, P., and Jacobs, M.N. (2023) The Cell Transformation Assay: A Historical Assessment of Current Knowledge of Applications in an Integrated Approach to Testing and Assessment for Non-Genotoxic Carcinogens. *Int. J. Mol. Sci.*, **24**.

Committee on Mutagenicity of Chemicals in Food, Consumer Products and the Environment.

Corton, J.C. *et al.* (2014) Mode of action framework analysis for receptor-mediated toxicity: The peroxisome proliferator-activated receptor alpha (PPARα) as a case study. *Crit. Rev. Toxicol.*, **44**, 1–49.

Corvi, R., Madia, F., Guyton, K.Z., Kasper, P., Rudel, R., Colacci, A., Kleinjans, J., and Jennings, P. (2017) Moving forward in carcinogenicity assessment: Report of an EURL ECVAM/ESTIV workshop. *Toxicol. Vitr.*, **45**, 278–286.

Couly, G.F., Coltey, P.M., and Le Douarin, N.M. (1993) The triple origin of skull in higher vertebrates: a study in quail-chick chimeras. *Development*, **117**, 409–429.

Deng, W., Wang, L., Xiong, Y., Li, J., Wang, Y., Shi, T., and Ma, D. (2015) The novel secretory protein CGREF1 inhibits the activation of AP-1 transcriptional activity and cell proliferation. *Int. J. Biochem. Cell Biol.*, **65**, 32–39.

Dixon, M.J., Marazita, M.L., Beaty, T.H., and Murray, J.C. (2011) Cleft lip and palate: synthesizing genetic and environmental influences. *Nat. Rev. Genet.*, **12**, 167.

Le Douarin, N.M., Ziller, C., and Couly, G.F. (1993) Patterning of Neural Crest Derivatives in the Avian Embryo: in Vivo and in Vitro Studies. *Dev. Biol.*, **159**, 24–49.

Dougherty, M., Kamel, G., Shubinets, V., Hickey, G., Grimaldi, M., and Liao, E.C. (2012) Embryonic fate map of first pharyngeal arch structures in the sox10: Kaede zebrafish transgenic model. *J. Craniofac. Surg.*, **23**, 1333–1337.

Drerup, C.M., Wiora, H.M., Topczewski, J., and Morris, J.A. (2009) Disc1 regulates foxd3 and sox10 expression, affecting neural crest migration and differentiation. *Development*, **136**, 2623–2632.

Eberhart, J.K. *et al.* (2008) MicroRNA Mirn140 modulates Pdgf signaling during palatogenesis. *Nat. Genet.*, **40**, 290–298.

Edison, R. and Muenke, M. (2003) The interplay of genetic and environmental factors in craniofacial morphogenesis: holoprosencephaly and the role of cholesterol. *Congenit. Anom. (Kyoto).*, **43**, 1–21.

Elcombe, C.R. *et al.* (2014) Mode of action and human relevance analysis for nuclear receptor-mediated liver toxicity: a case study with phenobarbital as a model constitutive androstane receptor (CAR) activator. *Crit. Rev. Toxicol.*, **44**, 64–82.

Etchevers, H.C., Dupin, E., and Le Douarin, N.M. (2019) The diverse neural crest: From embryology to human pathology. *Dev.*, **146**.
Frankish, H. (2003) 15 million new cancer cases per year by 2020, says WHO. *Lancet*, **361**, 1278.
Fu, J. and Taubman, M.B. (2013) EGLN3 inhibition of NF-κB is mediated by prolyl hydroxylase-independent inhibition of IκB kinase γ ubiquitination. *Mol. Cell. Biol.*, **33**, 3050–61.
Fujii, T., Sasaki, H., and Nishimura, H. (1969) Teratogenicity of caffeine in mice related to its mode of administration. *Jpn. J. Pharmacol.*, **19**, 134–138.
Fung, V.A., Barrett, J.C., and Huff, J. (1995) The carcinogenesis bioassay in perspective: application in identifying human cancer hazards. *Environ. Health Perspect.*, **103**, 680.
El Gendy, M.M., Kandil, A.M., Helal, M.A., and Zahou, F.M. (2015) The teratogenic effects of imatinib mesylate on rat fetuses. *Toxicol. Reports*, **2**, 654–663.
Gilbert, D. and Goldberg, L. (1965) Liver response tests. III. Liver enlargement and stimulation of microsomal processing enzyme activity. *Food Cosmet. Toxicol.*, **3**, 417–432.
Graham, A. (2001) The development and evolution of the pharyngeal arches. *J. Anat.*, **199**, 133–141.
Graham, A. and Richardson, J. (2012) Developmental and evolutionary origins of the pharyngeal apparatus. *Evodevo*, **3**.
Groh, K.J. *et al.* (2015) Development and application of the adverse outcome pathway framework for understanding and predicting chronic toxicity: II. A focus on growth impairment in fish. *Chemosphere*, **120**, 778–792.
Gundacker, C. and Ellinger, I. (2020) The unique applicability of the human placenta to the Adverse Outcome Pathway (AOP) concept: the placenta provides fundamental insights into human organ functions at multiple levels of biological organization. *Reprod. Toxicol.*, **96**, 273–281.
Gusenleitner, D., Auerbach, Scott S, Melia, T., Gómez, H.F., Sherr, D.H., and Monti, S. (2014) Genomic models of short-term exposure accurately predict long-term chemical carcinogenicity and identify putative mechanisms of action. *PLoS One*, **9**, e102579.
Gusenleitner, D., Auerbach, Scott S., Melia, T., Gómez, H.F., Sherr, D.H., and Monti, S. (2014) Genomic Models of Short-Term Exposure Accurately Predict Long-Term Chemical Carcinogenicity and Identify Putative Mechanisms of Action. *PLoS One*, **9**, e102579.
Habib, Z. (1978) Factors determining occurrence of cleft lip and cleft palate. *Surg. Gynecol. Obstet.*, **146**, 105–110.
Hall, A.P. *et al.* (2012) Liver Hypertrophy: a review of adaptive (adverse and non-adverse) changes-conclusions from the 3rd International ESTP expert workshop. *Toxicol. Pathol.*, **40**, 971–994.
Hammond, N.L. and Dixon, M.J. (2022) Revisiting the embryogenesis of lip and palate development. *Oral Dis.*, **28**, 1306–1326.
Hareng, L., Pellizzer, C., Bremer, S., Schwarz, M., and Hartung, T. (2005) The integrated project ReProTect: a novel approach in reproductive toxicity hazard assessment. *Reprod. Toxicol.*, **20**, 441–452.
Hayashi, M. (2022) Opinion: regulatory genotoxicity: past, present and future. *Genes Environ.*, **44**, 1–6.
He, J.H., Gao, J.M., Huang, C.J., and Li, C.Q. (2014) Zebrafish models for assessing developmental and reproductive toxicity. *Neurotoxicol. Teratol.*, **42**, 35–42.
Hernández, L.G., van Steeg, H., Luijten, M., and van Benthem, J. (2009) Mechanisms of non-genotoxic carcinogens and importance of a weight of evidence approach. *Mutat. Res. Mutat. Res.*, **682**, 94–109.
Hernández, L.G., Mennes, | W C, and Van Benthem, | J (2010) Toxicogenomics in carcinogenicity hazard assessment.
HILL, L.M. and KLEINBERG, F. (1984a) Effects of Drugs and Chemicals on the Fetus and Newborn (First of Two Parts). *Mayo Clin. Proc.*, **59**, 707–716.
HILL, L.M. and KLEINBERG, F. (1984b) Effects of Drugs and Chemicals on the Fetus and Newborn (Second of Two Parts). *Mayo Clin. Proc.*, **59**, 755–765.
Hockman, D. *et al.* (2019) A genome-wide assessment of the ancestral neural crest gene regulatory network. *Nat. Commun. 2019 101*, **10**, 1–15.
Hoerl, A.E. and Kennard, R.W. (2000) Ridge Regression: Biased Problems Nonorthogonal Estimation for. *Technometrics*, **42**, 80–86.
Hoke, R.A. and Ankley, G.T. (2005) Application of frog embryo teratogenesis assay-Xenopus to ecological risk assessment. *Environ. Toxicol. Chem.*, **24**, 2677–2690.
Huang, R. and Zhou, P.K. (2021) DNA damage repair: historical perspectives, mechanistic pathways and clinical translation for targeted cancer therapy. *Signal Transduct. Target. Ther. 2021 61*, **6**, 1–35.

Hyoun, S.C., Običan, S.G., and Scialli, A.R. (2012) Teratogen update: Methotrexate. *Birth Defects Res. Part A Clin. Mol. Teratol.*, **94**, 187–207.
Igarashi, Y., Nakatsu, N., Yamashita, T., Ono, A., Ohno, Y., Urushidani, T., and Yamada, H. (2015) Open TG-GATEs: A large-scale toxicogenomics database. *Nucleic Acids Res.*, **43**, D921–D927.
Inoue, A. *et al.* (2016) Comparative study of the zebrafish embryonic toxicity test and mouse embryonic stem cell test to screen developmental toxicity of human pharmaceutical drugs. *Fundam. Toxicol. Sci.*, **3**, 79–87.
Irie, N. and Kuratani, S. (2011) Comparative transcriptome analysis reveals vertebrate phylotypic period during organogenesis. *Nat. Commun. 2011 21*, **2**, 1–8.
Jacobs, M.N. *et al.* (2020) Chemical carcinogen safety testing: OECD expert group international consensus on the development of an integrated approach for the testing and assessment of chemical non-genotoxic carcinogens. *Arch. Toxicol.*, **94**, 2899–2923.
Jentink, J., Loane, M.A., Dolk, H., Barisic, I., Garne, E., Morris, J.K., and de Jong-van den Berg, L.T.W. (2010) Valproic Acid Monotherapy in Pregnancy and Major Congenital Malformations. *N. Engl. J. Med.*, **362**, 2185–2193.
Kamel, G., Hoyos, T., Rochard, L., Dougherty, M., Kong, Y., Tse, W., Shubinets, V., Grimaldi, M., and Liao, E.C. (2013) Requirement for frzb and fzd7a in cranial neural crest convergence and extension mechanisms during zebrafish palate and jaw morphogenesis. *Dev. Biol.*, **381**, 423–433.
Kee, Y. and Bronner-Fraser, M. (2005) To proliferate or to die: role of Id3 in cell cycle progression and survival of neural crest progenitors. *Genes Dev.*, **19**, 744–755.
Kimmel, C.B., Miller, C.T., Kruze, G., Ullmann, B., Bremiller, R.A., Larison, K.D., and Snyder, H.C. (1998) The Shaping of Pharyngeal Cartilages during Early Development of the Zebrafish. *Dev. Biol.*, **203**, 245–263.
Knapen, D., Vergauwen, L., Villeneuve, D.L., and Ankley, G.T. (2015) The potential of AOP networks for reproductive and developmental toxicity assay development. *Reprod. Toxicol.*, **56**, 52–55.
Knight, R.D., Nair, S., Nelson, S.S., Afshar, A., Javidan, Y., Geisler, R., Rauch, G.J., and Schilling, T.F. (2003) lockjaw encodes a zebrafish tfap2a required for early neural crest development. *Development*, **130**, 5755–5768.
Knudsen, T.B., Pierro, J.D., and Baker, N.C. (2021) Retinoid signaling in skeletal development: Scoping the system for predictive toxicology. *Reprod. Toxicol.*, **99**, 109–130.
Knudsen, T.B. and Kleinstreuer, N.C. (2011) Disruption of embryonic vascular development in predictive toxicology. *Birth Defects Res. Part C Embryo Today Rev.*, **93**, 312–323.
Konstandi, M., Shah, Y.M., Matsubara, T., and Gonzalez, F.J. (2013) Role of PPARα and HNF4α in stress-mediated alterations in lipid homeostasis. *PLoS One*, **8**, e70675.
Kozhemyakina, E., Lassar, A.B., and Zelzer, E. (2015) A pathway to bone: signaling molecules and transcription factors involved in chondrocyte development and maturation. *Development*, **142**, 817–831.
Kulesa, P., Ellies, D.L., and Trainor, P.A. (2004) Comparative analysis of neural crest cell death, migration, and function during vertebrate embryogenesis. *Dev. Dyn.*, **229**, 14–29.
Kuratani, S. (2005) Craniofacial development and the evolution of the vertebrates: The old problems on a new background. *Zoolog. Sci.*, **22**, 1–19.
Lan, Y., Xu, J., and Jiang, R. (2015) Cellular and Molecular Mechanisms of Palatogenesis. *Curr. Top. Dev. Biol.*, **115**, 59.
Laurencikiene, J., Stenson, B.M., Nordström, E.A., Agustsson, T., Langin, D., Isaksson, B., Permert, J., Rydén, M., and Arner, P. (2008) Evidence for an important role of CIDEA in human cancer cachexia. *Cancer Res.*, **68**, 9247–9254.
Leung, V.Y.L. *et al.* (2011) SOX9 Governs Differentiation Stage-Specific Gene Expression in Growth Plate Chondrocytes via Direct Concomitant Transactivation and Repression. *PLOS Genet.*, **7**, e1002356.
Li, J., Shi, Y., Sun, J., Zhang, Y., and Mao, B. (2011) Xenopus Reduced Folate Carrier Regulates Neural Crest Development Epigenetically. *PLoS One*, **6**, e27198.
Li, Y., Zhang, X., Hu, T., Han, L., Li, R., Wen, J., and Zhang, M. (2014) Asparagine synthetase expression and its potential prognostic value in patients with NK/T cell lymphoma. *Oncol Rep*, **32**, 853–859.
Lichtenstein, P., Holm, N. V., Verkasalo, P.K., Iliadou, A., Kaprio, J., Koskenvuo, M., Pukkala, E., Skytthe, A., and Hemminki, K. (2000) Environmental and heritable factors in the causation of cancer--analyses of cohorts of twins from Sweden, Denmark, and Finland. *N. Engl. J. Med.*, **343**,

78–85.
Liebelt, E.L. *et al.* (2007) NTP-CERHR Expert Panel Report on the reproductive and developmental toxicity of hydroxyurea. *Birth Defects Res. Part B Dev. Reprod. Toxicol.*, **80**, 259–366.
Ling, I.T., Rochard, L., and Liao, E.C. (2017) Distinct requirements of wls, wnt9a, wnt5b and gpc4 in regulating chondrocyte maturation and timing of endochondral ossification. *Dev. Biol.*, **421**, 219–232.
Liu, S., Narumi, R., Ikeda, N., Morita, O., and Tasaki, J. (2020) Chemical-induced craniofacial anomalies caused by disruption of neural crest cell development in a zebrafish model. *Dev. Dyn.*, **249**, 794–815.
Lumsden, A., Sprawson, N., and Graham, A. (1991) Segmental origin and migration of neural crest cells in the hindbrain region of the chick embryo. *Development*, **113**, 1281–1291.
Ma, Z. lai, Wang, G., Cheng, X., Chuai, M., Kurihara, H., Lee, K.K.H., and Yang, X. (2014) Excess caffeine exposure impairs eye development during chick embryogenesis. *J. Cell. Mol. Med.*, **18**, 1134.
Maronpot, R.R., Yoshizawa, K., Nyska, A., Harada, T., Flake, G., Mueller, G., Singh, B., and Ward, J.M. (2010) Hepatic enzyme induction: histopathology. *Toxicol. Pathol.*, **38**, 776–795.
Matsumoto, H. *et al.* (2009) Discrimination of carcinogens by hepatic transcript profiling in rats following 28-day administration. *Cancer Inform.*, **7**, 253–269.
Mattison, D.R. (2010) Environmental Exposures and Development. *Curr. Opin. Pediatr.*, **22**, 208.
McKeown, S.J., Lee, V.M., Bronner-Fraser, M., Newgreen, D.F., and Farlie, P.G. (2005) Sox10 overexpression induces neural crest-like cells from all dorsoventral levels of the neural tube but inhibits differentiation. *Dev. Dyn.*, **233**, 430–444.
Meulemans, D. and Bronner-Fraser, M. (2004) Gene-Regulatory Interactions in Neural Crest Evolution and Development. *Dev. Cell*, **7**, 291–299.
Minchin, J.E.N. and Hughes, S.M. (2008) Sequential actions of Pax3 and Pax7 drive xanthophore development in zebrafish neural crest. *Dev. Biol.*, **317**, 508–522.
Mork, L. and Crump, G. (2015) Zebrafish Craniofacial Development: A Window into Early Patterning. *Curr. Top. Dev. Biol.*, **115**, 235–269.
Nagahori, H., Suzuki, N., Le Coz, F., Omori, T., and Saito, K. (2016) Prediction of in vivo developmental toxicity by combination of Hand1-Luc embryonic stem cell test and metabolic stability test with clarification of metabolically inapplicable candidates. *Toxicol. Lett.*, **259**, 44–51.
Nagata, K., Washio, T., Kawahara, Y., and Unami, A. (2014) Toxicity prediction from toxicogenomic data based on class association rule mining. *Toxicol. Reports*, **1**, 1133–1142.
Narumi, R., Liu, S., Ikeda, N., Morita, O., and Tasaki, J. (2020) Chemical-Induced Cleft Palate Is Caused and Rescued by Pharmacological Modulation of the Canonical Wnt Signaling Pathway in a Zebrafish Model. *Front. cell Dev. Biol.*, **8**, 592967.
National Research Council . ed. (2011) The Guide for the Care and Use of Laboratory Animals 8th ed. Washington: National Academies Press.
Nishimura, Y., Inoue, A., Sasagawa, S., Koiwa, J., Kawaguchi, K., Kawase, R., Maruyama, T., Kim, S., and Tanaka, T. (2016) Using zebrafish in systems toxicology for developmental toxicity testing. *Congenit. Anom. (Kyoto).*, **56**, 18–27.
Peng, C. *et al.* (2014) A critical role for ZDHHC2 in metastasis and recurrence in human hepatocellular carcinoma. *Biomed Res. Int.*, **2014**, 832712.
Peters, J.M., Cattley, R.C., and Gonzalez, F.J. (1997) Role of PPAR alpha in the mechanism of action of the nongenotoxic carcinogen and peroxisome proliferator Wy-14,643. *Carcinogenesis*, **18**, 2029–2033.
Piersma, A.H. *et al.* (2022) Pluripotent stem cell assays: Modalities and applications for predictive developmental toxicity. *Curr. Res. Toxicol.*, **3**, 100074.
Plant, N. and Aouabdi, S. (2009) Nuclear receptors: the controlling force in drug metabolism of the liver? *Xenobiotica*, **39**, 597–605.
Poswillo, D. (1988) The aetiology and pathogenesis of craniofacial deformity. *Development*, **103 Suppl**, 207–212.
Price, Catherine J, Marr, Melissa C, Myers, C.B., Seely, J.C., Heindel, J.J., Schwetzt', B.A., Price, C J, and Marr, M C (1996) North Carolina 27709; and tDevelopmental and Reproductive Toxicology Group, National Toxicology Program. *Fundam. Appl. Toxicol.*, **34**, 176–187.
R??mer, M., Eichner, J., Metzger, U., Templin, M.F., Plummer, S., Ellinger-Ziegelbauer, H., and Zell, A. (2014) Cross-platform toxicogenomics for the prediction of non-genotoxic hepatocarcinogenesis in

rat. *PLoS One*, **9**, e97640.
Rada-Iglesias, A., Bajpai, R., Prescott, S., Brugmann, S.A., Swigut, T., and Wysocka, J. (2012) Epigenomic annotation of enhancers predicts transcriptional regulators of human neural crest. *Cell Stem Cell*, **11**, 633–648.
Rao, A. and LaBonne, C. (2018) Histone deacetylase activity has an essential role in establishing and maintaining the vertebrate neural crest. *Dev.*, **145** (15):dev163386 .
Rätsch, G., Sonnenburg, S., and Schäfer, C. (2006) Learning interpretable SVMs for biological sequence classification. *BMC Bioinformatics*, **7 Suppl 1**, S9.
Roberts, N.J., Vogelstein, J.T., Parmigiani, G., Kinzler, K.W., Vogelstein, B., and Velculescu, V.E. (2012) The Predictive Capacity of Personal Genome Sequencing. *Sci. Transl. Med.*, **4**, 133ra58.
Rocha, M., Singh, N., Ahsan, K., Beiriger, A., and Prince, V.E. (2020) Neural crest development: Insights from the zebrafish. *Dev. Dyn.*, **249**, 88.
Rochard, L., Monica, S.D., Ling, I.T.C., Kong, Y., Roberson, S., Harland, R., Halpern, M., and Liao, E.C. (2016) Roles of Wnt pathway genes wls, wnt9a, wnt5b, frzb and gpc4 in regulating convergent-extension during zebrafish palate morphogenesis. *Dev.*, **143**, 2541–2547.
Römer, M., Eichner, J., Metzger, U., Templin, M.F., Plummer, S., Ellinger-Ziegelbauer, H., and Zell, A. (2014) Cross-platform toxicogenomics for the prediction of non-genotoxic hepatocarcinogenesis in rat. *PLoS One*, **9**, e97640.
Rowe, V.K., Wolf, M.A., Weil, C.S., and Smyth, H.F. (1959) The toxicological basis of threshold limit values: 2. Pathological and biochemical criteria. *Am. Ind. Hyg. Assoc. J.*, **20**, 346–349.
Ruberte, E., Dolle, P., Chambon, P., and Morriss-Kay, G. (1991) Retinoic acid receptors and cellular retinoid binding proteins : II. Their differential pattern of transcription during early morphogenesis in mouse embryos. *Development*, **111**, 45–60.
Sachana, M., Willett, C., Pistollato, F., and Bal-Price, A. (2021) The potential of mechanistic information organised within the AOP framework to increase regulatory uptake of the developmental neurotoxicity (DNT) in vitro battery of assays. *Reprod. Toxicol.*, **103**, 159–170.
Saili, K.S., Zurlinden, T.J., Schwab, A.J., Silvin, A., Baker, N.C., Hunter, E.S., Ginhoux, F., and Knudsen, T.B. (2017) Blood-brain barrier development: Systems modeling and predictive toxicology. *Birth Defects Res.*, **109**, 1680–1710.
Schilling, T.F. and Kimmel, C.B. (1997) Musculoskeletal patterning in the pharyngeal segments of the zebrafish embryo. *Development*, **124**, 2945–2960.
Scholz, S., Fischer, S., Gündel, U., Küster, E., Luckenbach, T., and Voelker, D. (2008) The zebrafish embryo model in environmental risk assessment - Applications beyond acute toxicity testing. *Environ. Sci. Pollut. Res.*, **15**, 394–404.
Schulte-Hermann, R., Hoffman, V., Parzefall, W., Kallenbach, M., Gerhardt, A., and Schuppler, J. (1980) Adaptive responses of rat liver to the gestagen and anti-androgen cyproterone acetate and other inducers. II. Induction of growth. *Chem. Biol. Interact.*, **31**, 287–300.
Selderslaghs, I.W.T., Blust, R., and Witters, H.E. (2012) Feasibility study of the zebrafish assay as an alternative method to screen for developmental toxicity and embryotoxicity using a training set of 27 compounds. *Reprod. Toxicol.*, **33**, 142–154.
Serbedzija, G.N., Fraser, S.E., and Bronner-Fraser, M. (1990) Pathways of trunk neural crest cell migration in the mouse embryo as revealed by vital dye labelling. *Development*, **108**, 605–612.
Shaw, I.C. and Jones, H.B. (1994) Mechanisms of non-genotoxic carcinogenesis. *Trends Pharmacol. Sci.*, **15**, 89–93.
Sheth, S.S. *et al.* (2006) Hepatocellular carcinoma in Txnip-deficient mice. *Oncogene*, **25**, 3528–3536.
Shwartz, Y., Farkas, Z., Stern, T., Aszódi, A., and Zelzer, E. (2012) Muscle contraction controls skeletal morphogenesis through regulation of chondrocyte convergent extension. *Dev. Biol.*, **370**, 154–163.
Simões-Costa, M. and Bronner, M.E. (2015) Establishing neural crest identity: a gene regulatory recipe. *Development*, **142**, 242–257.
Simões-Costa, M. and Bronner, M.E. (2013) Insights into neural crest development and evolution from genomic analysis. *Genome Res.*, **23**, 1069–1080.
Singh, S., Arcaroli, J., Chen, Y., Thompson, D.C., Messersmith, W., Jimeno, A., and Vasiliou, V. (2015) ALDH1B1 is crucial for colon tumorigenesis by modulating Wnt/β-Catenin, Notch and PI3K/Akt signaling pathways. *PLoS One*, **10**, e0121648.
Sisson, B.E., Dale, R.M., Mui, S.R., Topczewska, J.M., and Topczewski, J. (2015) A role of glypican4 and wnt5b in chondrocyte stacking underlying craniofacial cartilage morphogenesis. *Mech. Dev.*, **138 Pt 3**, 279–290.

Smithells, R.W. and Newman, G.H. (1992) SYNDROME OF THE MONTH Recognition of thalidomide defects. *Med Genet*, **29**, 716–723.
Sokal, R.R., Oden, N.L., Rosenberg, M.S., and Thomson, B.A. (2000) Cancer incidences in Europe related to mortalities, and ethnohistoric, genetic, and geographic distances. *Proc. Natl. Acad. Sci. U. S. A.*, **97**, 6067–6072.
Southard-Smith, E.M., Kos, L., and Pavan, W.J. (1998) Sox10 mutation disrupts neural crest development in Dom Hirschsprung mouse model. *Nat. Genet.*, **18**, 60–64.
Strähle, U. *et al.* (2012) Zebrafish embryos as an alternative to animal experiments--a commentary on the definition of the onset of protected life stages in animal welfare regulations. *Reprod. Toxicol.*, **33**, 128–132.
Suster, M.L., Kikuta, H., Urasaki, A., Asakawa, K., and Kawakami, K. (2009) Transgenesis in Zebrafish with the Tol2 transposon system. *Methods Mol. Biol.*, **561**, 41–63.
Suter, L., Babiss, L.E., and Wheeldon, E.B. (2004) Toxicogenomics in predictive toxicology in drug development. *Chem. Biol.*, **11**, 161–171.
Suzuki, S., Pitchakarn, P., Ogawa, K., Naiki-Ito, A., Chewonarin, T., Punfa, W., Asamoto, M., Shirai, T., and Takahashi, S. (2013) Expression of glutathione peroxidase 2 is associated with not only early hepatocarcinogenesis but also late stage metastasis. *Toxicol.*, **311**, 115–123.
Swartz, M.E., Sheehan-Rooney, K., Dixon, M.J., and Eberhart, J.K. (2011) Examination of a palatogenic gene program in zebrafish. *Dev. Dyn.*, **240**, 2204–2220.
Szabo-Rogers, H.L., Smithers, L.E., Yakob, W., and Liu, K.J. (2010) New directions in craniofacial morphogenesis. *Dev. Biol.*, **341**, 84–94.
Teixidó, E., Kießling, T.R., Krupp, E., Quevedo, C., Muriana, A., and Scholz, S. (2019) Automated Morphological Feature Assessment for Zebrafish Embryo Developmental Toxicity Screens. *Toxicol. Sci.*, **167**, 438–449.
TeSlaa, J.J., Keller, A.N., Nyholm, M.K., and Grinblat, Y. (2013) Zebrafish Zic2a and Zic2b regulate neural crest and craniofacial development. *Dev. Biol.*, **380**, 73–86.
Thoolen, B. *et al.* (2010) Proliferative and nonproliferative lesions of the rat and mouse hepatobiliary system. *Toxicol. Pathol.*, **38**, 5S-81S.
Tibshirani. R (1996) Regression shrinkage and selection via the Lasso. *J. R. Stat. Soc. Ser. B Stat. Methodol.*, **58**, 267–288.
Tollefsen, K.E. *et al.* (2014) Applying Adverse Outcome Pathways (AOPs) to support Integrated Approaches to Testing and Assessment (IATA). *Regul. Toxicol. Pharmacol.*, **70**, 629–640.
Tomatis, L. *et al.* (1997) Avoided and avoidable risks of cancer. *Carcinogenesis*, **18**, 97–105.
Tugwood, J.D., Aldridge, T.C., Lambe, K.G., Macdonald, N., and Woodyatt, N.J. (1996) Peroxisome Proliferator-activated Receptors: Stuctures and Function. *Ann. N. Y. Acad. Sci.*, **804**, 252–265.
Uehara, T. *et al.* (2011) Prediction model of potential hepatocarcinogenicity of rat hepatocarcinogens using a large-scale toxicogenomics database. *Toxicol. Appl. Pharmacol.*, **255**, 297–306.
Villeneuve, D. *et al.* (2014) Investigating Alternatives to the fish early-life stage test: A strategy for discovering and annotating adverse outcome pathways for early fish development. *Environ. Toxicol. Chem.*, **33**, 158–169.
Villeneuve, D.L. *et al.* (2014) Adverse Outcome Pathway (AOP) Development I: Strategies and Principles. *Toxicol. Sci.*, **142**, 312–320.
Wada, N., Javidan, Y., Nelson, S., Carney, T.J., Kelsh, R.N., and Schilling, T.F. (2005) Hedgehog signaling is required for cranial neural crest morphogenesis and chondrogenesis at the midline in the zebrafish skull. *Development*, **132**, 3977–3988.
Watanabe, T. *et al.* (2012) Discrimination of genotoxic and non-genotoxic hepatocarcinogens by statistical analysis based on gene expression profiling in the mouse liver as determined by quantitative real-time PCR. *Mutat. Res. Toxicol. Environ. Mutagen.*, **747**, 164–175.
Weil, C.S. and McCollister, D.D. (1963) Safety evaluation of chemicals, relationship between short-and long-term feeding studies in designing an effective toxicity test. *J. Agric. Food Chem.*, **11**, 486–491.
Westerfield, M. (2000) The Zebrafish Book: A Guide for the Laboratory Use of Zebrafish (Danio Rerio) 4th ed. University of Oregon Press.
Yamashita, A., Inada, H., Chihara, K., Yamada, T., Deguchi, J., and Funabashi, H. (2014) Improvement of the evaluation method for teratogenicity using zebrafish embryos. *J. Toxicol. Sci.*, **39**, 453–464.
Yan, Y.L. *et al.* (2005) A pair of Sox: distinct and overlapping functions of zebrafish sox9 co-orthologs in craniofacial and pectoral fin development. *Development*, **132**, 1069–1083.

Yauk, C.L., Harrill, A.H., Ellinger-Ziegelbauer, H., van der Laan, J.W., Moggs, J., Froetschl, R., Sistare, F., and Pettit, S. (2020) A cross-sector call to improve carcinogenicity risk assessment through use of genomic methodologies. *Regul. Toxicol. Pharmacol.*, **110**.104526

Yoon, A., Pham, B., and Dipple, K. (2016) Genetic Screening in Patients with Craniofacial Malformations. *J. Pediatr. Genet.*, **5**, 220–224.

You, Y. *et al.* (2016) Sorting nexin 10 acting as a novel regulator of macrophage polarization mediates inflammatory response in experimental mouse colitis. *Sci. Rep.*, **6**, 20630.

Yu, Q., Wang, X., Wang, L., Zheng, J., Wang, J., and Wang, B. (2016) Knockdown of asparagine synthetase (ASNS) suppresses cell proliferation and inhibits tumor growth in gastric cancer cells. *Scand. J. Gastroenterol.*, **51**, 1–7.

Yu, X. and Li, Z. (2015) TOX gene: a novel target for human cancer gene therapy. *Am. J. Cancer Res.*, **5**, 3516–24.

Zhang, B. *et al.* (2013) Asparagine synthetase is an independent predictor of surgical survival and a potential therapeutic target in hepatocellular carcinoma. *Br. J. Cancer*, **109**, 14–23.

Zigmond, E. *et al.* (2015) Suppression of hepatocellular carcinoma by inhibition of overexpressed ornithine aminotransferase. *ACS Med. Chem. Lett.*, **6**, 840–844.

Zogg, C.K., Zogg, C.K., Zogg, and K., C. (2014) Phosphoglycerate dehydrogenase: potential therapeutic target and putative metabolic oncogene. *J. Oncol.*, **2014**, 524101.

Zúñiga-García, V., Chávez-López, M. de G., Quintanar-Jurado, V., Gabiño-López, N.B., Hernández-Gallegos, E., Soriano-Rosas, J., Pérez-Carreón, J.I., and Camacho, J. (2015) Differential expression of ion channels and transporters during hepatocellular carcinoma development. *Dig. Dis. Sci.*, **60**, 2373–83.

Appendix

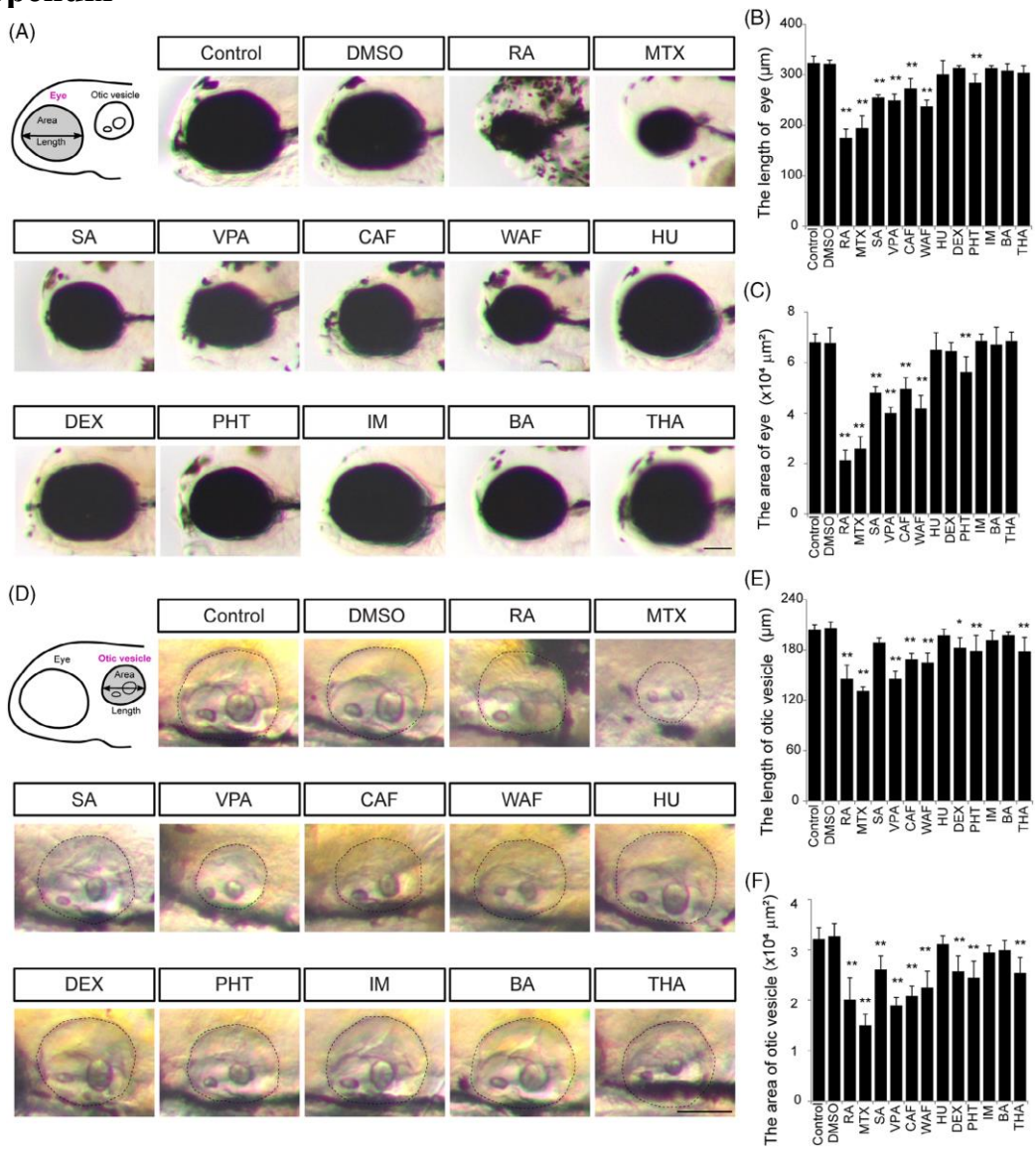

Figure S 1. Defects in eye and otic vesicle were observed in teratogen-treated embryos. (A) Schematic image and bright field images of the eye. Anterior is to the left. (B, C) Quantification of the length and area of the eye. (D) Schematic image and bright field images of the otic vesicle. (E, F) Quantification of the length and area of the otic vesicle. Asterisks indicate statistically significant differences between groups ($^{*}p<0.05$, $^{**}p<0.01$, n=5). Scale bars: 100 μm.

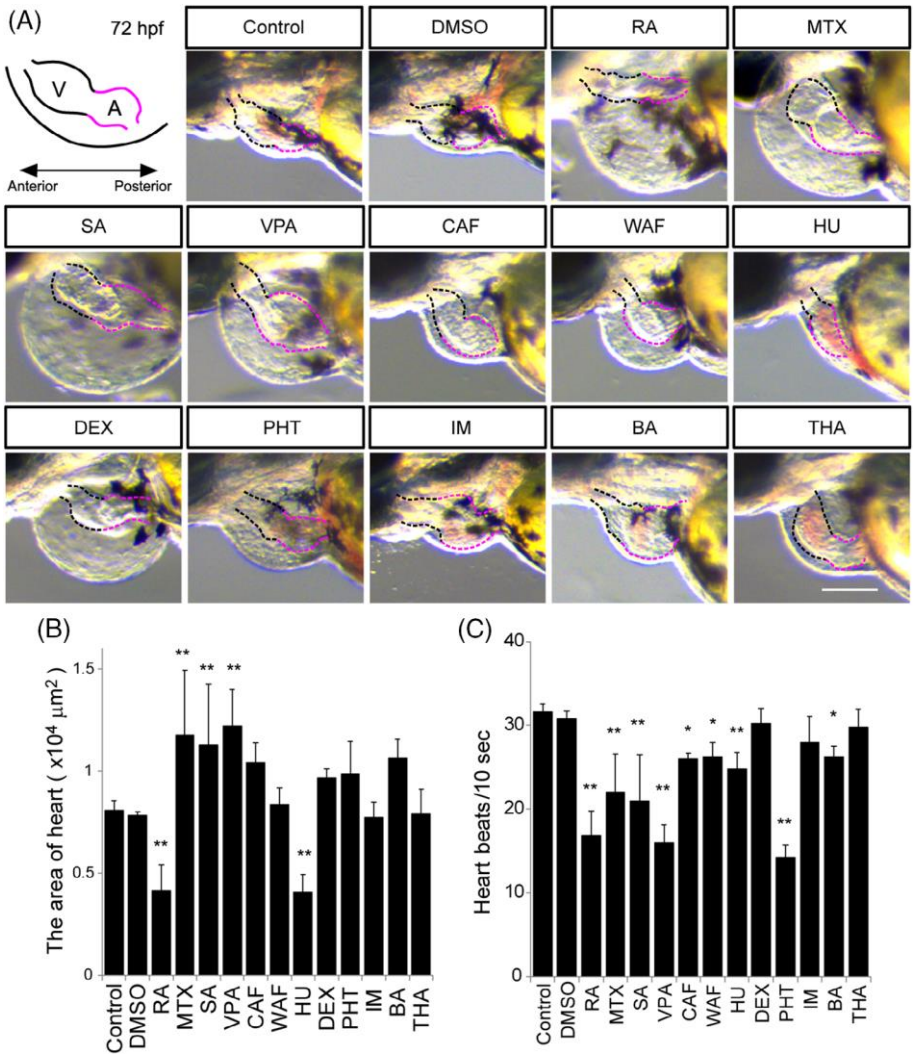

Figure S 2. Morphological defects of the heart and measurement of the heart beat rate. (A) Illustration of the embryonic heart at 72 hpf. V stands for the ventricle marked by the black-dotted line. A stands for the atrium marked by the red-dotted line. (B) Heart beat rate was calculated in a 10-second window. Asterisks indicate statistically significant differences between groups ($^{*}p<0.05$, $^{**}p<0.01$, n=3).

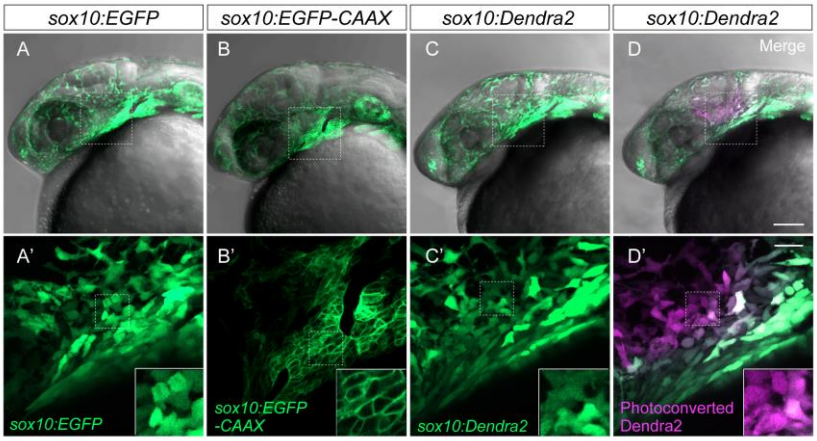

Figure S 3. Transgenic lines established in the present study. Lateral view of the three transgenic lines at 24 hpf. (A) *sox10:EGFP*, (B) *sox10:EGFP-CAAX*, (C–D) *sox10:Dendra2*. (A'-D') Enlarged view of the white rectangles in the panel A-D. Scale bars: (A–D) 100 µm, (A'–D') 25 µm.

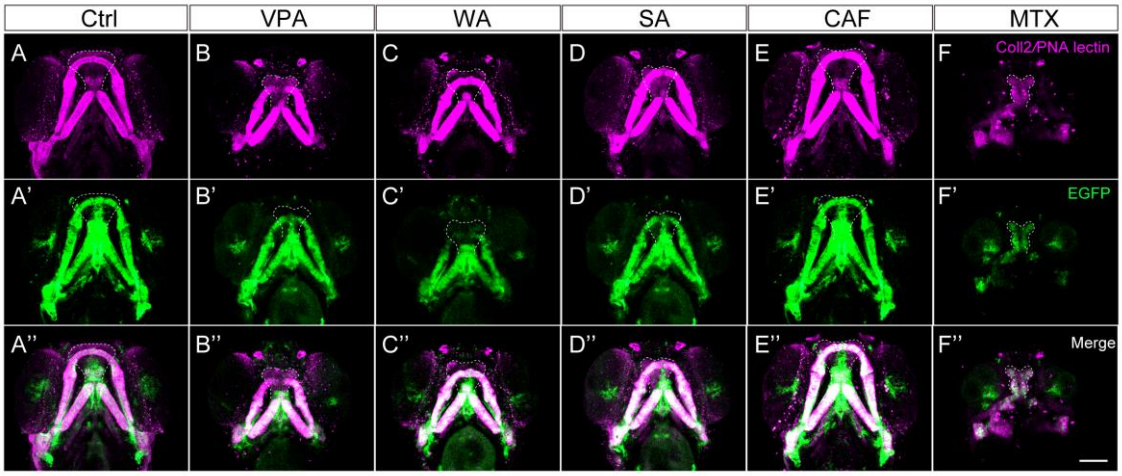

Figure S 4. Craniofacial anomalies in teratogen-treated *sox10:EGFP-CAAX* zebrafish embryos at 96 hpf. The zebrafish were treated with the following teratogens and displayed craniofacial malformations: A, Ctrl, E3 control. B, VPA, valproic acid. C, WAF, warfarin. D, SA, salicylic acid. E, CAF, caffeine. F, MTX, methotrexate. Immunofluorescence staining was performed with anti-coll2 antibody and PNA lectin (A–F), and anti-GFP antibody (A'–F'). Scale bar: 100 µm.

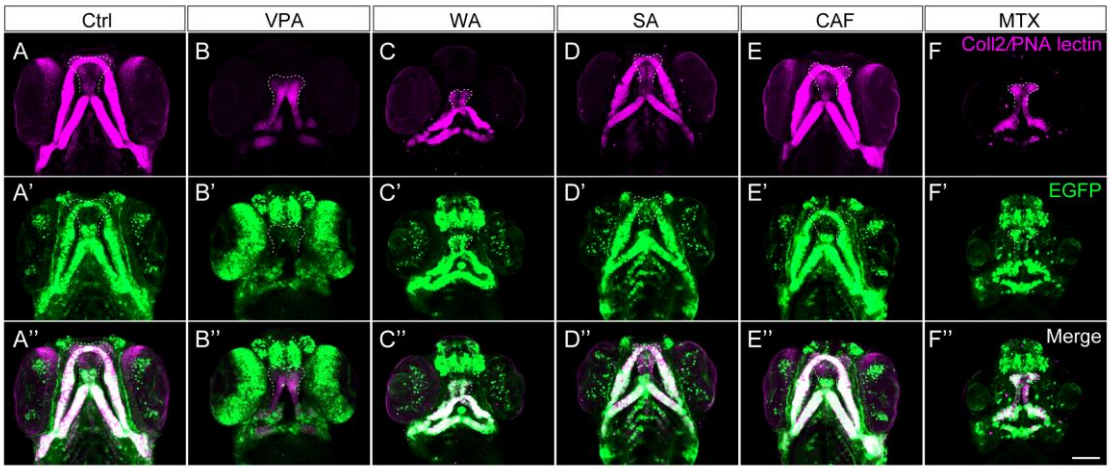

Figure S 5. Craniofacial anomalies in teratogen-treated *sox10:Dendra2* zebrafish embryos at 96 hpf. The *sox10:Dendra2* embryos were treated with the following teratogens and displayed craniofacial malformations: A, Ctrl, E3 control. B, VPA, valproic acid. C, WAF, warfarin. D, SA, salicylic acid. E, CAF, caffeine. F, MTX, methotrexate. Immunofluorescence staining was performed with anti-coll2 antibody and PNA lectin (A–F), and anti-GFP antibody (A'–F'). Scale bar: 100 µm.

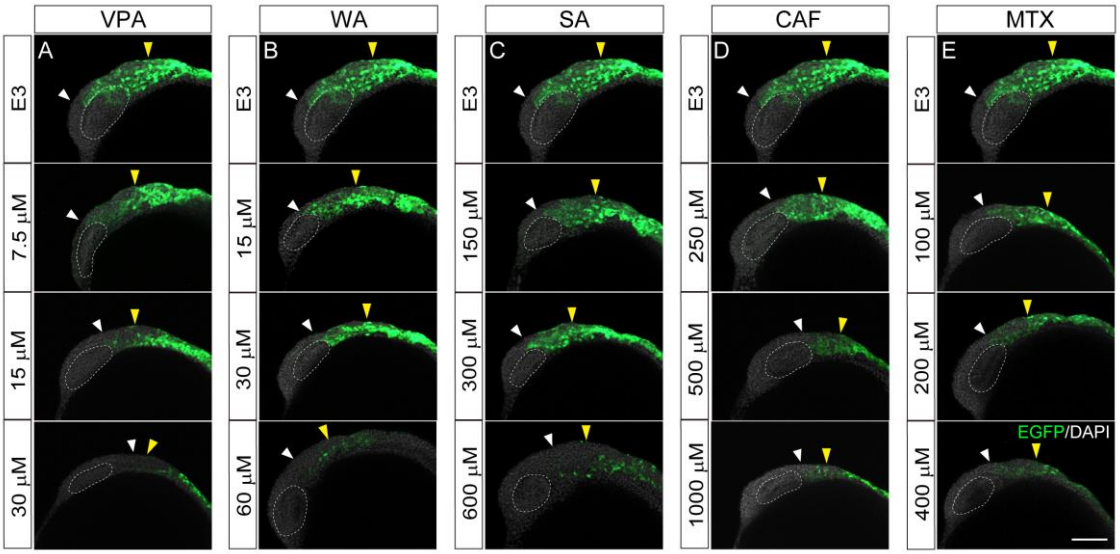

Figure S 6. Dose-dependent inhibition of CNCC migration. (A-E) Inhibitory effect on CNCC migration. Teratogens were treated at the following concentrations: (A) Valproic acid (VPA, 7.5, 15, 30 μM). (B) Warfarin (WA, 15, 30, 60 μM). (C) Salicylic acid (SA, 150, 300, 600 μM). (D) Caffein (CAF, 250, 500, 1000 μM). Methotrexate (MTX, 100, 200, 400 μM).

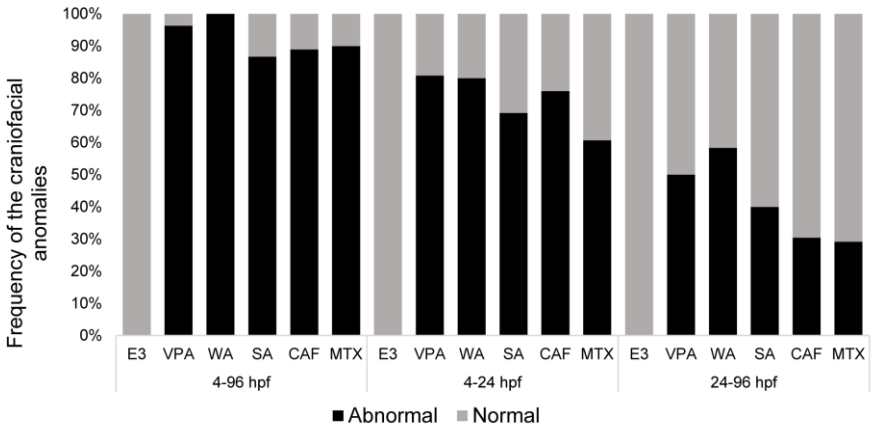

Figure S 7. CNCCs migration was crucial for craniofacial development. The frequency of craniofacial anomalies in the control and teratogen-exposed embryos with different exposure periods. n = 10–30.